Local Correlation: Implementation and Application to Molecular Response Properties

Nicholas Joel Russ

Dissertation submitted to the faculty of the
Virginia Polytechnic Institute and State University
in partial fulfillment of the requirements for the degree of

Doctor of Philosophy
In
Chemistry

T. Daniel Crawford, Chair
John R. Morris
Diego Troya
Jimmy W. Viers
Gordon T. Yee

17 April 2006
Blacksburg, Virginia

Keywords: coupled cluster, CC2, local correlation, optical rotation, polarizability

Local Correlation: Implementation and Application to Molecular Response Properties

Nicholas J. Russ

(Abstract)

One of the most promising methods for surmounting the high-degree polynomial scaling wall associated with electron correlating wave function methods is the local correlation technique of Pulay and Saebø. They have proposed using a set of localized occupied and virtual orbitals free of the canonical constraint commonly employed in quantum chemistry, resulting in a method that scales linearly (in the asymptotic limit) with molecular size. Pulay and Saebø first applied their methods to configuration interaction and later to Møller-Plesset perturbation theory. Werner *et al.* have have extended the local correlation scheme of Pulay and Saebø to coupled-cluster theory.

One of the pitfalls of the local correlation methods developed by Pulay and Saebø is the dependence of domain selection on the molecular geometry. In other words, as the geometry changes the domain structure of the local correlation calculation can change also, leading to discontinuities in the potential energy surface. We have examined the size of these discontinuities for the homolytic bond cleavage of fluoromethane and the heterolytic bond dissociation of singlet ketene and propadienone.

Properties such as polarizabilities and optical rotation are realized through linear response theory, where the Hamiltonian is subject to an external perturbation and the wave function is allowed to respond to the applied perturbation. Within the context of local correlation it is necessary to understand how the domain structure alters in response to an applied perturbation. We have proposed using solutions to the CPHF equations (coupled-perturbed Hartree-Fock) in order to predict the correlation response to an applied perturbation. We have applied this technique to the calculation of polarizabilities, with very favorable results, and also to optical rotation, with mixed results.

Acknowledgments

This dissertation has been realized through the hard work and commitment of many individuals. I would like to thank:

- First and foremost I would like to thank Jesus Christ for His ultimate sacrifice.
- My beautiful wife, Jen, your hard work over this time in our lives has been an inspiration to me. I love you very much.
- My parents, your love and support throughout my life have place me in a position to succeed.
- Prof. T. Daniel Crawford, your guidance and wisdom have been pivotal to my success as a graduate student.
- Graduate students: Christopherson Smythe and Mary Tam, Postdocs: Victor M Rosas-Garcia, Seung-Joon Kim, Rollin King and Micah Abrams.
- Thanks Starbucks for providing focus juice, a great working atmosphere as well as friendly employees.

Contents

List of Figures

List of Tables

Chapter 1

A Brief Survey of Conventional Techniques

One of the most fundamental quantities to quantum chemistry is the (electronic) wave function, Ψ, which depends on the spatial and spin coordinates of all electrons in a molecular system,

$$\Psi(x_1, y_1, z_1, s_1, x_2, y_2, z_2, s_2, \ldots, x_N, y_N, z_N, s_N) \tag{1.1}$$

where N is the number of electrons in the system. Finding the wave function for a particular molecular system is tantamount to solving the (time-independent, electronic) Schrödinger equation,

$$\hat{H}\Psi = E\Psi \tag{1.2}$$

where $\hat{H}$ is the Hamiltonian operator and E is the associated energy. The form of the (electronic) Hamiltonian operator, within the Born-Oppenheimer approximation[1] is

$$\hat{H} = -\frac{1}{2}\sum_{i}^{N}\nabla_i^2 - \sum_{i\alpha}^{NM}\frac{Z_\alpha}{r_{i\alpha}} + \frac{1}{2}\sum_{ij}^{NN}\frac{1}{r_{ij}}. \tag{1.3}$$

where Z_α is the charge on nuclear center α, $r_{i\alpha}$ is the distance between electron i and nucleus α and r_{ij} is the distance between electrons i and j. The first two terms in eqn. 1.3 are electron

operators describing the kinetic energy of the electrons and the nuclear-electronic attraction energy, respectively. The third term in eqn. 1.3 precludes the ability to solve the Schrödinger equation (eqn. 1.2) exactly for all but a handful of systems. As a result, we are forced to make approximations by introducing a basis set and assuming certain forms of the wave function. And so begins our journey through the landscape of quantum chemistry.

The Hamiltonian operator can be rewritten using second-quantization[2–4] as

$$\hat{H} = \sum_{pq} \langle p|h|q\rangle a_p^\dagger a_q + \frac{1}{4} \sum_{pqrs} \langle pq||rs\rangle a_p^\dagger a_q^\dagger a_s a_r \tag{1.4}$$

where $a_p^\dagger$ and a_p are creation and annihilation operators, respectively. The first term of eqn. 1.4 includes the kinetic and electron-nuclear attraction energies. The second term in eqn. 1.4 portrays the $\frac{1}{r_{12}}$ in a basis of $\{\psi_p\}$, usually taken to be MOs (molecular orbitals).

1.1 Single Configuration Theory

The most common starting point for solving the Schrödinger equation is to assume the wave function can be written as a single Slater determinant, or configuration, following the form

$$|0\rangle = \left(\frac{1}{N!}\right)^{\frac{1}{2}} \begin{vmatrix} \psi_1(r_1) & \psi_2(r_1) & \dots & \psi_N(r_1) \\ \psi_1(r_2) & \psi_2(r_2) & \dots & \psi_N(r_2) \\ \vdots & \vdots & \ddots & \vdots \\ \psi_1(r_N) & \psi_2(r_N) & \dots & \psi_N(r_N) \end{vmatrix} \tag{1.5}$$

where r_1 includes all spatial and spin coordinates of electron 1. This is known as Hartree-Fock theory and is a good starting guess. But, there is a major oversimplification inherent to the fundamental assumption, a lack of electron correlation.

The Hartree-Fock approximation converts the many-body problem of electron-electron interaction into a one-body problem through the use of the Fock operator in the Hartree-Fock equations:

$$\hat{f}\psi_p = \epsilon_p \psi_p \tag{1.6}$$

where ϵ_p is and eigenvalue of the Fock operator and the energy associated with molecular orbital ψ_p. The form of the Fock operator is

$$\hat{f} = \hat{h} + \sum_i (\hat{J}_i - \hat{K}_i) \tag{1.7}$$

where $\hat{h}$ is the core Hamiltonian (includes kinetic energy of the electrons and electron-nuclear attraction energy), $\hat{J}$ and $\hat{K}$ are the coulomb and exchange operators, respectively. Mathematically, the coulomb and exchange operators have the form

$$\hat{J}_i(x_2)\psi_p(x_1) = \int dx_2 \left[\psi_i^*(x_2)\frac{1}{r_{12}}\psi_i(x_2)\right]\psi_p(x_1) \tag{1.8}$$

$$\hat{K}_i(x_2)\psi_p(x_1) = \int dx_2 \left[\psi_i^*(x_2)\frac{1}{r_{12}}\psi_p(x_2)\right]\psi_i(x_1) \tag{1.9}$$

Combining the coulomb and exchange operators as in eqn. 1.7 describes the Hartree-Fock potential, $\hat{\nu}^{HF}$, and is defined

$$\nu^{HF} = \sum_i (\hat{J}_i - \hat{K}_i) \tag{1.10}$$

Employing the Fock operator results in a wave function that lacks instantaneous interaction (correlation) between electrons. In other words, each electron sees the other $N-1$ electrons as an averaged electronic field[5] instead of individual electrons in real time and space undergoing collisions and various other interactions. Correlating the motions of electrons in a system allows the entire system to relax and lower the total molecular energy.

Commonly, the Hartree-Fock equations are solved by introducing an atomic orbital basis in order to write the molecular orbitals as linear combinations of the atomic orbitals:

$$\psi_p = \sum_\mu C_\mu^p \phi_\mu \tag{1.11}$$

where ϕ_μ is an AO (atomic orbital) and ϕ_p is an MO (molecular orbital). Solving the Hartree-Fock equations in the presence of atomic orbital basis functions was first proposed in 1951 by Roothaan.[6] The Hartree-Fock equations can be rewritten in terms of an AO basis set, using matrix notation, *e.g.*,

$$\mathbf{FC} = \epsilon\mathbf{SC} \tag{1.12}$$

Where the AO basis overlap matrix, $S_{\mu\nu} = \langle\mu|\nu\rangle$, appears due to the lack of orthonormality within the AO basis functions.

The MO coefficients are determined by variationally optimizing the energy of the Hartree-Fock equations with the constraint that the MOs must remain orthonormal:

$$\langle\psi_p|\psi_q\rangle = S_{pq} = \delta_{pq} \tag{1.13}$$

where the S_{pq} are referred to as the overlap integrals and δ_{pq} is the usual Kronecker delta which equals 1 if $p = q$ and 0 if $p \neq q$. This is tantamount to finding MOs that force the occupied-virtual blocks of the Fock matrix to zero,

$$f_{ia} = f_{ai} = 0 \tag{1.14}$$

where $i, j, k, \ldots$ and $a, b, c, \ldots$ represent occupied and virtual MOs, respectively. A single Fock matrix element, defined

$$f_{pq} = h_{pq} + \sum_i \langle pi||qi\rangle, \tag{1.15}$$

where $p, q, r, \ldots$ represent a general MO (either occupied or virtual). The second term in eqn. 1.15 is a sum over antisymmetric two electron integrals in Dirac notation,

$$\langle pi||qi\rangle = \langle pi|qi\rangle - \langle pi|iq\rangle \tag{1.16}$$

and

$$\langle pi|qi\rangle = \int dx_1 \int dx_2 \; \psi_p^*(x_1)\psi_i^*(x_2)\frac{1}{r_{12}}\psi_q(x_1)\psi_i(x_2). \tag{1.17}$$

Commonly, there is a second restriction placed on the MOs, such that the Fock matrix must be diagonal,

$$f_{p\neq q} = 0. \tag{1.18}$$

MOs that satisfy this condition are called canonical MOs. Requiring canonical MOs has the advantage of simplifying the mathematical expressions, but at the cost of spatially delocalized orbital plots. We will address this issue in the local correlation section. Assuming canonical

MOs, the Hartree-Fock energy is

$$E = \sum_i h_{ii} + \frac{1}{2}\sum_{ij}\langle ij||ij\rangle. \tag{1.19}$$

Looking back at eqn. 1.4, we can rewrite the second-quantized form of the Hamiltonian operator for a specific reference, such as the Hartree-Fock reference by subtracting the reference expectation value:

$$\hat{H}_N \equiv \hat{H} - \langle 0|\hat{H}|0\rangle \tag{1.20}$$

where $|0\rangle$ is the Hartree-Fock reference, $|\Phi_0\rangle$, and $\hat{H}_N$ is defined as the normal-ordered Hamiltonian operator. Through algebraic manipulation, a more explicit form of the normal-ordered second-quantized Hamiltonian operator is derived as

$$\hat{H}_N = \sum_{pq} f_{pq}\{a_p^\dagger a_q\} + \frac{1}{4}\sum_{pqrs}\langle pq||rs\rangle\{a_p^\dagger a_q^\dagger a_s a_r\}. \tag{1.21}$$

where the use of curly brace denotes the normal-ordered form of the creation and annihilation operator string. The first term of eqn. 1.21 is defined as the normal-ordered Fock operator and the second term is the normal-ordered two-electron operator. eqn. 1.21 may be simplified to

$$\hat{H}_N = \hat{F}_N + \hat{V}_N. \tag{1.22}$$

We will return to this form of the Hamiltonian operator at the discussions of perturbation and coupled-cluster theories.

1.1.1 Static Field Molecular Properties in Hartree-Fock Theory

Calculating properties like a dipole moment, polarizability, magnetic moment, magnetizability, *etc.*, are accessible via a perturbational expansion of the Hamiltonian and subsequent differentiation of the energy with respect to the perturbing field.[7] While we are not actually interested in calculating Hartree-Fock level properties, we will be using the resulting coupled-perturbed Hartree-Fock equations to modify domain structures for response-type

calculations within a local correlation framework, *vide infra*. The Hamiltonian can be expanded by perturbation order as

$$\hat{H} = \hat{H}_0 + \lambda\hat{P}_1 + \lambda^2\hat{P}_2 + \ldots \tag{1.23}$$

where $\hat{P}_n$ are perturbation operators with a strength determined by λ. Differentiating the energy with respect to the perturbation and evaluating at $\lambda = 0$ yields

$$\begin{aligned} \frac{\partial E}{\partial \lambda} &= \frac{\partial}{\partial \lambda}\langle 0|\hat{H}_0 + \lambda\hat{P}_1 + \lambda^2\hat{P}_2|0\rangle\Big|_{\lambda=0} \\ &= 2\langle\frac{\partial}{\partial\lambda}0|\hat{H}_0|0\rangle + \langle 0|\hat{P}_1|0\rangle \end{aligned} \tag{1.24}$$

where $|0\rangle$ is the Hartree-Fock wave function and we have assumed real orbitals. Looking at the first term in eqn. 1.24, we can use the chain rule to give

$$2\langle\frac{\partial}{\partial\lambda}0|\hat{H}_0|0\rangle = 2\frac{\partial C}{\partial\lambda}\langle\frac{\partial}{\partial C}0|\hat{H}_0|0\rangle \tag{1.25}$$

Eqn. 1.25 is equal to 0 because of the variational nature of the Hartree-Fock wave function (*i.e.*, $\frac{\partial}{\partial C}|0\rangle = 0$). Therefore, the derivative of the energy is equal to the expectation value of the derivative of the Hamiltonian, *e.g.*,

$$\frac{\partial}{\partial\lambda}\langle 0|\hat{H}|0\rangle = \langle 0|\frac{\partial}{\partial\lambda}\hat{H}|0\rangle \tag{1.26}$$

and the Hartree-Fock wave function obeys the Hellmann-Feynman theorem.[8] Before deriving expressions for specific properties and perturbations, it is helpful to first differentiate one- and two-electron integrals with respect to a generic real perturbation, λ.

Differentiating a general one-electron integral with respect to a real perturbation λ yields

$$\begin{aligned} \frac{\partial}{\partial\lambda}h_{pq} &= \frac{\partial}{\partial\lambda}\sum_{\mu\nu}C_\mu^p h_{\mu\nu}C_\nu^q \\ &= \sum_{\mu\nu}\left[(\frac{\partial}{\partial\lambda}C_\mu^p)h_{\mu\nu}C_\nu^q + C_\mu^p(\frac{\partial}{\partial\lambda}h_{\mu\nu})C_\nu^q + C_\mu^p h_{\mu\nu}(\frac{\partial}{\partial\lambda}C_\nu^q)\right] \\ &= h_{pq}^\lambda + \sum_{\mu\nu}\left[(\sum_t U_{pt}^\lambda C_\mu^t)h_{\mu\nu}C_\nu^q + C_\mu^p h_{\mu\nu}(\sum_t U_{qt}^\lambda C_\nu^t)\right] \\ &= h_{pq}^\lambda + \sum_t\left(U_{pt}^\lambda h_{tq} + U_{qt}^\lambda h_{pt}\right) \end{aligned} \tag{1.27}$$

where we have made several steps in one series of equations. The U_{pt}^{λ} define the set of derivative coefficients by a linear combination of the original set of MO coefficients, *e.g.*,

$$\frac{\partial}{\partial\lambda}C_{\mu}^{p} = \sum_{t} U_{pt}^{\lambda} C_{\mu}^{t} \tag{1.28}$$

The notation, h_{pq}^{λ}, represents the derivative of the quantity in the AO basis transformed to the MO basis, *e.g.*,

$$h_{pq}^{\lambda} = \sum_{\mu\nu} C_{\mu}^{p} (\frac{\partial}{\partial\lambda} h_{\mu\nu}) C_{\nu}^{q} \tag{1.29}$$

It is important to note that the AO basis derivative transformed to the MO basis is not equal to the MO basis derivative, *i.e.*,

$$h_{pq}^{\lambda} \neq \frac{\partial}{\partial\lambda} h_{pq} \tag{1.30}$$

Differentiating a general one-electron operator reveals a pattern that can be exploited to quickly elucidate the form of the derivative overlap and two-electron integrals. Differentiating the MO basis overlap integrals reveals a unique relationship between U_{pq} and S_{pq}.

$$\begin{aligned} \frac{\partial}{\partial\lambda} S_{pq} &= S_{pq}^{\lambda} + \sum_{t} \left(U_{pt}^{\lambda} S_{tq} + U_{qt}^{\lambda} S_{pt} \right) \\ &= S_{pq}^{\lambda} + U_{pq}^{\lambda} + U_{qp}^{\lambda} = 0 \end{aligned} \tag{1.31}$$

recalling that $S_{pq} = \delta_{pq}$ from eqn. 1.13. The two-electron integrals follow the same pattern already outlined by the one-electron integrals, but with a few more terms:

$$\frac{\partial}{\partial\lambda}\langle pq||rs\rangle = \langle pq||rs\rangle^{\lambda} + \sum_{t} \left(U_{pt}^{\lambda}\langle tq||rs\rangle + U_{qt}^{\lambda}\langle pt||rs\rangle + U_{rt}^{\lambda}\langle pq||ts\rangle + U_{st}^{\lambda}\langle pq||rt\rangle \right) \tag{1.32}$$

Combining the results of eqns. 1.27, 1.31 and 1.32, we can write the complete derivative of the Hartree-Fock energy with respect to a generic real perturbation, λ, as

$$\frac{\partial E}{\partial\lambda} = \sum_{i} h_{ii}^{\lambda} + \frac{1}{2}\sum_{ij}\langle ij||ij\rangle^{\lambda} - \sum_{i} S_{ii}^{\lambda} f_{ii} \tag{1.33}$$

where we have used the definition of a Fock matrix element from eqn. 1.7.

So far we have looked at integrals with respect to a real perturbation λ. Since we will be using solutions to the CPHF (*vide infra*) equations to predict domain structures for both

polarizabilities and optical rotation we must also consider integral derivatives with respect to an imaginary perturbation, which is introduced in the magnetic operator employed in the calculations of optical rotation. The only difference that arises when differentiating with respect to an imaginary perturbation is a negative sign when operating on the bra of an integral.[9] For example, a one- and two-electron integral differentiated with respect to an imaginary perturbation, γ, yields

$$\frac{\partial}{\partial\gamma}h_{pq} = h^{\gamma}_{pq} + \sum_{t}(-U^{\gamma}_{pt}h_{tq} + U^{\gamma}_{qt}h_{pt}) \tag{1.34}$$

and

$$\frac{\partial}{\partial\gamma}\langle pq||rs\rangle = \langle pq||rs\rangle^{\gamma} + \sum_{t}(-U^{\gamma}_{pt}\langle tq||rs\rangle - U^{\gamma}_{qt}\langle pt||rs\rangle + U^{\gamma}_{pr}\langle pq||ts\rangle + U^{\gamma}_{st}\langle pq||rt\rangle), \tag{1.35}$$

respectively. Also, differentiating the MO basis overlap integrals with respect to an imaginary perturbation gives

$$\frac{\partial}{\partial\gamma}S_{pq} = S^{\gamma}_{pq} - U^{\gamma}_{pq} + U^{\gamma}_{qp} = 0 \tag{1.36}$$

We can use the above expressions for differentiating integrals with respect to a real perturbation, λ, and an imaginary perturbation, γ, to calculate properties specific to an electric and magnetic field perturbation in order to calculate polarizabilities and magnetizabilities, respectively.

Static Polarizability and 'Pseudo-'Magnetizability via Analytic Derivatives

Calculating a polarizability requires a perturbing electric field as described in eqn. 1.23, which can be rewritten as,

$$\hat{H} = \hat{H}_0 + \hat{\mu}_e\mathbf{F} \tag{1.37}$$

where $\hat{\mu}_e$ is the electric dipole moment operator and $\mathbf{F}$ is the field strength. The static field polarizability can be calculated as the negative of the second derivative of the energy with respect to an electric field perturbation,[7,10] *e.g.*,

$$\alpha_{xy} = -\frac{\partial^2 E}{\partial x\partial y} \tag{1.38}$$

where α_{xy} is one element of the polarizability tensor and x is one component of the electric field perturbation, $\mathbf{F}$. The dipole moment is defined as the negative of the first derivative of the energy with respect to the dipole moment operator,[7,10]

$$\mu^x = -\frac{\partial E}{\partial x}. \tag{1.39}$$

Using the definition of the electric dipole moment in eqn. 1.38, we can rewrite the polarizability as

$$\alpha_{xy} = \frac{\partial \mu^x}{\partial y} = \frac{\partial \mu^y}{\partial x} \tag{1.40}$$

Differentiating the energy with respect to an electric field perturbation yields the dipole moment as

$$\begin{aligned} \frac{\partial E}{\partial x} &= -\mu^x \\ &= -\langle 0|\mu_e^x|0\rangle \\ &= \sum_i d_{ii}^x \end{aligned} \tag{1.41}$$

where d_{ii}^x are the electric dipole moment integrals and are defined as

$$d_{pq}^x = -\langle p|\mu_e^x|q\rangle \tag{1.42}$$

Differentiating the dipole moment integrals appearing in the above equation yields the polarizability.

Since the dipole moment integrals involve only one electron operators, we can use the form of a one-electron derivative to write the polarizability as

$$\begin{aligned} \alpha_{xy} &= \frac{\partial \mu^y}{\partial x} = \sum_{pi}(U_{pi}^x d_{pi}^y + U_{pi}^x d_{ip}^y) \\ &= 2\sum_{pi} U_{pi}^x d_{pi}^y \\ &= 2\sum_{ai} U_{ai}^x d_{ai}^y + 2\sum_{ij} U_{ij}^x d_{ij}^y \\ &= 2\sum_{ai} U_{ai}^x d_{ai}^y + \sum_{ij}(U_{ij}^x + U_{ji}^x) d_{ij}^y \\ &= 2\sum_{ai} U_{ai}^x d_{ai}^y \end{aligned} \tag{1.43}$$

where we have omitted the second-order derivative term d_{pq}^{yx} which is commonly considered unimportant and usually ignored.[10] Also, the AO basis functions do not depend on the electric field perturbation, meaning $S_{pq}^{x} = 0$. As a result, eqn. 1.31 can be rewritten as

$$U_{pq}^{x} = -U_{qp}^{x} \tag{1.44}$$

which has been used in the derivation of eqn. 1.43. What remains now is to solve for the set of MO derivative coefficients, U_{ai}.

The magnetizability is defined analogously to the polarizability; a magnetic perturbation is applied to the Hamiltonian followed by differentiating the energy with respect to the magnetic field. Rewriting the Hamiltonian including a magnetic field perturbation yields,

$$\hat{H} = \hat{H}_0 + \hat{m}\mathbf{B} \tag{1.45}$$

where $\hat{m}$ is the magnetic moment operator and $\mathbf{B}$ is the strength of the magnetic field. Differentiating the energy with respect to a magnetic field is more cumbersome than an electric field, not only due to the imaginary nature of the magnetic moment operator, but also due to the fact that more quantities depend on the magnetic field, which gives rise to more terms in the derivative expression.[7] Since we are not interested in calculating magnetizabilities we instead choose to mimic the equation for calculating polarizabilities and compute a 'pseudo-'magnetizability as

$$\Gamma_{xy} = 2\sum_{ai} U_{ai}^{x} g_{ai}^{y} \tag{1.46}$$

where g_{ai}^{y} are magnetic dipole moment integrals. We must now solve for the set of U_{ai} for both an electric and magnetic field perturbation.

Coupled-Perturbed Hartree-Fock Equations (CPHF)

The coupled-perturbed Hartree-Fock[9–12] (CPHF) equations provide a route to for solve the set of MO derivative coefficients. The variational condition for the Hartree-Fock equations

is that the occupied-virtual blocks of the Fock matrix must be zero (see eqn. 1.14). The derivative of the Fock matrix must also yield zeros in the occupied-virtual blocks, *e.g.*,

$$\frac{\partial}{\partial\lambda} f_{ai} = \frac{\partial}{\partial\lambda} f_{ia} = 0 \tag{1.47}$$

Differentiating the f_{ai} matrix elements with respect to real perturbation λ will provide a set of coupled equations that can be iterated to obtain the set of MO derivative coefficients, U_{ai}^{λ}. The analytic form of $\frac{\partial}{\partial\lambda} f_{ai}$ is

$$0 = f_{ai}^{\lambda} + \sum_{j} U_{aj}^{\lambda} f_{ji} - \sum_{b} U_{bi}^{\lambda} f_{ab} - \sum_{bj} U_{bj}^{\lambda} A_{aibj} \tag{1.48}$$

where we have used an A_{aibj} quantity defined as

$$\begin{aligned} A_{aibj} &= \langle ab||ij\rangle + \langle aj||ib\rangle \\ &= 2\langle ab|ij\rangle - \langle ab|ji\rangle - \langle aj|bi\rangle \end{aligned} \tag{1.49}$$

The U_{ai}^{λ} coefficients are solved in a very similar manner to the T_1-amplitude equations in coupled-cluster theory, *vide infra*.

For the case of an imaginary perturbation, γ, the CPHF equations become

$$0 = f_{ai}^{\gamma} - \sum_{j} U_{aj}^{\gamma} f_{ji} + \sum_{b} U_{bi}^{\gamma} f_{ab} - \sum_{bj} U_{bj}^{\gamma} B_{aibj} \tag{1.50}$$

where we have used a B_{aibj} quantity defined as

$$\begin{aligned} B_{aibj} &= -\langle ab||ij\rangle + \langle aj||ib\rangle \\ &= \langle ab|ji\rangle - \langle aj|bi\rangle \end{aligned} \tag{1.51}$$

It is worth noting that we do not incorporate the solutions to the CPHF equations into the calculation of any properties within the scope of this research. Instead, we have merely used the U_{ai} coefficients, which represent the orbital response to an applied perturbation, predict the correlated wave function response to the applied perturbation. This technique provides an *a priori* domain selection with respect to an applied perturbation.

1.2 Enter Electron Correlation

Electrons are constantly colliding and scattering in Cartesian space. These types of motions are not included in the Hartree-Fock wave function. Accounting for this behavior in orbital space is equivalent to including multiple configurations into the wave function.[13]

Electron correlation is required for an accurate description of the wave function. Hartree-Fock theory accounts for approximately 98% of total energy, the remaining 2% is called the correlation energy. This may seem like a small percentage, but its effect can qualitatively change the properties of a molecular system.[13–16]

1.3 Configuration-Interaction Theory

In Hartree-Fock theory, only a single determinant is used to describe the total wave function, with all of the electrons in the energetically lowest molecular orbitals. Configuration-interaction uses this single determinant as a reference from which to add a series of singly, doubly, triply, *etc.* excited determinants. The order of excitation refers to the number of electrons being excited; *e.g.* a doubly excited determinant means that two electrons are removed from their occupied orbitals and placed into unoccupied orbitals.

The exact form of the wave function can be described by a linear combination of all unique determinants. This would require an infinite basis set, but since we are forced to use a finite basis, we can only include the unique determinants within the confines of the chosen basis.[17] Configuration-interaction (CI), like many other correlated methods, integrates electron correlation by incorporating a linear combination of excited determinants into the wave function.[18–20]

$$|\Psi_{CI}\rangle = (1 + \hat{C})|0\rangle \tag{1.52}$$

where $|\Psi_{CI}\rangle$ is the CI wave function, $|0\rangle$ is the reference determinant, and $\hat{C}$ is the excitation operator. The $\hat{C}$ operator can be expanded as $\hat{C} = \hat{C}_1 + \hat{C}_2 + \hat{C}_3 + \cdots$, where the operator

$\hat{C}_1$ generates all single excitations, $\hat{C}_2$ generates all double excitations, *etc.* The truncation of the excitation operator determines the level of CI theory. Truncation at $\hat{C} = \hat{C}_1 + \hat{C}_2$ defines CISD; $\hat{C} = \hat{C}_1 + \hat{C}_2 + \hat{C}_3$ defines CISDT. The general form of a $\hat{C}_n$ operator is

$$\hat{C}_n \equiv \left(\frac{1}{n!}\right)^2 \sum_{ij\ldots ab\ldots}^{n} c_{ij\ldots}^{ab\ldots} a_a^\dagger a_b^\dagger \ldots a_j a_i \tag{1.53}$$

The excitation operator, $\hat{C}$, provides the excited determinants from which configuration-interaction is able to describe electron correlation.

CI is a tried and true method in quantum chemistry. In fact, full CI (FCI) provides the exact solution to the electronic Schrödinger equation within a given basis set.[21] Full CI means that all possible excited determinants, within the given basis set, have been incorporated into the wave function. The quality of performance in other quantum chemical methods are often determined by comparison to FCI.[22–30] The only drawback of FCI is the computational expense, scaling as $O(N!)$, where N is some measure of the system size. This makes FCI a realistic option for only very small molecules with small basis sets.

1.4 Perturbation Theory

One of the simplest ways to incorporate electron correlation into the system is though perturbation theory. The Hamiltonian is split into two parts, a zeroth order part and a perturbation as

$$\hat{H} = \hat{H}_0 + \lambda \hat{V} \tag{1.54}$$

where λ is an used as a bookkeeping tool for perturbation order and $\hat{V}$ represents the first-order Hamiltonian. The division in the Hamiltonian can be imposed on the Schrödinger equation to partition the Schrödinger equation by order:

$$\lambda = 0 \qquad \hat{H}_0|0\rangle = E^{(0)}|0\rangle \tag{1.55}$$

$$\lambda = 1 \qquad \hat{H}_0|\psi^{(1)}\rangle + \hat{V}|0\rangle = E^{(0)}|\psi^{(1)}\rangle + E^{(1)}|0\rangle \tag{1.56}$$

$$\lambda = 2 \qquad \hat{H}_0|\psi^{(2)}\rangle + \hat{V}|\psi^{(1)}\rangle = E^{(0)}|\psi^{(2)}\rangle + E^{(1)}|\psi^{(1)}\rangle + E^{(2)}|0\rangle \tag{1.57}$$

Where $|0\rangle$ are eigenfunctions of the zeroth-order Hamiltonian, $\hat{H}_0$, and we have limited our discussion to ground state energies.

Left projecting the above equations by $\langle 0|$ yields expressions for the energy at various perturbation orders:

$$E^{(0)} = \langle 0|\hat{H}_0|0\rangle \tag{1.58}$$

$$E^{(1)} = \langle 0|\hat{V}|0\rangle \tag{1.59}$$

$$E^{(2)} = \langle 0|\hat{V}|\psi^{(1)}\rangle \tag{1.60}$$

Within the context of electronic structure theory and using the Hartree-Fock wave function as the reference, solving the energy through first-order returns only the Hartree-Fock energy. The first correction to the Hartree-Fock energy is obtained at second-order. Eqn. 1.60 implies that the first-order wave function is required to calculate the second-order energy. Defining an analytic form of the first-order wave function requires a deeper look at the first-order Schrödinger equation. We will look at the definition of the first-order wave function in terms of Møller-Plesset perturbation theory.

MP2

Møller-Plesset theory[31] is a specific form of perturbation theory where the reference is strictly the Hartree-Fock wave function and Hamiltonian is partitioned as in eqn. 1.21, *i.e.*,

$$\hat{F}_N = \hat{H}_0 \tag{1.61}$$

$$\hat{V}_N = \hat{V} \tag{1.62}$$

Looking at the second-order correction to the energy, MP2, we can rewrite eqn. 1.60 as

$$E_{MP2} = \langle 0|\hat{V}_N|\psi^{(1)}\rangle \tag{1.63}$$

Again, finding the first-order wave function requires an in-depth look at the first-order Schrödinger equation:

$$\hat{F}_N|\psi^{(1)}\rangle + \hat{V}_N|0\rangle = 0 \tag{1.64}$$

As is common practice for Rayleigh-Schrødinger perturbation theory, the first-order wave function can be written as a linear combination of eigenfunctions of the zeroth-order Hamiltonian ($|\psi^{(0)}\rangle = \sum_n c_n^{(1)}|0\rangle$). Plugging this into eqn. 1.64 yields

$$\sum_n c_n^{(1)} \hat{F}_N|0\rangle + \hat{V}_N|0\rangle = 0 \tag{1.65}$$

Solving for the $c_n^{(1)}$ coefficients now becomes a question of what can be left-projected onto eqn. 1.65 to produce a non-zero result. The reference cannot produce a non-zero result due to the definition of a normal-ordered operator (eqn. 1.22). The set of singles, $\{\langle\Phi_i^a|\}$ cannot produce a non-zero result due to Brillouin's theorem.[17] The set of triples and higher, $\{\langle\Phi_{ijk\ldots}^{abc\ldots}|\}$, is not able to produce a non-zero result due to Slater's rules.[17] However, the set of doubles, $\{\langle\Phi_{ij}^{ab}|\}$, is able to produce a non-trivial solution to the set of coefficients:

$$\sum_{ijab} t_{ij}^{ab} \langle\Phi_{ij}^{ab}|\hat{F}_N|0\rangle + \langle\Phi_{ij}^{ab}|\hat{V}_N|0\rangle = 0 \tag{1.66}$$

where we have replaced the $c_n^{(1)}$ with t_{ij}^{ab} to maintain consistency with coupled-cluster theory, *vide infra*.

Eqn. 1.66 can easily be solved using diagrammatic techniques[4,32] to obtain an algebraic expression:

$$\sum_e \left(t_{ij}^{ae} f_{be} - t_{ij}^{be} f_{ae}\right) - \sum_m \left(t_{im}^{ab} f_{mj} - t_{jm}^{ab} f_{im}\right) + \langle ab||ij\rangle = 0 \tag{1.67}$$

Assuming canonical orbitals (eqn. 1.18) the above equation can be further simplified to

$$t_{ij}^{ab} = \frac{\langle ab||ij\rangle}{\epsilon_i + \epsilon_j - \epsilon_a - \epsilon_b} \tag{1.68}$$

where ϵ_p is the energy associated with orbital ψ_p and the denominator of the above expression is commonly referred to as an energy denominator. Looking back at eqn. 1.63, we can plug in the set of doubles to define the MP2 energy as

$$E_{MP2} = \sum_{ijab} t_{ij}^{ab} \langle 0|\hat{V}_N|0\rangle \tag{1.69}$$

We already know the form of the t_{ij}^{ab} amplitudes, the other part of the above equation can be analyzed diagrammatically to obtain a final form of the MP2 energy as

$$E_{MP2} = \frac{1}{4} \sum_{ijab} \frac{|\langle ij||ab\rangle|^2}{\epsilon_i + \epsilon_j - \epsilon_a - \epsilon_b} \tag{1.70}$$

The MP2 energy expression is non-iterative, scaling as $\mathcal{O}(N^4)$ and is relatively inexpensive to compute.

The ability to solve the t_{ij}^{ab} amplitudes through a one-time calculation rather than iteratively as achieved by assuming canonical orbitals. If the Fock matrix is not diagonal, as is the case for a local-correlation calculation, the MP2 t_{ij}^{ab} amplitudes must be solved iteratively. However, the savings inherent in a local-correlation calculation more than make up for the iterative algorithm.

1.5 Coupled-Cluster Theory

Coupled-cluster theory address the lack of electron correlation in a Hartree-Fock reference determinant by using an exponential *ansatz* of excitation operators as

$$|\Psi_{CC}\rangle = e^{\hat{T}} |0\rangle . \tag{1.71}$$

Where $\hat{T} = \hat{T}_1 + \hat{T}_2 + \hat{T}_3 + \ldots$ decomposed into single excitations, double excitations, *etc.* The general form of an excitation operator, in second quantization, is given as

$$\hat{T}_n \equiv \left(\frac{1}{n!}\right)^2 \sum_{ij\ldots ab\ldots}^{n} t_{ij\ldots}^{ab\ldots} \{a_a^\dagger a_b^\dagger \ldots a_j a_i\} \tag{1.72}$$

The $\hat{T}$ operator is identical to the $\hat{C}$ operator of CI theory. The only difference between to the two is the manner in which they are used in their respective theories. CI theory uses the $\hat{C}$ operator linearly, eqn. 1.52, while coupled-cluster theory adopts an exponential form, eqn. 1.71.

Looking back to eqn. 1.71, we can use a power series expansion of an exponential to rewrite eqn. 1.71

$$|\Psi_{CC}\rangle = \left(1 + \hat{T} + \frac{1}{2!}\hat{T}^2 + \frac{1}{3!}\hat{T}^3 + \ldots\right)|0\rangle \tag{1.73}$$

Using the power series expansion of an exponential operator may not seem beneficial, but the series naturally truncates at $\hat{T}^4$. This is a result of the Hamiltonian operator being at most a two-body and retaining only connected terms.

Using the coupled-cluster wave function in the Schrödinger equation yields,

$$\hat{H}e^{\hat{T}}|0\rangle = E_{CC}e^{\hat{T}}|0\rangle. \tag{1.74}$$

Suppose we multiply on the left by $e^{-\hat{T}}$,

$$\bar{H}|0\rangle = E_{CC}|0\rangle \tag{1.75}$$

where the over-bar denotes a similarity transformed operator (*e.g.* $\bar{H} = e^{-\hat{T}}\hat{H}e^{\hat{T}}$). Left projecting eqn. 1.75 by the reference yields the coupled-cluster energy,

$$\langle 0|\bar{H}|0\rangle = E_{CC} \tag{1.76}$$

Assuming the $\hat{T}$ operator has been truncated at $\hat{T} = \hat{T}_1 + \hat{T}_2$, (CCSD) we can left project by the set of singles, $\{\langle\Phi_i^a|\}$, and doubles, $\{\langle\Phi_{ij}^{ab}|\}$, to obtain the amplitude defining equations:

$$\langle\Phi_i^a|\bar{H}|0\rangle = 0 \tag{1.77}$$

$$\langle\Phi_{ij}^{ab}|\bar{H}|0\rangle = 0 \tag{1.78}$$

The T-amplitude equations are a set of coupled nonlinear equations that must be solved iteratively. Solving this set of equations can be a computationally demanding task scaling as $O(N^6)$ for CCSD.

CC2

CC2 has been designed by Christiansen *et al.* to be a computationally less demanding approximation to CCSD,[33] scaling as $O(N^5)$. The difference between CC2 and CCSD is found

only in the doubles amplitude equation. The singles amplitude equation has been preserved to allow for orbital relaxation in linear-response calculations.[34] In order for the T_1's to be included in their entirety, Christiansen *et al.* propose the use of a T_1 similarity transformation of the Hamiltonian operator, *i.e.*,

$$\hat{\bar{H}} = e^{-T_1} \hat{H}_N e^{T_1} \tag{1.79}$$

where the hat above the over-bar denotes an "incomplete" similarity transformation. In this case, we have omitted the T_2 in the similarity transformation even though the full $\hat{T}$ operator in CC2 is $\hat{T}_1 + \hat{T}_2$.

Incorporating concepts from perturbation theory, singles are regarded as second-order parameters due to their lack of contribution in the MP2 energy expression (eqn. 1.66). However, Christiansen *et al.* have chosen to treat T_1 amplitudes as zeroth-order parameters to ensure their inclusion in all aspects of the CC2 model and return an energy complete through second order, whereas the CCSD energy is correct through third order.

Reformulating the CCSD equations using the T_1 similarity Hamiltonian along with commutator notation yields

$$\langle \Phi_i^a | \hat{\bar{H}} + [\hat{\bar{H}}, T_2] | 0 \rangle = 0 \tag{1.80}$$

$$\langle \Phi_{ij}^{ab} | \hat{\bar{H}} + [\hat{\bar{H}}, T_2] + \tfrac{1}{2}[[\hat{\bar{H}}, T_2], T_2] | 0 \rangle = 0 \tag{1.81}$$

Using this same notation, the T_2 equation for CC2 is

$$\langle \Phi_{ij}^{ab} | [F_N, T_2] + \hat{\bar{H}} | 0 \rangle = 0 \tag{1.82}$$

The T_2 equation of CC2 is much less computationally demanding the CCSD analogue. The CC2 T_2 amplitude equations can be written in an MP2-like expression using the T_1 similarity transformation notation:

$$t_{ij}^{ab} = \frac{\langle ab | \hat{\bar{}} ij \rangle}{\epsilon_i + \epsilon_j - \epsilon_a - \epsilon_b} \tag{1.83}$$

The CC2 T_1 equation (eqn. 1.80) reveals the coupling of the T_1 amplitudes to themselves resulting in a necessarily iterative procedure to solve the T amplitude equations. Even

though MP2 and CC2 both scale as $\mathcal{O}(N^5)$, CC2 is computationally more demanding due, in part, to the iterative nature of CC2.

We have chosen to implement CC2 for many of our local methods due to its decreased scaling as compared to CCSD, allowing the opportunity to perform calculations on larger molecular system that would otherwise be unattainable for CCSD. The concepts and algorithms discovered for CC2 will be directly transferable to CCSD. One of the drawbacks to MP2 theory is its lack of a well-defined response function making it difficult or impossible to calculate second-order properties. CC2 offers an ideal framework for assessing the merits and shortcomings associated with local correlation methods.

1.5.1 Coupled-Cluster Linear-Response Theory

The ability to calculate properties such as dipole polarizabilities, optical rotation, magnetizabilities, oscillator strengths, rotational strengths, spin-spin coupling constants, *etc.* (also known as second-order properties) are all obtainable through response theory. Subjecting the Hamiltonian to a perturbation of the form

$$\hat{H} = \hat{H}_N + \beta\hat{V} \tag{1.84}$$

where $\beta\hat{V}$ is an external perturbation applied to the molecular system. The property of interest determines the type of perturbation that must be applied to the Hamiltonian (see Table 1.1).

The groundwork for calculating response-type properties within coupled-cluster theory was laid out by Koch and Jørgensen in 1990[35] in their seminal paper on coupled-cluster response functions and later revisited by Pedersen and Koch in 1997.[36] The linear response of the coupled-cluster wave function for operator $\hat{\mathbf{A}}$ perturbed by $\hat{\mathbf{B}}$ is governed by

$$\langle\langle \mathbf{A}; \mathbf{B} \rangle\rangle_\omega = \frac{1}{2}\hat{C}^{\pm\omega}\hat{P}\left(\hat{A}(-\omega), \hat{B}(\omega)\right)\left[\langle 0|\hat{\Lambda}\left[\bar{A}, \hat{X}^B_\omega\right]|0\rangle + \frac{1}{2}\langle 0|\hat{\Lambda}\left[\left[\bar{H}, \hat{X}^A_\omega\right], \hat{X}^B_{-\omega}\right]|0\rangle\right]. \tag{1.85}$$

Table 1.1: A brief sampling of applied perturbations necessary for the calculation of particular properties.

Molecular Property	Perturbation
Polarizability	$-\vec{\mu} \cdot \mathbf{F}$
Magnetizability	$-\vec{m} \cdot \mathbf{B}$
NMR Chemical Shieldings	$\sum_k \frac{m_k \times r_k}{r_k^3} - \vec{m} \cdot \mathbf{B}$
Optical Rotation	$-\vec{\mu}_e \cdot \mathbf{F} - \vec{m} \cdot \mathbf{B}$

where the permutation operator, $\hat{C}^{\pm\omega}$, simultaneously changes signs on the chosen field frequency, ω, and takes the complex conjugate of the equation, while $\hat{P}(\hat{A}(-\omega), \hat{B}(\omega))$ permutes the property operators $\hat{A}$ and $\hat{B}$.

The lambda operator, $\hat{\Lambda}$, represents a set of de-excitation operators, similar to the $\hat{T}$ operator, but parametrizes the left-hand state of the coupled-cluster wave function:

$$\langle \Psi_{CC}| = \langle 0| \left(1 + \hat{\Lambda}\right) e^{-\hat{T}} \tag{1.86}$$

The Λ-amplitudes are determined by solving a set of coupled-linear equations:

$$\sum_{\nu} \langle 0|\Lambda|\nu\rangle\langle\nu|(\bar{H} - E)|\mu\rangle + \langle 0|\bar{H}|\mu\rangle = 0 \tag{1.87}$$

where $|\mu\rangle$ and $|\nu\rangle$ represent excited determinants relative to the reference, $|0\rangle$. The computational expense (scales as $\mathcal{O}(N^6)$ for CCSD) and storage requirements for solving the Λ-amplitude equations are similar to those of the T-amplitude equations.

The $\hat{X}_\omega^A$ operators in eqn. 1.85 are perturbed wave function amplitudes that must be solved iteratively through a set of coupled-linear equations, much like the Λ-amplitude equations:

$$\sum_{\mu} \langle \mu|(\bar{H} - \omega)|\nu\rangle\langle\nu|X_\omega^A|0\rangle + \langle\mu|\bar{A}|0\rangle = 0 \tag{1.88}$$

were ω is the frequency of the perturbation applied to the system. It is important to note that there is a different set of perturbed amplitude equations that must be solved for each

perturbation applied to the system. For example, calculating the optical rotation at a single frequency may require upwards of 12 different sets of perturbed amplitudes (*i.e.* eqn. 1.88 must be solved 12 times).

As is always the case in quantum chemistry, there is more than one way to skin Schrödinger's cat. Frequency independent response-type properties, such as static polarizabilities, can be calculated using a second-order energy derivative with respect to the perturbation of interest.[37] In the static limit of linear-response theory (*i.e.* when $\omega = 0$) the two approaches will yield the exact same result. However, the linear response approach offers a much more robust solution that is easily extendable to response-type properties which require frequency dependence, such as optical rotation.

Polarizability

The quantity of interest when performing polarizability calculations is the electric dipole-polarizability tensor, *e.g.*

$$\alpha_{xy}(\omega) = \frac{2}{\hbar} \sum_{n \neq 0} \frac{\omega_{n0} \langle 0|\mu_x|n\rangle \langle n|\mu_y|0\rangle}{\omega_{n0}^2 - \omega^2} \tag{1.89}$$

where the summation runs over all electronically excited states, ψ_n, each with an excitation energy of ω_{n0}. The value of α_{xy} is directly related to the value of the coupled-cluster linear-response function by

$$\alpha_{xy}(\omega) \equiv -\langle\langle \mu_x; \mu_y \rangle\rangle_\omega \tag{1.90}$$

which completely eliminates the costly sum over states approach of eqn. 1.89.

Comparing eqn. 1.90 to the general linear response function in eqn. 1.85, it is clear that both $\hat{A}$ and $\hat{B}$ operators have been set to components of the electric dipole moment operator, $\vec{\mu}$, defined as

$$\vec{\mu} = \sum_k q_k \vec{r}_k \tag{1.91}$$

The general coupled-cluster linear-response function of eqn. 1.85 can be rewritten more specifically for the calculation of static and frequency dependent polarizabilities as

$$\langle\langle\vec{\mu};\vec{\mu}\rangle\rangle = \frac{1}{2}\hat{C}\hat{P}\left(\hat{\mu},\hat{\mu}\right)\left[\langle 0|\hat{\Lambda}\left[\bar{\mu},\hat{X}^{\mu}\right]|0\rangle + \frac{1}{2}\langle 0|\hat{\Lambda}\left[\left[\bar{H},\hat{X}^{\mu}\right],\hat{X}^{\mu}\right]|0\rangle\right] \tag{1.92}$$

and

$$\langle\langle\vec{\mu};\vec{\mu}\rangle\rangle = \frac{1}{2}\hat{C}^{\pm\omega}\hat{P}\left(\hat{\mu}(-\omega),\hat{\mu}(\omega)\right)\left[\langle 0|\hat{\Lambda}\left[\bar{\mu},\hat{X}^{\mu}_{\omega}\right]|0\rangle + \frac{1}{2}\langle 0|\hat{\Lambda}\left[\left[\bar{H},\hat{X}^{\mu}_{\omega}\right],\hat{X}^{\mu}_{-\omega}\right]|0\rangle\right], \tag{1.93}$$

respectively. Performing a coupled-cluster static polarizability calculation ($\omega = 0$) would require only three sets of perturbed wave function amplitudes, one for each component of the electric dipole moment operator, $\vec{\mu}$. Computing a dynamic, frequency-dependent, polarizability calculation requires six sets of perturbed wave function amplitudes, one for each coordinate of $\vec{\mu}$ for both positive and negative frequencies of ω. Recall, each set of perturbed wave function amplitudes requires approximately the same computational expense and resources as the ground state T-amplitude equations resulting in a potentially very expensive calculation.

Optical Rotation

Similar to polarizabilities, the calculation of optical rotation is based on the β tensor developed by Rosenfeld[38] and defined as, *e.g.*

$$\beta_{xy}(\omega) = \frac{c}{3\pi h}\mathrm{Im}\sum_{n\neq 0}\frac{\omega\langle 0|\mu_x|n\rangle\langle n|m_y|0\rangle}{\omega_{n0}^2 - \omega^2}, \tag{1.94}$$

where the second integral in the numerator employs the magnetic dipole operator,

$$\vec{m} = \sum_k \frac{q_k}{2m_k}\vec{r}_k \times \vec{p}_k. \tag{1.95}$$

The β tensor is related to the coupled-cluster linear-response function by

$$\beta_{xy} \equiv -\mathrm{Im}\langle\langle\mu_x;m_y\rangle\rangle_{\omega}. \tag{1.96}$$

Again, avoiding the very costly sum over states approach implied by eqn. 1.94.

Averaging over all molecular orientations and relating the β tensor to the specific rotation, $[\alpha]_\omega$, leads to the following expression

$$[\alpha]_\omega = \frac{(72.0 \times 10^6)\hbar^2 N_A \omega}{c^2 m_e^2 M} \times \left[\frac{1}{3}\mathrm{Tr}(\beta)\right], \tag{1.97}$$

where the notation $\mathrm{Tr}(\beta)$ denotes the trace of β (summation of the diagonal components), N_A is Avogadro's number, c is the speed of light ($\frac{m}{s}$), m_e is the mass of an electron at rest (kg), and M is the molecular mass (amu).

Computing optical rotation is more demanding than even dynamic polarizabilities due to the use of both electric and magnetic dipole moment operators. For polarizabilities only μ_x, μ_y and μ_z perturbed wave function amplitudes are required. Calculating optical rotation also requires the sets of m_x, m_y and m_z perturbed wave function amplitudes. Also, since there is no such thing as a zero field frequency optical rotation, all calculations concerning optical rotation are performed at $\omega \neq 0$ require positive and negative variants for each of the perturbations. This result in a total of 12 perturbed wave function amplitudes that must be solved, each nearly as costly as the ground state T-amplitude equations. Calculating optical rotation at the coupled-cluster level of theory can be an extremely computationally demanding endeavor.

1.6 Conclusions

"Are coupled-cluster calculations of response-type properties worth the expense?" There are many sources in literature which compare the performance of coupled-cluster level optical rotation to other methods, such as density functional (DFT)[39–43] and Hartree-Fock[40] methods. Coupled-cluster level optical rotations usually agree with comparable experiments much more closely than DFT or Hartree-Fock,[40–43] especially when vibrational effects are taken into account.[44,45]

Unfortunately, the level of accuracy associated with coupled-cluster theory has come at the

expense of computational resources. DFT has similar computational demands to Hartree-Fock theory, scaling as $O(N^3)$ formally, but through recent developments, able to achieve linear scaling.[46–49] The ability to maintain the high accuracy of coupled-cluster calculations at a competitive resource expense of DFT or Hartree-Fock may be realized though the local correlation concepts pioneered by Saebø and Pulay.[50,51] The topic of local correlation as a means to reduce the scaling of coupled-cluster calculation will be the topic of the next chapter.

Chapter 2

Introduction to Local Correlation

2.1 Why Local Correlation

Hyper-accurate quantum chemical techniques, like coupled cluster theory, suffer from high-degree polynomial scaling. For example, CCSD scales as $\mathcal{O}(N^6)$, where N is some measure of system size. This means that if the system doubles in size the calculation will take, not twice as long, but approximately 64-times as long.

This high-degree scaling wall is due, in part, to the use of canonical orbitals. The delocalized nature of canonical MOs lead to an inability to truncate the wave function within a given excitation class. For example, the set of doubles included in CCSD must be included in its entirety, without truncation. There is no proven *a priori* method to detect and discard negligible configurations. By contrast, a set of localized occupied and virtual MOs would provide a spatial criterion to predict insignificant parts of the wave function and ultimately reduce the number of wave function parameters that need to be calculated.

There have been many attempts to reduce the high-degree polynomial scaling wall associated with correlation-including methods. Head-Gordon *et al.* have developed a dual-projection technique where the occupied space is projected against the virtual space and *vice versa*.[52–55]

Flocke and Bartlett have based their reduced-scaling method on natural bond orbitals which allow the occupied-virtual blocks of the Fock matrix to be non-zero.[56,57] The main drawback of the Flocke and Bartlett procedure is that the Hartree-Fock reference has been destroyed.

We have chosen to use the local correlation procedure pioneered by Saebø and Pulay[50,51,58–62] who demonstrated that localized orbitals are attainable by abandoning the canonical orbital formulation and employing separate localization schemes for the occupied and virtual spaces. Within this framework, there is a spatial criterion to discriminate and neglect insignificant pieces of the wave function. The local correlation method of Saebø and Pulay was first implemented in configuration-interaction theory[50,51] then later applied to many-body perturbation theory,[58–61] and extended to coupled-cluster theory for ground[63,64] and excited[65,66] states, as well as coupled-cluster response theory for static[67] and dynamic[68] polarizability. The current state-of-the-art in large scale calculation of ground state energies was performed by Schütz and Manby on 16 glycine molecules in only a few hours on a modern high performance workstation.[69]

2.2 Orbital Localization

A prerequisite of local correlation is a set of localized occupied and virtual orbitals. Occupied and virtual orbital subspaces are localized by two very different procedures. The reason for this is due to the inability to achieve sufficiently localized orbitals by one procedure and maintain the Hartree-Fock condition (eqn. 1.14).

Localizing the Occupied Space

Several methods have been proposed to localize occupied orbitals, including, Boys,[70,71] Edmiston-Ruedenberg[72,73] and Pipek-Mezey.[74] While we do not wish to spend much time discussing the localization of occupied MOs, it is helpful to mention the merits and shortcomings of each of these methods. All the procedures mentioned here require solving the

Hartree-Fock equations in a canonical basis followed by localization that does not destroy the Hartree-Fock condition.

The Boys localization procedure scales as $\mathcal{O}(N^3)$, which makes it a relatively fast procedure. The Boys procedure attempts to maximize the distance between orbital centers. Boys localization can have difficulty converging and often breaks symmetry as discussed by Boughton and Pulay.[75] Localized Boys orbitals cannot maintain π and σ symmetry separation of a double bond. The two bonds will mix to form a pair of "τ" or "banana" bonds.[75]

Edmiston-Ruedenberg (ER) localization seeks to maximize the orbital self-repulsion energies. ER localized orbitals are able to maintain σ-π separation and do not suffer from an inability to converge. The main drawback of the ER procedure is that it must be performed in the MO basis and therefore scales as $\mathcal{O}(N^5)$.

Pipek-Mezey (PM) localization offers the best of both worlds, so to speak. The scaling of the PM procedure is only $O(N^3)$ and it is able to maintain π and σ separation of double bonds. The localization criterion for the PM procedure is to minimize the number of atoms each orbital is associated with by maximizing electronic charge on as few atoms as possible.

Due to the merits and very few drawbacks of PM localization, we have chosen to use PM localized orbitals for all local-correlation calculations performed here. Also, work by Boughton and Pulay[75] suggest the localization procedure of the occupied space has little effect on the final local correlation calculation.

Localizing the Virtual Space

As mentioned above, the virtual space is localized by a completely different procedure than the occupied space due to the fact that similar methods to those used for the occupied space do not work for the virtual space.[50] Instead, the virtual space is restricted to a subset of the atomic orbital basis functions projected against the occupied MO space.[50,51] This is handled

by a projection operator as

$$|\tilde{\phi}_\mu\rangle = \left(1 - \sum_i^m |\psi_i\rangle\langle\psi_i|\right)|\phi_\mu\rangle = \sum_i^N |\phi_\nu\rangle \tilde{R}_{\nu\mu} \tag{2.1}$$

where quantities in the PAO (projected AO) basis are represented with a tilde and the $\tilde{\mathbf{R}}$ matrix defines a transformation between the AO basis and the PAO basis. Through algebraic manipulation we can elucidate the form of the transformation matrix as

$$\tilde{\mathbf{R}} = \mathbf{1} - \mathbf{DS}, \tag{2.2}$$

where $\mathbf{D}$ is "half" the usual Hartree-Fock density matrix,

$$D_{\mu\nu} = \sum_i C_\mu^i C_\nu^i, \tag{2.3}$$

and $\mathbf{S}$ is the overlap matrix in the AO basis,

$$S_{\mu\nu} = \langle\phi_\mu|\phi_\nu\rangle. \tag{2.4}$$

The PAO basis, $\{\tilde{\phi}_\mu\}$, defines our correlation space. Unfortunately, this PAO basis is an over-determined space compared to the original virtual MOs and therefore contains redundancies that must be dealt with to eliminate the m zero eigenvalues.

2.3 Local Truncation

Once localized MOs are obtained for the occupied and virtual spaces, the next step is to truncate the correlation space associated with each T-amplitude. For the case of CCSD or CC2 (CC2 is an $O(N^5)$ approximation to CCSD), a subset of the PAO space must be defined as the excitation space for each single and double excitation. The set of PAOs assigned to each occupied orbital is called its domain. If we choose not to truncate orbital domains, the calculated correlation energy will be identical to the canonical result. This provides a route to the "correct" correlation energy. If we wish to reduce the localization error in a calculation we can simply increase the orbital domains. The trade off for more accurate correlation energies is the increased cost of the calculation.

2.3.1 Singles Domains

The most common way of defining orbital domains was proposed by Boughton and Pulay,[75] referred to as the Boughton-Pulay completeness check defined by

$$f(\mathbf{R}') = \min\left\{\int(\psi_i - \psi_i')^2 d\tau\right\} = 1 - \sum_{\mu\in[i]}\sum_{\nu} C_\mu'^i S_{\mu\nu} C_\nu^i \tag{2.5}$$

where ψ_i' is an approximate occupied orbital comprised of the current orbital domain for $[i]$ and the MO coefficients, $C_\mu'^i$, are solved separately for each occupied orbital. We will refer to domains defined by the above equation as BP domains. Typically, a cutoff value of 0.02 for $f(\mathbf{R}')$ is sufficient to retain upwards of 98% of the correlation energy.[63,75] Basis functions are added atom-wise to the domain of $[i]$ until the criterion is satisfied. Since AOs (and PAOs) are added to the domain by atom, domains can be discussed in terms of atoms instead of individual AOs (or PAOs).

The set of AOs used to satisfy eqn. 2.5 for occupied orbital ψ_i defines the single excitation space for that particular occupied orbital after the set of AOs, $\{\phi_\mu\}$, has been transformed to the PAO basis, $\{\tilde{\phi}_\mu\}$, by eqn. 2.1. For example, single excitations from occupied orbital ψ_i into the canonical virtual space can be written as

$$\hat{t}_i = \sum_a t_i^a \{a_a^\dagger a_i\} \tag{2.6}$$

Using the definition of the virtual space defined earlier, eqn. 2.6 can be rewritten as

$$\hat{t}_i = \sum_{\tilde{\mu}} t_i^{\tilde{\mu}} \{a_{\tilde{\mu}}^\dagger a_i\} \tag{2.7}$$

where $\tilde{\mu}$ is an orbital in the PAO basis; specifically, only the Φ_μ's required to satisfy eqn. 2.5 are used in eqn. 2.7. Thus, only a subset of the full PAO basis, $\{\tilde{\phi}_\mu\}$, is used, resulting in fewer T_1-amplitudes that need to be calculated. In this sense, eqn. 2.5 defines the singles domains.

2.3.2 Pair Domains

Double excitations within canonical coupled-cluster theory are defined as

$$\hat{t}_{ij} = \frac{1}{2}\sum_{ab} t_{ij}^{ab}\{a_a^\dagger a_b^\dagger a_j a_i\}. \tag{2.8}$$

It is necessary to define pair (or doubles) domains for each ij pair. There are a number of ways to handle each ij pair depending on the distance, or bond connectivity, between each occupied orbital, ψ_i and ψ_j, setting up a hierarchy of importance. If the single domains of ψ_i and ψ_j have an atom in common we can call that particular ij pair a strong pair and treat them explicitly within the method we are using. The domain for a strong ij pair is taken to be the union of the individual domains for orbital i and j (*i.e.* $[ij] = [i] \cup [j]$).

Suppose ψ_i and ψ_j are separated by only one bond, about one a_0. The effect of this particular ij pair would not be as important as the strong pair described above. Occupied orbitals separated by one bond may be defined as the set of weak pairs. Further separation of orbitals ψ_i and ψ_j by two or more bonds can be used to define distant pairs and so forth.

Setting up the hierarchy of importance within the double excitation space allows different pairs to be calculated by various levels of theory. For example, suppose local correlation is being implemented within CCSD, all strong pairs can be treated explicitly by CCSD. Since the weak pairs are not as important as the strong pairs, they can be treated with a lower, and less expensive, level of theory, such as MP2 or CC2. Distant pairs can be completely ignored or treated by a multipole expansion.[76] Using a hierarchical method of pairs and levels of theory can greatly decrease computational time and resources while maintaining accurate energies compared to the canonical analogue.[64,77]

2.3.3 Local Domains for Response Calculations

One of the main questions that must be answered concerning local correlation calculations for the determination of response-type properties is, "How does an applied perturbation affect

the localizability, and ultimately the domains, of a molecular system?" The Boughton-Pulay completeness check described by eqn. 2.5 does not take into account the perturbation applied to the system for a response-type property calculation. Instead, we propose using solutions to the CPHF (coupled-perturbed Hartree-Fock) equations[11] to augment the BP domains.

Calculating polarizability within the context of Hartree-Fock theory requires solution of the CPHF equations. Solutions to the CPHF equations define the response of the orbitals themselves to the applied perturbation. Looking at polarizability, for example, a single component of the dipole polarizability tensor (*e.g.* α_{xy}) is determined by

$$\alpha_{xy} = \sum_i \sum_a U_{ai}^x \mu_{ai}^y, \tag{2.9}$$

where the U_{ai}^x are the solutions to the CPHF equations, and μ_{ai} are electric dipole integrals. The summation over virtual orbitals may be 'back-transformed' into the AO basis to yield

$$\alpha_{xy} = \sum_i \sum_\rho U_{\rho i}^x \mu_{\rho i}^y \tag{2.10}$$

where ρ denotes an AO basis function. Further decomposing eqn. 2.10 into atomic contributions per occupied orbital gives

$$\alpha_{xy}^{iA} = \sum_{\rho \in A} U_{\rho i}^x \mu_{\rho i}^y \tag{2.11}$$

where the summation over ρ includes only those basis functions centered on atom A.

Using eqn. 2.11 along with a certain cutoff criterion would be a mistake due to the fact that individual contributions from each AO can be either positive or negative, resulting in artifactually small domains. Instead, we choose to employ absolute values of individual AO contributions, leading to a completeness check similar in spirit to the original Boughton-Pulay criterion

$$\epsilon_{xy}^i = \sum_\rho \left| U_{\rho i}^x \mu_{\rho i}^y \right| - \sum_{\rho \in [i]} \left| U_{\rho i}^x \mu_{\rho i}^y \right|, \tag{2.12}$$

where the notation ($\rho \in [i]$) appearing in the summation of eqn. 2.12 indicates that only the AOs within the current estimated domain of orbital ψ_i are used.

The importance of this approach is that the domain selection now takes into account the perturbation that has been applied to the system. Recall from Table 1.1 that optical rotation is the summation of an electric and magnetic dipole perturbation. Including the effects of both these perturbations requires solving the CPHF equations twice, once for the electric dipole operator and once for the magnetic dipole moment operator. The domains used for an optical rotation calculation are taken to be the union of the CPHF-based domains from each perturbation.

2.4 Conclusions

One potential shortcoming of the local correlation method revealed in this chapter is the dependence of the domain structure on the geometric framework. In other words, the automatic domain selection of the BP completeness check can alter throughout the plot of a potential energy surface (PES). Such a change in the domain structure will result in a discontinuity on the PES. Looking at something like a bond dissociation, it is important to understand where these discontinuities may occur in relation to the equilibrium structure, what types of bond dissociation will result in discontinuities and how large they are. These topics will be addressed in Chapter 3.

In order to perform response-type calculation on large molecular systems using coupled-cluster theory, it is of utmost importance to understand how an applied perturbation to the Hamiltonian affects the localizability of the wave function. Calculating a static polarizability is one of the least computationally demanding response calculations and is a good starting point to understand the effects imposed on local correlation calculations by a perturbed Hamiltonian. Chapter 4. Extension of the concepts learned from static polarizabilities will be carried over and expanded upon through the study of local optical rotation calculations as performed in Chapter 5.

Chapter 3

Potential Energy Surface Discontinuities

3.1 Introduction

The rigorous computation of the properties of large molecules is one of the great challenges to *ab initio* quantum chemistry. Although hyper-accurate theoretical predictions of various properties of small molecules are now commonplace, the polynomial scaling wall of the most reliable methods such as coupled cluster theory [*e.g.*, the $\mathcal{O}(N^7)$ scaling of the popular CCSD(T) method] has prevented their routine application to molecules containing more than around ten non-hydrogen atoms. One of the most promising approaches to overcoming the scaling problem is through "local correlation", which was pioneered by Pulay and Saebø.[50,62] This idea relies on the fact that electron correlation effects in molecular systems with large band-gaps (insulators) should decrease asymptotically with the interorbital dis-

tance as $1/r^6$. By choosing a well-localized form for the molecular orbitals that parametrize the determinantal wave function expansion, one may limit orbital excitations/substitutions to occupied-virtual pairs that are in close proximity. This approach thus reduces the number of independent wave function coefficients one must compute and store, and thus reduces the computational order of the method, perhaps even to linear scaling. The local correlation concept has been applied successfully to many-body perturbation theory[53–55,58,59,62,77–79] and coupled cluster theory,[56,57,63,64,69,80–83] including triples correction.[84–88] theories. We note the particularly impressive work by Schütz on chains of up to sixteen glycine molecules at the LCCSD level of theory.[83]

One of the criticisms leveled at the Pulay-Saebø local correlation concept, however, stems from its dependence upon geometry-specific localization criteria. Specifically, the Pulay-Saebø scheme assigns to each localized occupied molecular orbital (MO) a "domain," i.e. a group of atoms whose atomic orbital basis functions (projected onto the unoccupied subspace) serve as that MOs excitation space.[62] These domains commonly correspond to bonded atoms (e.g. the carbon and oxygen atom participating in a carbonyl π-bond), lone pairs, *etc.*, depending upon the choice of localization criteria for the occupied space. (The Pipek-Mezey charge maximization method is perhaps the most commonly used localization definition.[74]) Unfortunately, if the molecular structure changes significantly, as in a dissociation or isomerization reaction, for example, the orbital domain structures may change as well, potentially leading to discontinuities in the resulting potential energy surface (PES). The local correlation methods advocated by Scuseria and co-workers[79,80] and by Head-Gordon and co-workers[53–55,84] have been designed to use atom-based domain structures that are thus geometry-independent.[89,90] However, the question remains: do PES discontinuities occur in practical applications of the Pulay-Saebø-based local correlation methods, such as those developed by Werner, Schütz, and co-workers, and, if so, what significance do they have?

The purpose of this work is to investigate these questions using three prototypical systems: the homolytic cleavage of the C−F bond in fluoromethane, CH_3F, and the heterolytic cleavage of the methylene C−C bond in singlet ketene, CH_2CO, and propadienone, CH_2CCO.

We have chosen these examples in part because of their small size, but also because the dissociation processes can still be correctly described by single-reference correlation methods such as CCSD and MP2.

3.2 Theoretical Background

In the ground-state local correlation approach developed by Pulay and Saebø, the orbital domain structure noted above limits the excitations generated by the cluster/excitation operators in the construction of the determinantal wave function. In the most widely used implementations of the Pulay-Saebø scheme, the occupied orbitals are chosen to be the charge-maximized functions defined by Pipek and Mezey.[74] These orbitals are conveniently orthonormal and well-localized in most cases. In the Pulay-Saebø approach, the unoccupied orbitals are defined as the set of nucleus-centered atomic orbitals (AOs), orthogonalized against the occupied space, but non-orthogonal to each other. For a given localized occupied orbital, ϕ_i, its virtual domain is chosen as the set of *atoms* whose associated projected AOs contribute most strongly to the total population of ϕ_i. This choice is implemented in an algorithmic manner using the completeness criterion suggested by Boughton and Pulay:[75]

$$f_i(\mathbf{C}') = \min\left\{\int (\phi_i - \phi_i')^2 \, d\tau\right\} = 1 - \sum_{\mu\in[i]}\sum_{\nu} C_\mu'^{\,i} S_{\mu\nu} C_\nu^i, \tag{3.1}$$

where ϕ' is the approximation to ϕ_i for the chosen set of AOs, ϕ_μ, with associated MO coefficients, $C_\mu'^{\,i}$ and C_μ^i, respectively. Thus, the size (*i.e.* the number of atoms) in the domain of a given occupied orbital is dependent solely on the choice of cutoff of the function $f_i(\mathbf{C}')$. A value of 0.02 preserves bonded atoms in well-localized systems and is commonly used for ground-state local-MP2 and local-CCSD calculations.[63] With the Boughton-Pulay criterion, single excitations out of occupied orbital, ϕ_i, are allowed only into projected-AO functions associated with those atoms in the orbital's domain. Pairwise excitations from orbitals ϕ_i and ϕ_j are chosen as the union of the orbitals' single-excitation domains, with additional decomposition into "strong" and "weak" pairs to further reduce the scaling of the

method.[62,63]

One drawback to the Pulay-Saebø approach that has been pointed out in the literature[55,84] is the dependence of the orbital domain structure (and thus the excitation/Fock space on which the wave function is defined) on the molecular structure. If the geometry changes significantly across the PES, e.g. as bonds are broken and formed, the orbital domain structure may change abruptly and a concomitant discontinuity in the PES will appear. Thus, local correlation methods defined in this way cannot adhere to the widely accepted ideal of a "theoretical model chemistry", first defined by Pople.[91]

On the other hand, Pulay and Saebø have argued that the changing structure of the correlating space with molecular geometry should be considered a feature of their method. In particular, the local correlation approach may lead to a reduction in intermolecular basis-set superposition error (BSSE),[92,93] in which the local wave function on one fragment benefits from the presence of AO basis functions on another nearby fragment resulting in overestimation of the computed dimerization energy. BSSE can have a substantial effect on fragmentation energies (ca. 2 kcal/mol or more) and is often reduced using so-called counterpoise corrections.[94] However, as Pulay and Saebø have discussed, for weakly interacting fragments, their local correlation method limits the intramolecular correlation space of occupied orbitals on a given fragment to (projected) AOs on that same fragment, thus reducing the correlation contribution to the BSSE.[61] The same advantage is expected for the Head-Gordon and the Scuseria approaches.

In this work, we seek to answer two important questions: (1) Under what circumstances can PES discontinuities occur in local correlation methods based on the Pulay-Saebø approach? and (2) What are the magnitudes of these discontinuities for typical systems?

3.3 Computational Details

Canonical-MO and local-MO second-order perturbation theory (MP2)[31] and coupled cluster singles and doubles (CCSD) calculations[32,95] were carried out for fluoromethane, CH_3F, singlet ketene, CH_2CO, and propadienone, CH_2CCO, using the PSI3 quantum chemical program package.[96] The local-CCSD approach we have implemented is a "pilot" program that uses the canonical-MO code to simulate the local correlation treatment. This method was briefly described by Pulay and Saebø in one of their earlier local correlation papers,[59] and was used by Hampel and Werner in their seminal paper on local-CCSD[63] and by Crawford and King in a recent extension of these methods to excited states via the local-EOM-CCSD approach.[65] No distinction was made between weak and strong pairs in these calculations, i.e., all localized pair domains were treated explicitly in the local-CCSD calculations. Core orbitals were held frozen in all these calculations, and a Boughton-Pulay completeness cutoff of 0.02 was used throughout. The correlation-consistent polarized-valence double-zeta (cc-pVDZ) basis set developed by Dunning was used for all calculations reported here.[97]

3.4 Homolytic Bond Dissociation: Fluoromethane

Fig. 3.1 plots the conventional and localized MP2 and CCSD potential energy curves for breaking the C−F bond in fluoromethane, CH_3F, with all other geometric parameters fixed at their CCSD/cc-pVDZ optimized values. Although this dissociation involves homolytic bond cleavage, the bond in question nominally involves only two electrons. Therefore, the CCSD approach is still capable of providing a qualitatively reasonable potential curve, though CCSD significantly overestimates the well depth.[98] On the other hand, the MP2 curve [as well as curves from perturbative methods such as CCSD(T)] will exhibit a characteristic "turnover" at long distances due to the narrowing of the HOMO-LUMO gap; the early stages of this phenomenon are already visible in the figure near $r(\mathrm{C{-}F) = 3.75}$ Å.

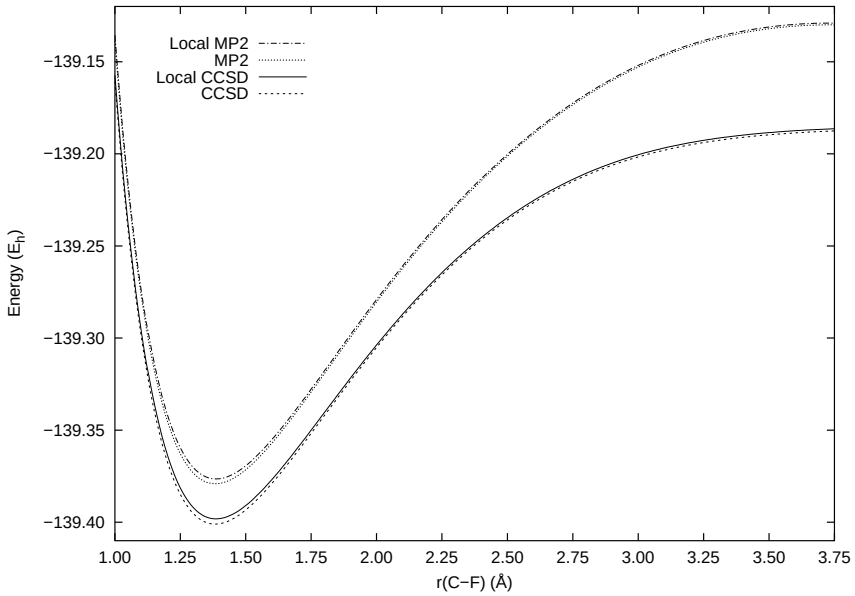

Figure 3.1: Canonical- and local-MO MP2 and CCSD potential energy curves (using the cc-pVDZ basis set) for the dissociation of the C−F bond in CH_3F.

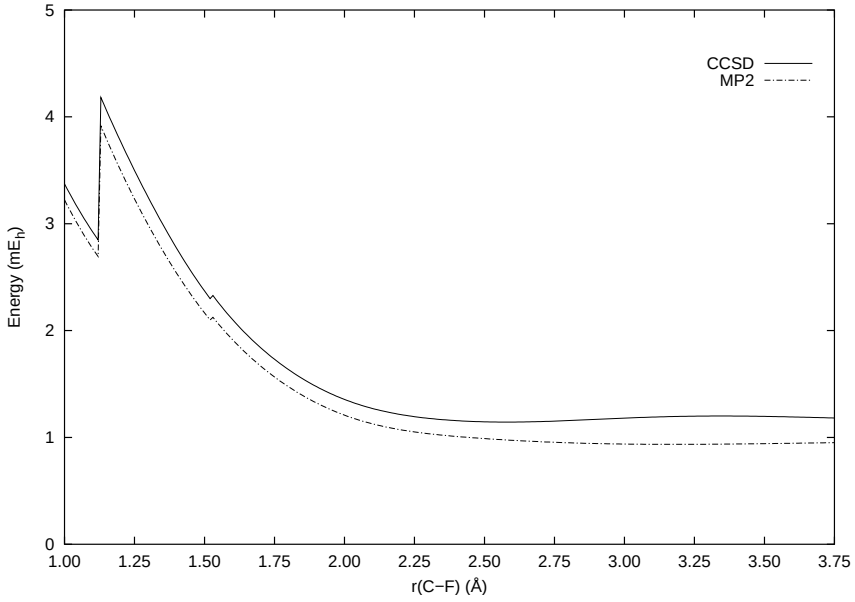

Figure 3.2: LMP2 and LCCSD localization errors (in mE_h) for dissociation of the C−F bond in CH_3F. The inner discontinuity corresponds to expansion of a fluorine lone-pair orbital domain for short bond lengths.

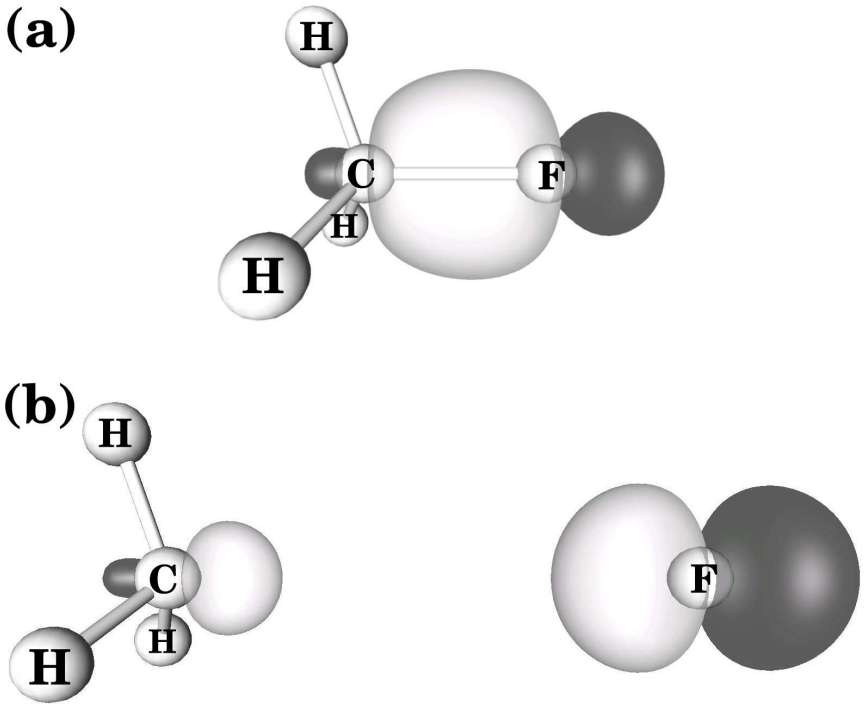

Figure 3.3: Contour plots of the Pipek-Mezey localized C−F bonding orbital of CH_3F (a) near the equilibrium geometry and (b) at dissociation.

The most striking feature of Fig. 3.1 is that there is clearly *no discontinuity* in either the LMP2 or the LCCSD energy in the bond-breaking region of the potential energy curve, indicating that the orbital domain structure remains constant for long C−F distances. (A discontinuity of about 1.0 mE_h occurs at very short C−F distances — less than 1.25 Å — due to expansion of the domain of a fluorine lone pair to include the carbon atom, as is visible in Fig. 3.2.) We emphasize that this lack of discontinuity in the dissociation region of the curve is not the result of user-defined constraints on the orbital domains, but instead stems naturally from the inability of the Pipek-Mezey scheme to truly localize the C−F "bonding" MO. Fig. 3.3 illustrates this point: near equilibrium and at dissociation the Pipek-Mezey localized C−F bonding MO clearly involves AOs on both fragments, CH_3 and F. That is, since the electrons in this MO are singlet-coupled and only occupied-orbital mixings are allowed, no charge-localization can occur, and the MO remains delocalized.

We may therefore conclude from these results that for *homolytic* bond-breaking, the Pulay-Saebø local-correlation approach will not necessarily lead to discontinuous potential energy surfaces, due to the natural (and appropriate) inability of orbital localization methods such as Pipek-Mezey to separate singlet-coupled charges on distant fragments. We also note that the coupled cluster method [as well as any correlation approach based on a spin-restricted Hartree-Fock (RHF) wave function] is not size-consistent for this type of bond-breaking process.

3.5 Heterolytic Bond Dissociation: Singlet Ketene

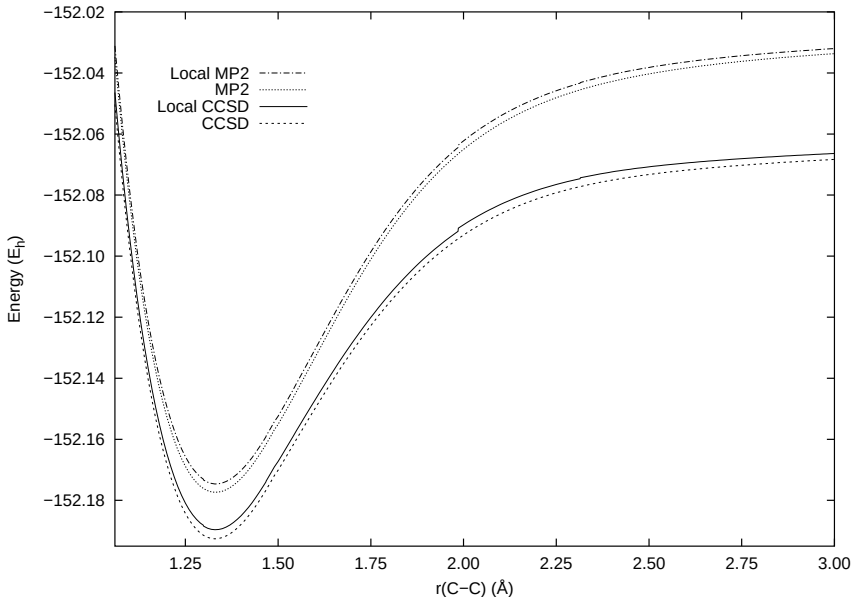

Figure 3.4: Canonical- and local-MO MP2 and CCSD potential energy curves (using the cc-pVDZ basis set) for the dissociation of the C−C bond in singlet ketene, CH_2CO. The structure was reoptimized at the CCSD/cc-pVDZ level of theory for each value of the C−C bond distance.

Given the above observation of a lack of PES discontinuity for homolytic bond cleavage in the LMP2 and LCCSD methods, we then chose to examine the effect of *heterolytic* bond cleavage on the orbital domain structure. The C−C double bond in singlet ketene, CH_2CO, provides

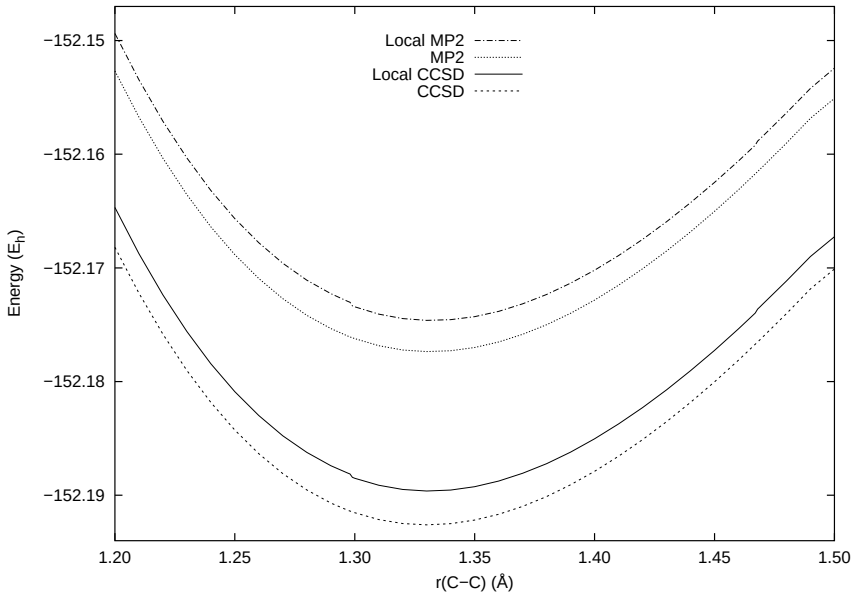

Figure 3.5: Closeup of the singlet ketene curves shown in Fig. 3.4 focused on the near-equilibrium "rearrangement" discontinuities described in the text.

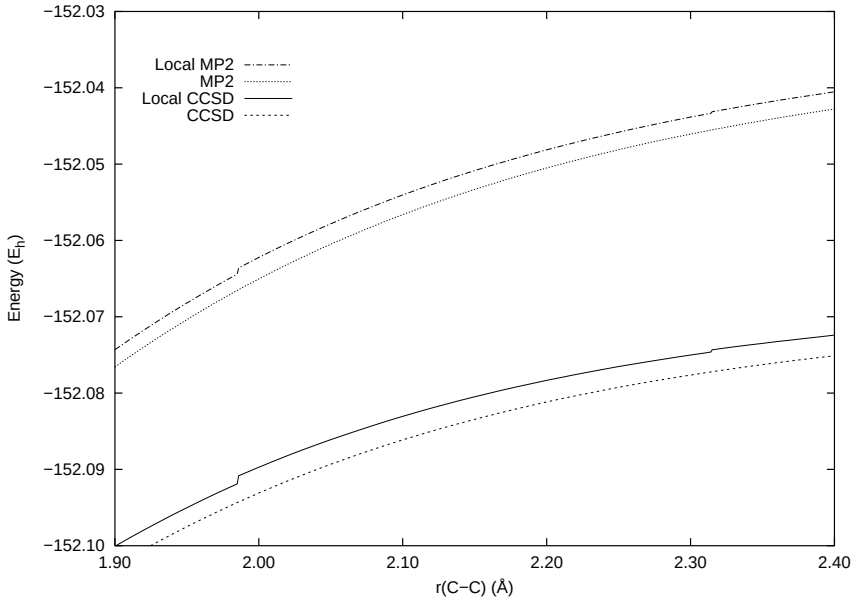

Figure 3.6: Closeup view of the singlet ketene curves shown in Fig. 3.4 focused on the outer π and σ bond-breaking discontinuities described in the text.

a useful example of this type of dissociation process. This species and its triplet counterpart have been extensively scrutinized both experimentally and theoretically to test the RRKM

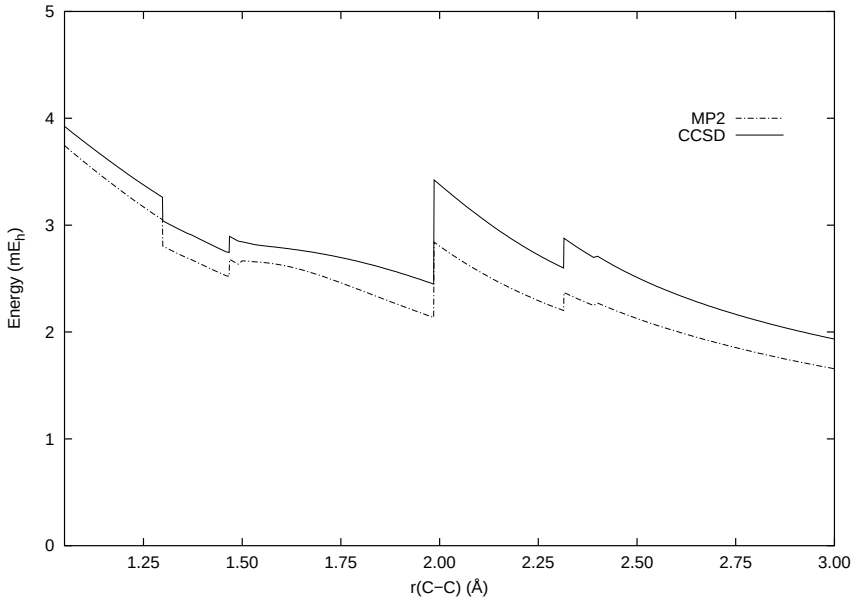

Figure 3.7: LMP2 and LCCSD localization errors (in mE_h) for singlet ketene dissociation, where the four discontinuities discussed in the text are clearly visible.

behavior of the rate constant for dissociation.[99–104] It is well known that the lowest singlet surface (i.e. dissociation to singlet methylene and carbon monoxide) proceeds through a C_s-symmetry structure, sometimes referred to in the literature as the C_s^{I} pathway.[99,105] We have followed this lowest-energy coordinate to ketene dissociation by computing the optimized CCSD/cc-pVDZ structure for different values of the C−C bond distance. At equilibrium the structure has C_{2v} symmetry, but falls to C_s symmetry as the C=C=O moiety bends up and out of the plane of the molecule near a r(C−C) bond distance of around 1.49 Å.

Figs. 3.4, 3.5, and 3.6 plot the conventional and local MP2 and CCSD potential energy curves for breaking the ketene C−C double bond. Unlike the CH_3F curve, the ketene PES exhibits a total of four discontinuities: two near the equilibrium geometry at ca. 1.298 and 1.467 and two in the dissociation regime at 1.985 and 2.314 Å. These discontinuities are better emphasized by plotting the localization error (i.e., the difference between the canonical and local energies), as shown in Fig. (3.7). The two inner discontinuities stem from changes in the valence-MO domain structures involving the C=C=O chain, while the two outer

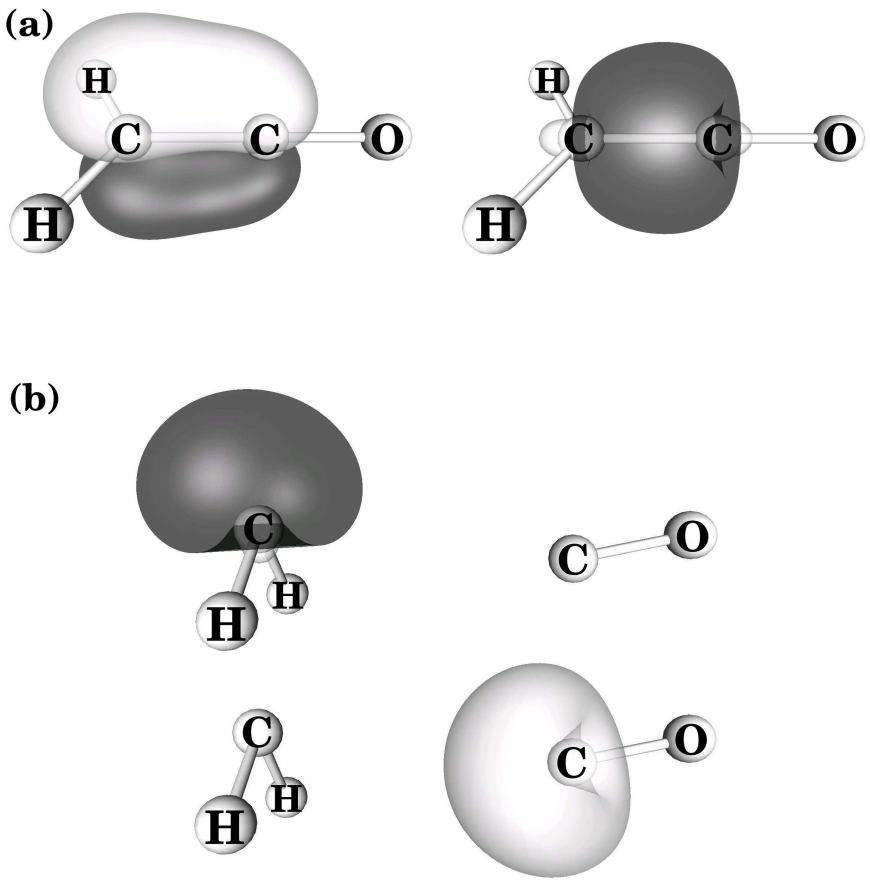

Figure 3.8: Contour plots of the relevant Pipek-Mezey localized orbitals for singlet ketene: (a) The π and σ bonding orbitals of near the equilibrium geometry; (b) the corresponding lone-pair dissociated MOs of singlet methylene and carbon monoxide.

discontinuities result from the bond breaking: the cleavage occurs heterolytically, with the part of the $\sigma - \pi$ double bond following the CO fragment and the remaining component following the methylene fragment. The two outer discontinuities appear separately in the curve because the corresponding orbital domain structures change at different points. This process is illustrated in Fig. 3.8, which plot contour surfaces of the relevant σ and π Pipek-Mezey localized orbitals near equilibrium and at dissociation.

As shown in Fig. 3.7 and in Table 3.1, the inner LCCSD discontinuities are small, 0.1-0.2

Table 3.1: Estimates of the sizes of the two LMP2 and LCCSD discontinuities on the dissociation surface of singlet ketene. Localization errors (ΔE) are computed as the difference between the canonical-MO and local-MO methods at the given value of r(C−C). The discontinuity size is estimated as the difference between the two errors at values of r(C−C) on either side of the orbital-domain shift. Total energies are given in E_h and energy differences in mE_h.

	MP2			CCSD		
	Correlation Energy			Correlation Energy		
r(C−C)	Canonical	Local	ΔE	Canonical	Local	ΔE
1.298	-0.437156	-0.434105	3.051	-0.452480	-0.449219	3.261
1.299	-0.437208	-0.434404	2.804	-0.452529	-0.449490	3.039
Discontinuity	—	—	-0.247	—	—	-0.222
1.467	-0.445013	-0.442492	2.521	-0.460006	-0.457261	2.745
1.468	-0.445049	-0.442370	2.679	-0.460042	-0.457147	2.895
Discontinuity	—	—	0.158	—	—	0.150
1.985	-0.422345	-0.420210	2.135	-0.450137	-0.447689	2.449
1.986	-0.422290	-0.419450	2.841	-0.450101	-0.446678	3.423
Discontinuity	—	—	0.706	—	—	0.974
2.314	-0.409867	-0.407666	2.201	-0.441556	-0.438958	2.598
2.315	-0.409843	-0.407474	2.369	-0.441540	-0.438662	2.878
Discontinuity	—	—	0.168	—	—	0.280

mE_h, while the outer ones are larger at 0.3-1.0 mE_h, of the same order of magnitude as the localization error (i.e., the difference in the canonical and local CCSD energies). The source of this difference is related to the structure of the orbital domains and the orbital energies. The inner discontinuities stem from rearrangements in the orbital domain structure of the localized HOMO-1, which is a bonding MO on the carbon monoxide; for r(C=C) value less

than 1.298 Å and greater than 1.468 Å, the domain of this MO is limited to projected AOs on the CO moiety, but in between these values the domain includes AOs on the methylene carbon. These changes result naturally from the Boughton-Pulay criterion in eqn. (3.1). The outer discontinuities, on the other hand, corresponding to actual bond breaking, with the skip at 1.985 Å corresponding essentially to breaking of the π component of the C−C double bond and the skip at 2.314 Å to breaking of the σ component. The former discontinuity is larger because it involves the HOMO, while the latter orbital is significantly lower in energy.

3.6 Heterolytic Bond Dissociation: Propadienone

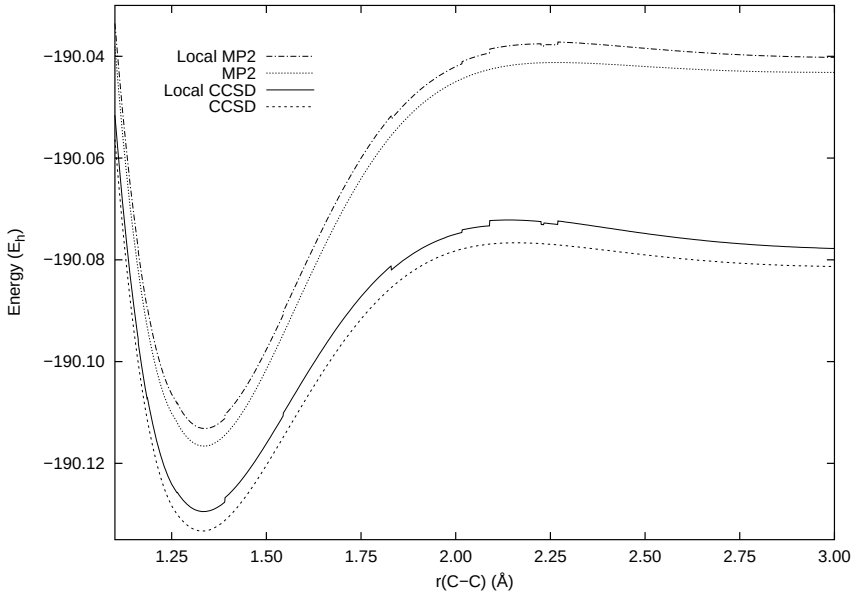

Figure 3.9: Canonical- and local-MO MP2 and CCSD potential energy curves (using the cc-pVDZ basis set) for the dissociation of the central C−C bond in singlet propadienone, CH_2CCO. The structure was reoptimized at the CCSD/cc-pVDZ level of theory for each value of the C−C bond distance.

As a second test of discontinuities arising in heterolytic bond cleavage, we considered singlet propadienone, CH_2CCO, which is clearly related to ketene, but whose electronic structure is somewhat more complicated by increased conjugation. Unlike ketene, propadienone has C_s

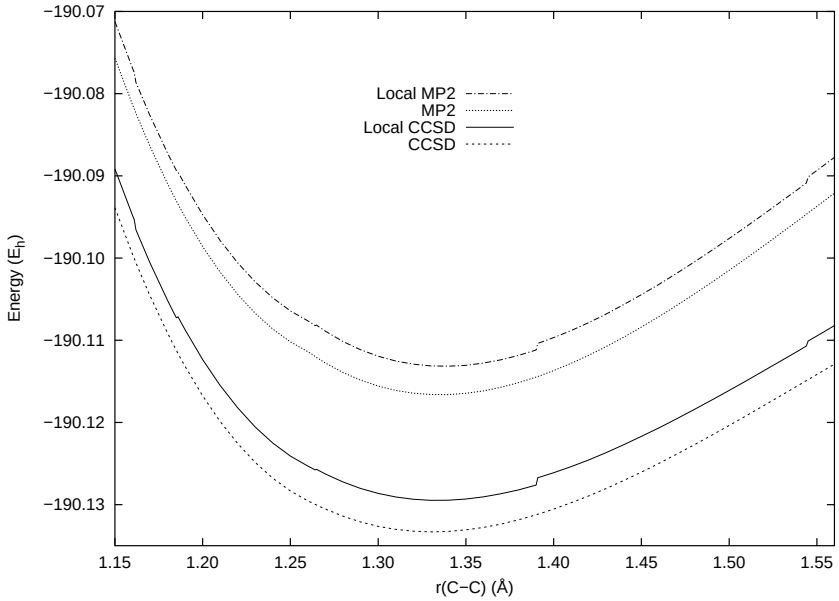

Figure 3.10: Closeup of the singlet propadienone curves shown in Fig. 3.9 focused on the near-equilibrium "rearrangement" discontinuities described in the text.

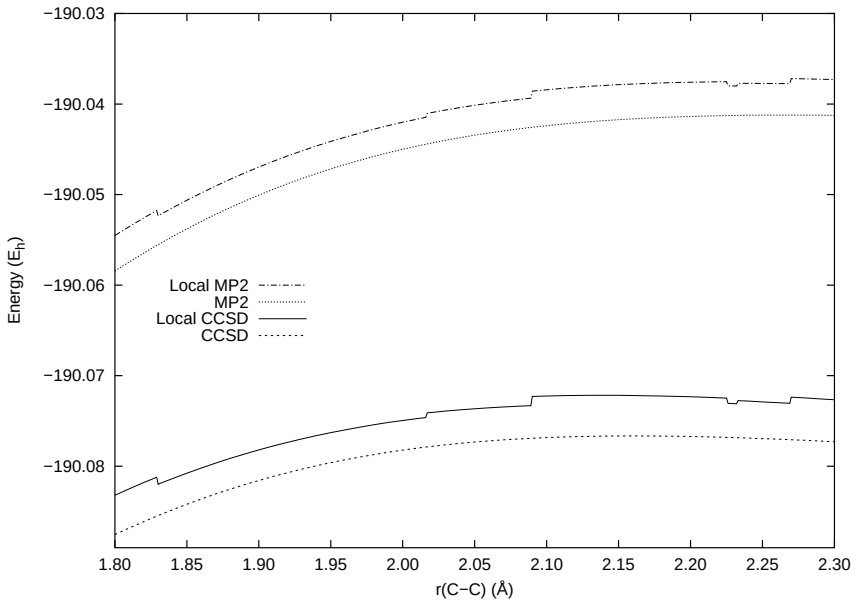

Figure 3.11: Closeup of the singlet propadienone curves shown in Fig. 3.9 focused on the bond-breaking region described in the text.

symmetry at equilibrium (r(C−C) = 1.34 Å), with a "kink" in its cumulenic chain discussed previously by East.[106] At very short C−C bond distances (ca. 1.26 Å) the propadienone

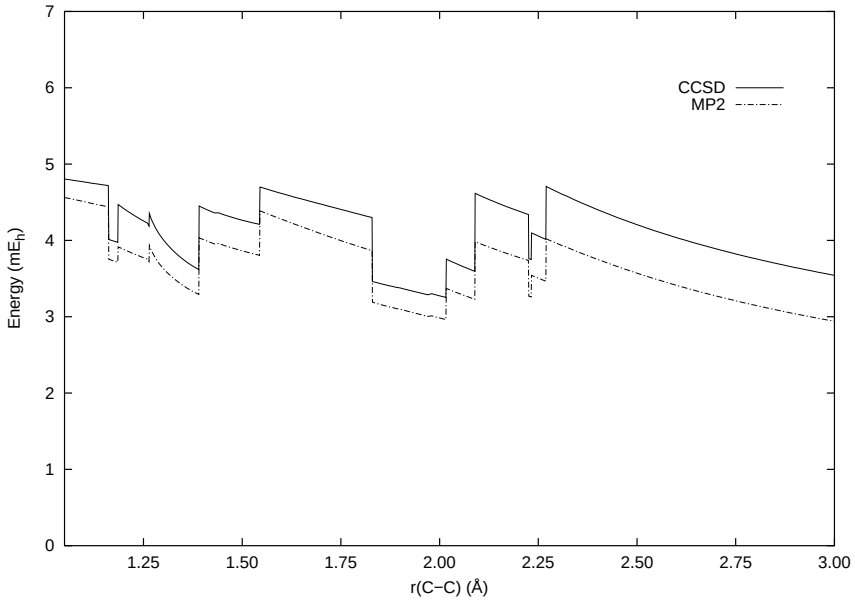

Figure 3.12: LMP2 and LCCSD localization errors (in mE_h) for singlet propadienone dissociation, where the ten discontinuities discussed in the text are more clearly visible.

structure has C_{2v} symmetry. As in the ketene case, we have chosen to follow the minimum-energy dissociation path by computing the CCSD/cc-pVDZ optimized structure at each value of the C−C distance leading to carbon monoxide and the lowest singlet state of vinylidene.

Figs. 3.9, 3.10 and 3.11 plot the conventional and local MP2 and CCSD potential energy curves for breaking the central C−C bond of propadienone. In this case, the curve exhibits a total of ten discontinuities, including five near the equilibrium geometry at 1.161, 1.185, 1.264, 1.390, and 1.544 Å, ranging in size from 0.1 to 0.8 mE_h, and five in the bond breaking region at 1.829, 2.089, 2.225, 2.232, and 2.269 Å, ranging from 0.3 to 1.0 mE_h, again on the same order as the localization error. As is evident from Fig. 3.12, which plots the localization error as a function of the central C−C distance, several of the discontinuities correspond to shifts back-and-forth in the orbital domain structures leading to a "jagged," unphysical appearance to the PES.

3.7 Conclusions

We have examined the occurrence of discontinuities in the potential energy surfaces given by the LMP2 and LCCSD local correlation methods based on the orbital domain approach of Pulay and Saebø. We find that for "pure" homolytic bond cleavage, as illustrated by breaking the C−F bond in fluoromethane, no such discontinuities appear due to the natural tendency of the Pipek-Mezey localized orbitals to remain delocalized between the separating fragments. On the other hand, for heterolytic bond cleavage and for shifts in the the bond structure of conjugated systems, multiple discontinuities can occur, even in the vicinity of the equilibrium geometry, far from the bond-breaking regime. These discontinuities are usually small, but can often be of the same magnitude as the localization error (ca. 1 mE_h), as illustrated above by singlet ketene and propadienone. The existence of such discontinuities prevents these types of local correlation models from adhering to the definition of a "theoretical model chemistry".[91]

Chapter 4

Local Correlation Applied to Static Polarizabilities

4.1 Introduction

A variety of molecular properties, including dipole polarizabilities and hyperpolarizabilities, optical rotation, magnetizabilities, oscillator strengths, rotational strengths, spin-spin coupling constants, *etc.* are all accessible via so-called response theory.[107] One of the simplest *ab initio* approaches to response theory is realized in the random phase approximation (RPA) [also known as time-dependent Hartree-Fock theory (TDHF)],[108] in which the Hartree-Fock wave function is allowed to evolve under the influence of a time-dependent perturbation, while maintaining its single-determinant structure. More recently, time-dependent density-functional theory (TDDFT) has emerged as an efficient approach to incorporating electron correlation effects into the modeling of response properties.[109,110] Unfortunately, a com-

mon shortcoming of modern density functionals is their inability to describe correctly diffuse excited electronic states, such as Rydberg or charge-transfer states, often leading to qualitatively incorrect descriptions of the effect of frequency dispersion on the related response properties.[41]

Coupled cluster theory,[32,95,111,112] one of the most reliable quantum chemical methods, also provides a convenient approach to response properties.[35] For many small molecules, the coupled cluster linear response (CC-LR) approach has been found to give polarizabilities, optical rotation, and other properties that compare superbly to experiment, often to within only a few percent error.[42,113] Unfortunately, this high accuracy is limited to only small molecules, containing at most a few atoms, due to the high-degree polynomial scaling of coupled cluster methods with molecule size [*e.g.*, $\mathcal{O}(N^6) - \mathcal{O}(N^7)$]. For example, a coupled cluster singles and double linear-response (CCSD-LR) optical rotation calculation of the amino acid valine would require approximately one week on modern high-performance computational hardware with a state-of-the-art quantum chemical program. A similar computation on the valine dimer, however, would require more than a year to complete. This polynomial scaling wall represents the greatest obstacle to the application of high-level quantum mechanics to mainstream chemistry.

Local correlation, a concept pioneered by Pulay and Saebø, provides one possible route over the scaling wall through a judicious choice of molecular orbital (MO) basis.[50,62] The "canonical" MOs, although convenient, are delocalized over the entire molecular framework and often lead to overestimation of electronic interactions on spatially distant atoms. Pulay and Saebø demonstrated that if one abandons canonical MOs and instead chooses a more localized orbital form, vast numbers of electronic wave-function parameters become negligible and may thus be ignored. By limiting excitation components to unoccupied/virtual orbitals that are within certain "domains" of a given occupied orbital or orbital pair, one can *a priori* organize the wave-function calculation to exclude components that are expected to be small. This approach is tantamount to correlating only the motions of electrons on parts of the molecule that are in close proximity. The local correlation concept was originally applied

to many-body perturbation theory,[53,62,78,79] but more recently has found success in ground-state[54,63,69,80,83] and excited-state[65,66] calculations, as well as a recent implementation of dipole moments and static polarizabilities.[67]

In this work, we consider the extension of the local correlation approach to both static and dynamic molecular response properties. In particular, we have modified our canonical-MO CCSD-LR program to simulate the effect of local truncation on the perturbed and unperturbed wave functions in order to judge the ability of various orbital domain definitions to reproduce untruncated CCSD-LR polarizabilities. We find that an extension of the "standard" orbital domains using a Hartree-Fock-level estimate of the atomic polarizability contributions provides a reliable route to defining a local-CCSD-LR approach. We have tested the method on two one-dimensional systems: helium-atom chains and n-alkanes, as well as on several other representative molecules, including N-acetylglycine and N-methylacetamide.

4.2 Theoretical Approach

Molecular properties such as dipole polarizabilities, optical rotation, *etc.* may be computed with the CC-LR model through the linear response function, which governs the change in the expectation value of operator $\hat{A}$ with respect to perturbation $\hat{B}$:

$$\langle\langle \mathbf{A};\mathbf{B}\rangle\rangle_\omega = \frac{1}{2}\hat{C}^{\pm\omega}\hat{P}\left(\mathbf{A}(-\omega),\mathbf{B}(\omega)\right)\left[\langle 0|\hat{\Lambda}\left[\bar{\mathbf{A}},\hat{X}^{\omega}_{\mathbf{B}}\right]|0\rangle + \frac{1}{2}\langle 0|\hat{\Lambda}\left[\left[\bar{H},\hat{X}^{\omega}_{\mathbf{A}}\right],\hat{X}^{-\omega}_{\mathbf{B}}\right]|0\rangle\right] \quad (4.1)$$

where $|0\rangle$ is the Hartree-Fock reference state, the overbar denotes the similarity transformation of the given operator [*e.g.*, $\bar{H} = \exp(-\hat{T})\hat{H}\exp(\hat{T})$], and $\hat{\Lambda}$ is a cluster operator parametrizing the coupled cluster "left-hand" ground-state wave function (developed also in coupled cluster analytic energy gradient theory).[95] The permutation operator $\hat{C}^{\pm\omega}$ simultaneously changes signs on the the chosen field frequency, ω, and takes the complex conjugate of the equation, while $\hat{P}(\hat{A},\hat{B})$ permutes the property operators $\hat{A}$ and $\hat{B}$. For example, the dipole polarizability is the negative of the linear response function with both $\mathbf{C}$ and $\mathbf{D}$ taken to be the electric dipole operator, μ. The perturbed wave functions, $\hat{X}^{\omega}_{\mathbf{A}}$, are determined by

solving the system of linear equations

$$\langle\Phi_i|(\bar{H}-\omega)|\Phi_j\rangle\langle\Phi_j|\hat{X}^{\omega}_{\mathbf{A}}|0\rangle = -\langle\Phi_i|\bar{\mathbf{A}}|0\rangle, \tag{4.2}$$

where the Φ_i represent excited determinants. It is worth noting that the eigenvalues of the response matrix on the left-hand side of the above equation (sometimes referred to in the literature as the coupled cluster Jacobian matrix) are related to the excitation energies of the system, an approach to UV/Vis spectra known as the equation-of-motion coupled cluster (EOM-CC) method.[114] Thus, the linear response function exhibits first-order poles at the excitation energies, as required by the underlying perturbation theory. We further note that the above definition of the response function does not include orbital relaxation explicitly, but instead uses single excitations to account for these effects . This approach is necessary in coupled cluster methods with fixed orbitals in order to avoid the occurrence of artifactual CPHF poles.[35,107]

In the local correlation approach developed by Pulay and Saebø, excitations generated by the cluster operator, $\hat{T}$, are limited to orbital "domains" (subsets of the virtual orbital space).[62] In a locally correlated CC-LR approach, this truncation must be applied not only to the ground-state $\hat{T}$ operator, but also to its left-hand counterpart, $\hat{\Lambda}$, as well as to the perturbed wave functions defined in eqn. 4.2. Furthermore, in order for response properties computed using analytic expressions such as eqn. 4.1 above to match those using finite-field (numerical differentiation) techniques, the orbital domain structure must be consistent throughout all facets of the calculation.

In the current work, the occupied orbitals are chosen to be the charge-maximized functions described by Pipek and Mezey.[74] These functions are conveniently orthonormal and well localized, in most cases, to chemically intuitive bond types. (i.e. σ, π, lone pairs, *etc.*) The virtual orbitals are constructed by projecting out all occupied pieces of the original atomic orbital (AO) basis set. These projected AOs (PAOs) are orthogonal to the occupied space, but not to each other.

Given the above definition of localized orbitals (which is identical to that used in the original

work by Pulay and Saebø[62]), we assign to each occupied orbital ϕ_i a domain — a subset of the full PAO space — which becomes the orbital's correlation space. For ground-state energies, the most common domain definition is that based on the Boughton-Pulay completeness criterion.[63,75] However, while these domains are generally sufficient for the recovery of *ca.* 98% of the correlation energy,[50,63] they are inadequate to describe correlation effects within field-perturbed wave functions (*vide infra*). We therefore propose a new domain selection scheme that explicitly incorporates the perturbation into the construction of the domains *via* the coupled-perturbed Hartree-Fock (CPHF) equations.

Within Hartree-Fock theory, a single component of the dipole polarizability tensor (*e.g.*, α_{xy}) may be determined using

$$\alpha_{xy} = \sum_{i}^{\text{occ}} \sum_{a}^{\text{vir}} U_{ai}^{x} \mu_{ai}^{y}, \tag{4.3}$$

where i and a index occupied and virtual MOs, respectively, the U_{ai}^{x} are the solutions to the CPHF equations, and μ_{ai}^{y} are electric dipole integrals. The summation over the virtual orbitals may be "back-transformed" into the AO basis to give

$$\alpha_{xy} = \sum_{i}^{\text{occ}} \sum_{\rho}^{\text{AO}} U_{\rho i}^{x} \mu_{\rho i}^{y}, \tag{4.4}$$

where ρ denotes AO basis functions. eqn. 4.4 can be further decomposed into atomic contributions per occupied orbital as

$$\alpha_{xy}^{iA} = \sum_{\rho \in A}^{\text{AO}} U_{\rho i}^{x} \mu_{\rho i}^{y}, \tag{4.5}$$

where the summation includes only the basis functions on atom A.

One could use eqn. 4.5 to define the domain for occupied orbital ϕ_i: if the contribution of α_{xy}^{iA} exceeds a prescribed cutoff, then the PAOs on atom A, would be included in the domain. However, such an approach would hide the fact that individual AO contributions on the same atom can be either positive or negative, thus leading to artifactually small domain sizes. We therefore choose an alternative approach using the absolute values of the individual AO

contributions, leading to a completeness check in the spirit of the original Boughton-Pulay criterion:

$$\epsilon_{xy}^{i} = \sum_{\rho}^{\mathrm{AO}} \left| U_{\rho i}^{x} \mu_{\rho i}^{y} \right| - \sum_{\rho \in [i]}^{\mathrm{AO}} \left| U_{\rho i}^{x} \mu_{\rho i}^{y} \right| , \tag{4.6}$$

where the notation $\rho \in [i]$ indicates that the summation includes only those AOs within the current estimated domain of orbital ϕ_i. Atoms are first ranked by decreasing value of the above "pseudo"-polarizability contribution, and then incorporated into the domain until the value of ϵ_{xy}^{i} falls below a certain percentage cutoff. The final domain of orbital ϕ_i is taken to be the set of PAOs on the atoms included in eqn. 4.6 as well as those already incorporated through the original Boughton-Pulay procedure. The domains obtained from this CPHF-based approach are necessarily larger than those using the Boughton-Pulay completeness check alone, which results in increased computational expense.

The domains are determined immediately following the Hartree-Fock reference calculation and, as noted above, must be held constant throughout the entire response calculation. Pairwise excitations of orbitals ϕ_i and ϕ_j are chosen as the union of the orbitals' single-excitation domains, with additional decomposition into "strong" and "weak" pairs to further reduce the scaling of the method.[62,63] However, because of the unique role of the single excitations to account for orbital relaxation, as noted earlier, we choose to leave the $\hat{T}_1$, $\hat{\Lambda}_1$, and $\hat{X}_1$ cluster operators untruncated. In an efficient, production-level code, some truncation of the singles will be necessary, but even for very large-distance cutoffs, the wave function will remain compact.

We note that Korona, Pflüger, and Werner have also reported recently a local-CC approach to polarizabilities.[67] Their scheme differs from the present method in that the domains are chosen based on a bond-connectivity/nearest-neighbor criterion using atomic covalent radii. While this approach was found to produce small localization errors (less than 0.5%), the performance of the method degrades considerably if orbital relaxation is omitted, with errors approaching 10% or more. As noted above, for frequency-dependent polarizabilities, a qualitatively correct pole structure can be maintained only if the orbital response is included

indirectly (*via* single excitations, as above) or through explicit orbital optimization.[115] Thus, one purpose of the present work is to develop a scheme that reproduces the untruncated properties with or without direct orbital contributions.

We also should point out that the current analysis focuses only on the truncation of the orbital domain structure, and does not consider additional reduction in the number of correlated pairs. Our future efforts in this arena will be directed towards development of a weak-pair scheme, analogous to the use of local-MP2 energies in ground-state local-CCSD methods. However, one important complication in the case of frequency-dependent properties is the coupling between the strong- and weak-pair domains, which may be ignored for ground-state energies, but could introduce artifactual poles in polarizabilities, for example.

4.3 Computational Details

Canonical- and local-MO CCSD-LR polarizability calculations using spin-restricted Hartree-Fock (RHF) orbitals were carried out using the PSI3 quantum chemical program package.[96] Although the current work reports only static polarizabilities, the program is also capable of computing frequency-dependent polarizabilities, according to eqn. 4.2. The local-CCSD approach we have implemented here is a "pilot" program that uses our canonical-MO code to simulate the local correlation treatment. This method was briefly described by Saebø and Pulay in one of their earlier local correlation articles,[59] by Hampel and Werner in their seminal paper on local-CCSD[63] and by Crawford and King in a recent extension of these methods to excited states via the local equation-of-motion (EOM)-CCSD approach.[65] As mentioned earlier, no distinction was made between weak and strong pairs in these calculations, i.e., all localized pair domains were treated explicitly in the local-CCSD calculations. This allows us to confine our analysis strictly to the orbital domain truncation.

Test calculations of the local-CCSD-LR scheme were carried out on helium-atom chains, *n*-alkanes, and the pseudo-linear series of molecules glycine, N-acetylglycine, N-methylformamide,

and N-methylacetamide. Helium-chain calculations used the diffuse-augmented correlation-consistent polarized-valence double-zeta (aug-cc-pVDZ) basis set by Dunning and co-workers.[97,116] All other calculations used the split-valence 6-31G* and 6-31+G* basis sets of Pople and co-workers.[117] (Basis sets were obtained from the Extensible Computational Chemistry Environment Basis Set Database, Version 12/03/03, as developed and distributed by the Molecular Science Computing Facility, Environmental and Molecular Sciences Laboratory which is part of the Pacific Northwest Laboratory.)

4.4 Benchmark Calculations

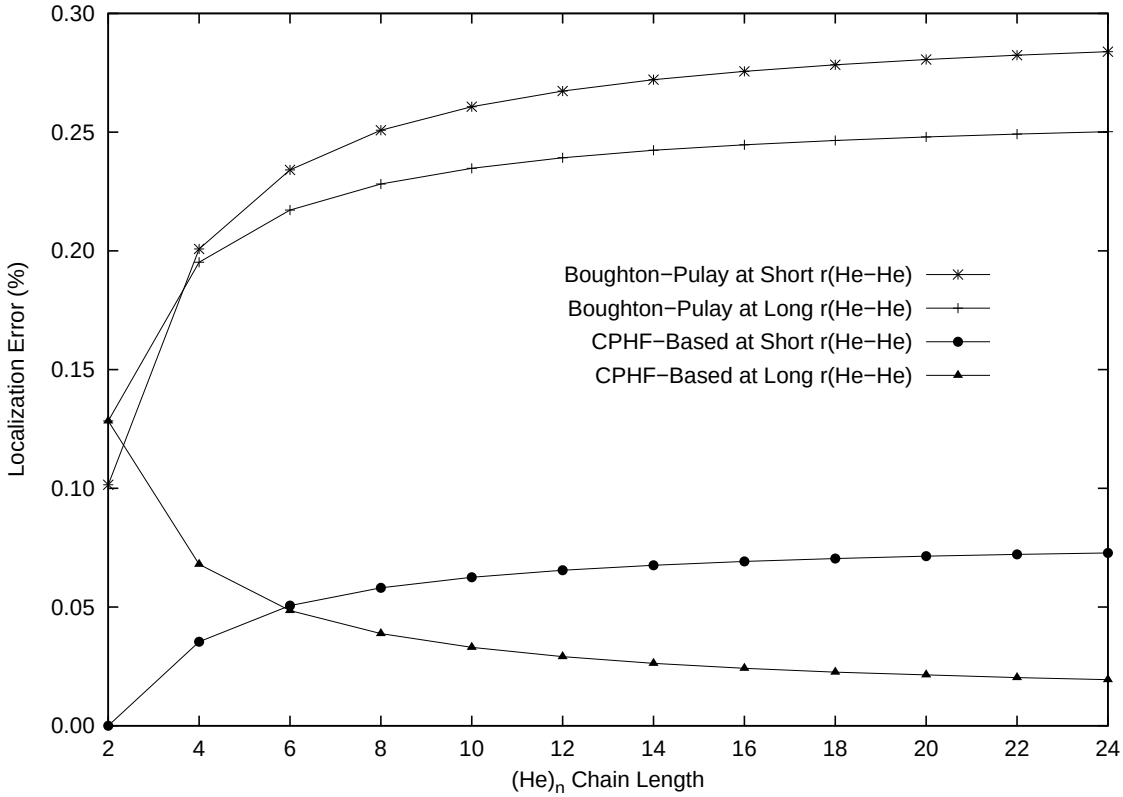

Figure 4.1: Localization errors (%) for CCSD/aug-cc-pVDZ polarizabilities (α_{zz}) for helium-atom chains (at He−He distances of 2.0 and 2.986 Å) using Boughton-Pulay and CPHF-based domain structures, with cutoffs of 0.02 and 0.05 respectively.

Fig. 4.1 plots the localization error in the largest components of the CCSD/aug-cc-pVDZ polarizability for helium chains ranging from 2-24 atoms at two different bond lengths: 2.0 Å and 2.986 Å(the CCSD/aug-cc-pVQZ optimized geometry of He_2). Table 4.1 reports the corresponding data for the shorter bond distance, which is representative, as well as the total polarizabilities and canonical versus local double-excitation amplitude ratios. Both bond lengths correspond to well-localized systems — indeed, the Pipek-Mezey localized occupied orbitals are simply $1s$ AOs on each atom — involving primarily dispersion-force interactions. This example therefore represents a "best-case" scenario for local-CC schemes and allows us to measure the minimum capabilities of the proposed approach. Two different double-excitation domain structures were used: the standard Boughton-Pulay domains obtained with a cutoff of 0.02 and CPHF-based domains with a cutoff of 0.05. (As described above, for appropriate comparison, single-excitations remained untruncated for both sets of calculations.) These cutoffs lead to Boughton-Pulay domains consisting of only single atoms, and CPHF-based domains of at most three atoms.

As expected, the localization errors for both domain types is small (less than 0.5% in all cases), though the Boughton-Pulay domains naturally lead to errors approximately five times larger than the CPHF-domains, and, for greater interatomic interactions, the former will be inadequate (*vide infra*). The key observation here, however, is that for the short He−He distance results, both the Boughton-Pulay and CPHF-based domain structures lead to maximum values in the localization error: approximately 0.30% and 0.075%, respectively. In other words, the polarizability is not a completely delocalized property in this system, and a local-CC model can recover the canonical-CC result to within a finite percentage, even for an infinite system. We also note that the CPHF-domains for the long-bond chains actually lead to a *decrease* in the localization error with increasing chain length, a result obviously attributable to the decreased He−He interaction coupled with overdetermined domain sizes.

Fig. 4.2 plots the number of canonical (untruncated) double-excitation amplitudes versus the number of local (truncated) amplitudes used to obtain the T_2 amplitude ratios given in Table 4.1 for the two domain choices for r(He−He) = 2.0 Å. All three curves show quadratic

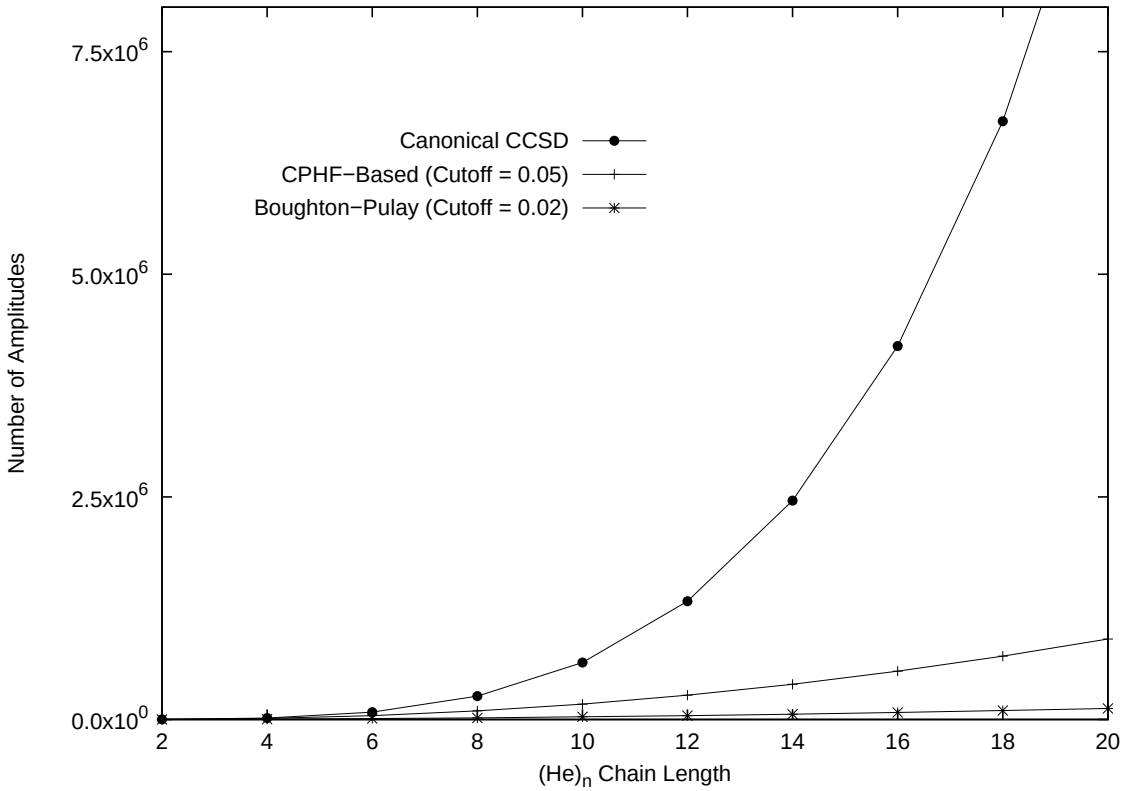

Figure 4.2: Number of canonical- and local-CCSD/aug-cc-pVDZ double-excitation amplitudes for helium-atom chains at an interatomic distance of 2.0 Å.

behavior (only very subtly in the Boughton-Pulay case), which is expected here because all occupied-orbital pairs are included in the current analysis. The crossover point between the canonical and local curves occurs at He_4 for the CPHF-based domains and immediately at He_2 for the Boughton-Pulay domains.

Alkanes provide a slightly more difficult problem for localization schemes for response properties than helium chains because they test bonding interactions, but they remain well localized because of their lack of conjugation. Fig. 4.3 plots the localization error in the largest components of the CCSD/6-31G* static polarizability for odd-numbered n-alkane chains ranging from three (propane) to nine (nonane) carbon atoms using the Hartree-Fock/6-31G** optimized geometry for each alkane. Table 4.3 reports the corresponding data, as well as the total polarizabilities and T_2 amplitude ratios. CPHF-based domain structures were used for

Table 4.1: Canonical- and local-CCSD-LR static polarizabilities (in a.u.) and % localization errors of helium chains at an interatomic distance of 2.0 Å with the aug-cc-pVDZ basis set. Boughton-Pulay domains were determined using a cutoff of 0.02, and CPHF-based domains using a cutoff of 0.05. T_2 ratios are defined as the ratio of the number of canonical-MO (untruncated) doubles-amplitudes to the number of local-MO (truncated) amplitudes.

	Canonical	Boughton-Pulay Domains			CPHF-Based Domains		
$(He)_n$	α_{zz}	α_{zz}	% Error	T_2 Ratio	α_{zz}	% Error	T_2 Ratio
2	2.779	2.776	0.1015	0.791	2.779	0.0000	1.266
4	5.653	5.641	0.2008	0.257	5.651	0.0354	0.939
6	8.536	8.516	0.2341	0.123	8.532	0.0506	0.629
8	11.422	11.390	0.2508	0.072	11.416	0.0581	0.428
10	14.310	14.273	0.2607	0.047	14.301	0.0625	0.306
12	17.198	17.152	0.2673	0.033	17.187	0.0655	0.228
14	20.087	20.032	0.2721	0.024	20.073	0.0676	0.176
16	22.976	22.912	0.2756	0.019	22.960	0.0692	0.140
18	25.865	25.793	0.2784	0.015	25.846	0.0704	0.114
20	28.754	28.673	0.2806	0.012	28.733	0.0714	0.094
22	31.643	31.553	0.2824	0.010	31.620	0.0722	0.079
24	34.532	34.434	0.2839	0.009	34.507	0.0728	0.067

Fig. 4.3 and Table 4.3 with cutoffs ranging from 0.05 to 0.20.

With the smallest cutoff used here of 0.05, the localization errors remain small, below 0.3%, while larger cutoffs lead to errors of up to 2.0% with a cutoff of 0.20. Concomitantly, the average domain size varies as well, with the smallest domains (3-4 atoms) for a cutoff of 0.20 and the largest (6-9 atoms) for 0.05. Thus, the crossover point between the canonical- and local-CC-LR methods shifts towards larger alkanes as the cutoff decreases, with the

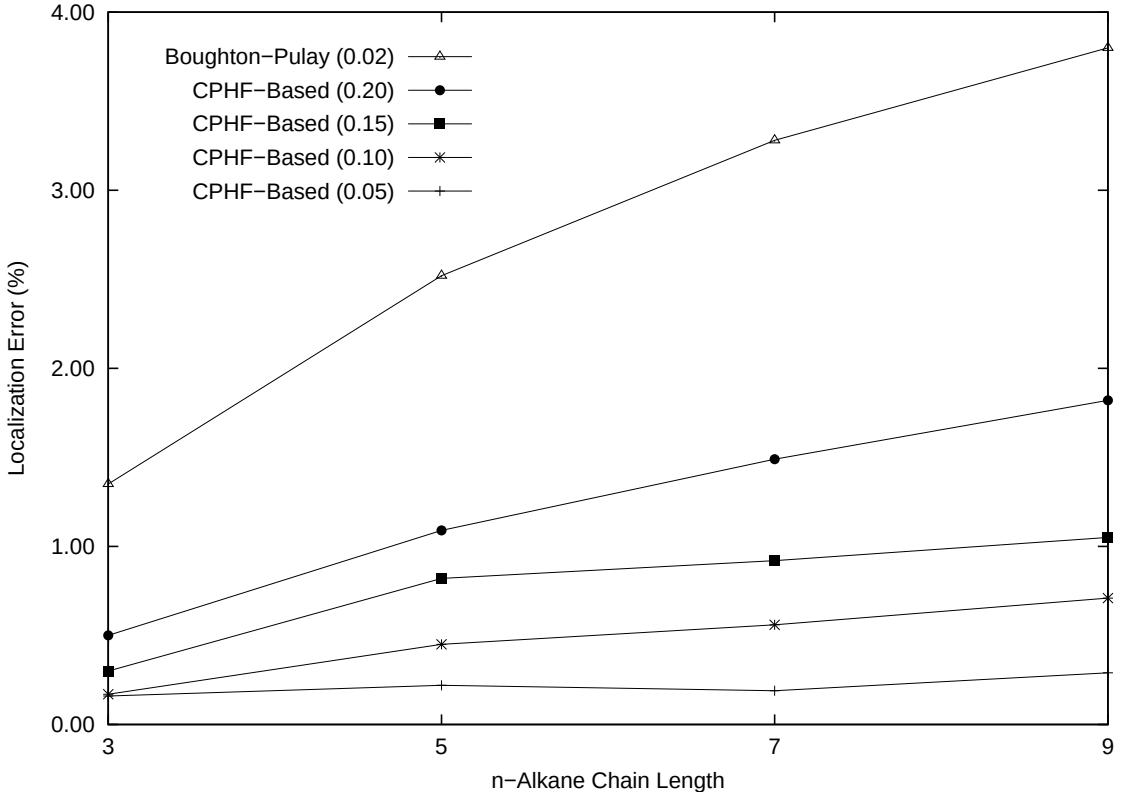

Figure 4.3: Localization errors (%) for CCSD/6-31G* polarizabilities (α_{xx}) for n-alkane chains using CPHF-based domains with cutoffs ranging from 0.05-0.20.

0.20-cutoff crossover occurring immediately at propane and that for the 0.05 cutoff extended to heptane (cf. Table 4.3). In addition, for each choice of CPHF cutoff the change in the localization error decreases with chain length, as can be seen most clearly from Fig. 4.3. For the 0.15 cutoff, for example, the error appears to be converging towards a value between 1.00 and 1.25%, while for the 0.05 cutoff, the converged error will likely be less than 0.4%. (Note that the "kink" observed in the localization error for each cutoff is related to inherent symmetry in the alkane chains, the numerical precision of the CPHF polarizabilities, and the use of separately optimized geometries for each alkane.)

We consider a 1% localization error in the polarizability to be the maximum acceptable loss, and from the data in Table 4.3 and Fig. 4.3, one thus might assume that a CPHF domain cutoff of 0.10 is reasonable to maintain an efficient localization. However, we find that the

Table 4.2: Canonical- and local-CCSD-LR static polarizabilities (in a.u.) and % localization errors of n-alkane chains with the 6-31+G* basis set for a CPHF-based domain cutoff of 0.20. T_2 ratios are defined as in Table 4.1.

	Canonical	CPHF-Based Domains (0.20)		
n-Alkane	α_{zz}	α_{zz}	% Error	T_2 Ratio
propane	37.73	37.66	0.19	1.05
pentane	65.44	65.06	0.59	0.81
heptane	94.62	93.90	0.75	0.68
nonane	124.45	123.34	0.89	0.54

localization error is reduced as the basis set quality improves. Table 4.2 reports similar data as in Table 4.3, but only for a 0.20 CPHF cutoff using a 6-31+G* basis set, which includes diffuse s- and p-type functions. The localization error in this case drops by a factor of two relative to that using the 6-31G* basis. This improvement results entirely from a natural increase in the average domain size, from 3-4 atoms with the 6-31G* basis to 4-5 atoms with the 6-31+G* basis. In addition, the crossover point between the canonical- and local-CC methods shifts from propane to pentane.

In order to test more general electronic structure patterns, we have also considered several other pseudo-linear molecules, including N-methylformamide, glycine, N-methylacetamide, and N-acetylglycine. Table 4.4 reports the CCSD-LR static polarizabilities for these molecules using both Boughton-Pulay domains (with a 0.02 cutoff) and CPHF-based domains (with cutoffs at 0.10 and 0.20) using the 6-31+G* basis set. For the Boughton-Pulay domains, the localization errors are, as expected, much too large, exceeding 3.0% even with N-acetylglycine. The CPHF-based domains, however, are much better behaved, giving localization errors of less than 1.0%, even with a cutoff of 0.20, or less than 0.5% with the tighter cutoff of 0.10. The cost of this improvement, however, is the increase in the average domain size, ranging from only 1-3 atoms with the Boughton-Pulay domains to 4-6 atoms with the

0.10-cutoff CPHF-based domains. This, of course, leads to greater computational expense, with expanded crossover points in the doubles amplitudes to beyond N-methylacetamide with the smallest cutoff.

Table 4.3: Canonical- and local-CCSD-LR static polarizabilities (in a.u.) and % localization errors of n-alkane chains with the 6-31G* basis set for several CPHF-based domain cutoffs ranging from 0.05 to 0.20. T_2 ratios are defined as in Table 4.1.

	Canonical	0.05			0.10			0.15			0.20		
n-alkane	α_{zz}	α_{zz}	% Error	T_2 Ratio	α_{zz}	% Error	T_2 Ratio	α_{zz}	% Error	T_2 Ratio	α_{zz}	% Error	T_2 Ratio
propane	34.45	34.40	0.16	1.29	34.39	0.17	1.22	34.35	0.30	1.05	34.28	0.50	0.92
pentane	60.10	59.97	0.22	1.05	59.83	0.45	0.86	59.61	0.82	0.70	59.44	1.09	0.61
heptane	87.45	87.28	0.19	0.88	86.96	0.56	0.65	86.64	0.92	0.55	86.14	1.49	0.41
nonane	115.56	115.23	0.29	0.67	114.74	0.71	0.48	114.34	1.05	0.41	113.46	1.82	0.28

Table 4.4: Canonical- and local-CCSD-LR static polarizabilities (in a.u.) and % localization errors of several non-saturated pseudo-linear molecules using the 6-31+G* basis set. Boughton-Pulay domains were determined using a cutoff of 0.02 and CPHF-based domains using cutoffs of 0.10 and 0.20. T_2 ratios are defined as in Table 4.1.

	Canonical	BP Domains			CPHF-Based Domains (0.10)			CPHF-Based Domains (0.20)		
	α_{zz}	α_{zz}	% Error	T_2 Ratio	α_{zz}	% Error	T_2 Ratio	α_{zz}	% Error	T_2 Ratio
N-methylformamide	43.10	42.37	1.68	0.54	43.07	0.05	1.19	42.96	0.31	0.99
Glycine	43.83	42.67	2.66	0.35	43.78	0.11	1.09	43.71	0.28	0.88
N-methylacetamide	55.02	53.50	2.76	0.35	54.85	0.30	1.06	54.59	0.77	0.77
N-acetylglycine	78.41	75.96	3.12	0.18	78.28	0.17	0.84	77.92	0.62	0.58

4.5 Conclusions

We have implemented a reduced-scaling coupled cluster approach to molecular response properties, such as dipole polarizabilities, optical rotation, *etc.*, using a Pulay-Saebø localization structure based on orbital excitation domains defined using CPHF contributions to the perturbed wave functions. After testing on several benchmark systems, including He-atom chains, linear alkanes, and molecules as large as N-acetylglycine, we conclude that this approach can provide polarizabilities comparable to canonical-MO calculations to within 1% given appropriately chosen cutoffs, even without direct inclusion of orbital relaxation contributions. This scheme is necessarily more computationally demanding than that used for ground-state energy calculations, but the crossover between non-local and local methods remains within reach of production-level implementation.

Chapter 5

Local Correlation Applied to Optical Rotation

5.1 Introduction

Natural products chemistry and drug discovery employ various techniques for elucidating absolute configurations of naturally occurring chemical compounds. The most reliable method is x-ray crystallography on the compound itself or a derivative that incorporates a known stereocenter. Unfortunately, x-ray crystallography is not always feasible. When this is the case, chemists often turn to NMR spectral analysis and chiroptical methods like optical rotation, electronic and vibrational circular dichroism, etc., sometimes resorting to partial, or total, synthesis of the compound from known starting materials. Assignment of absolute configuration by these methods can take upwards of a decade, indeed 14 years elapsed between the discovery of Bistramide C to assigning the absolute configuration of the naturally occurring product.[118] The ability to accurately and quickly predict chiroptical properties by computational methods may greatly speed-up this long, arduous process.

Recently, calculations of optical rotation,[39–42,119–123] electronic circular dichroism,[124–126] vi-

brational circular dichroism,[126–128] vibrational Raman optical activity[129–131] and vibrational contributions to optical rotation[45,126,132] have become much more routine on small molecular systems. Among the methods listed here optical rotation is the most popular for experimental chemists and has the largest amount of experimental data, causing the greatest surge in computational methods. Seemingly, computational chemistry is well suited to aid chemists in the assignment of natural products. In fact, optical rotation calculations have been performed to help deduce the absolute configuration of previously unassigned enantiomers for some relatively small molecules.[133] However, the greatest obstacles to computational quantum chemistry are the computational resources and amount of time required to perform optical rotation calculations.

Optical rotation, as well as many other chiroptical properties, are accessible through response theory.[107] One of the simplest manifestations of response theory within *ab initio* methods is the random phase approximation (RPA) (also known as time-dependent Hartree-Fock theory (TDHF)),[108,134] in which the Hartree-Fock wave function is allowed to respond to a time-dependent perturbation while maintaining its single determinant structure. Based on this same model, time-dependent density-functional theory (TDDFT) has become one of the most popular methods for response type properties due to its inclusion of electron correlation at relatively low computational demands.[109,110] It is well known that DFT suffers from an inability to correctly predict excitation energies (especially for diffuse and charge transfer type excited states) which leads to inaccurate predictions of optical rotation.[41,42]

Coupled cluster theory,[32,95,111,112] one of the most reliable quantum chemical methods, provides calculations of response type properties via coupled cluster linear-response theory (CC-LR).[35] In fact, calculations of excitation energies,[135] polarizabilities,[113] optical rotation,[39–42] etc., have been shown to give errors within only a few percent. This level of accuracy does not come without a great cost in computational resources. The self consistent field methods (*e.g.* Hartree-Fock and DFT) scale as $\mathcal{O}(N^3)$ (this is only a formal scaling, much effort has been made to bring the scaling of SCF methods down to linear in the asymptotic limit[47,136]) compared to the accurate coupled cluster singles and doubles method (CCSD)

which scales as $\mathcal{O}(N^6)$, where N is some measure of system size. For example, a CCSD-LR optical rotation calculation on [4]-triangulane requires approximately ten days on a modern high performance workstation. An analogous calculation on [9]-triangulane (approximately twice the size of [4]-triangulane) would require nearly two years to complete, while the same calculation using Hartree-Fock or DFT would still be feasible. This high-degree polynomial scaling wall is the bane of electron correlation quantum chemical methods, such as coupled cluster theory.

This high-degree polynomial scaling has little to no physical justification since dispersion is a short-range interaction. The source of the scaling issues associated with electron correlation methods is commonly attributed to the use of canonical MOs. While mathematically convenient, canonical MOs result in orbital contour plots that incorporate significant contributions from most atomic orbitals (AOs) and lead to highly delocalized MO pictures. As a result, there is no *a priori* selection scheme to determine (and ignore) negligible pieces of the wave function within a given excitation class (i.e. if doubles are included in the wave function, then all possible doubles must be calculated, not just a subset of the doubles).

Many local ansäetze have been proposed to achieve reduced scaling within electron correlation calculations. Head-Gordon *et al.* have developed a technique where the occupied space is projected against the virtual space and *vice versa* to achieve localized MOs (molecular orbitals). Domains are then chosen to be only the virtual orbitals that are on the same atom as the occupied orbital.[53,54] This has the advantage or maintaining smooth potential energy surfaces, free of discontinuities, which is a shortcoming of many other local correlation schemes.[137] Flocke and Bartlett have based their local correlation methods on NBOs (natural bond orbitals) by allowing the occupied-virtual blocks of the Fock matrix to be non-zero (but small) they achieve a well localized basis from which to perform local correlation with the caveat that the Hartree-Fock reference has been destroyed.[56]

We have chosen to use the local correlation scheme pioneered by Pulay and Saebø,[50,62] who demonstrated that localized orbitals are attainable by abandoning the canonical orbital for-

mulation and employing separate localization schemes for the occupied and virtual spaces. Within this framework there is now a spatial criterion to discriminate and neglect insignificant pieces of the wave function. The local correlation method of Pulay and Saebø was first applied to many-body perturbation theory,[59–61] than extended to coupled cluster theory for ground[63] and excited states,[65,66] as well as to coupled cluster response theory for the calculation of static[67] and dynamic[68] polarizabilities. The current state-of-the art in large scale local correlation calculation of ground state energies was performed by Schütz and Manby on 16 Glycine molecules in only a few hours on a modern high performance workstation.[69]

The purpose of this work is to extend our previous work on local response properties for calculating polarizabilities[68] to the calculation of optical rotation. We have modified our canonical-MO CC-LR program to simulate the effect of local truncations on the unperturbed and perturbed amplitudes and ultimately the optical rotation as compared to the canonical-MO (untruncated) approach. There are several new features we have added to our pilot CC-LR code. 1) CC2 has been implemented to allow calculations on larger molecular systems (CC2[33] is an approximation to CCSD and scales as $\mathcal{O}(N^5)$ instead of $\mathcal{O}(N^6)$ for CCSD.) 2) The ability to calculate optical rotations at the CC2 level of theory for canonical- and local-MO calculations has been implemented. 3) Even though the state of the pilot code was able to perform frequency dependent calculations at the time of our previous publication, we chose to concentrate on static polarizabilities, but take full advantage of frequency dependent capable code for optical rotations. 4) Magnetic field dependent CPHF-based (coupled-perturbed Hartree-Fock) domain selection has been introduced to account for the nature of the Rosenfeld β tensor.[38] Previously, only electric field perturbations were used when calculating polarizabilities. We have tested this new domain selection algorithm on the one-dimensional 1-fluoroalkane system ranging from 1-fluoropropane to 1-fluoroundecane and a series of [n]-triangulanes from [4]-[6]-triangulane and β-pinene

5.2 Theoretical Approach

The quantum mechanical foundation for calculating optical rotation has been known since 1928, first proposed by Rosenfeld.[38] Through the use of time-dependent perturbation theory, one can derive the Rosenfeld β tensor as:

$$\beta(\omega) = \frac{c}{3\pi h}\mathrm{Im}\sum_{n\neq 0}\frac{\langle 0|\boldsymbol{\mu}|n\rangle\langle n|\mathbf{m}|0\rangle}{\omega_{n0}^2-\omega^2} \tag{5.1}$$

where $\boldsymbol{\mu}$ and $\mathbf{m}$ are electric and magnetic dipole moment operators, respectively, the summation runs over all excited states, $|n\rangle$, ω_{n0} is the excitation energy of state $|n\rangle$, and ω is the incident frequency. The sum over states approach is very computationally expensive, and fortunately, can be avoided through the use of linear-response theory.[138]

Koch *et al.* have developed the linear-response function for a coupled-cluster wave function[35] relating the β tensor to the CC-LR (coupled-cluster linear-response) function by

$$\beta_{xy}(\omega) = -\mathrm{Im}\langle\langle\boldsymbol{\mu};\mathbf{m}\rangle\rangle_\omega \tag{5.2}$$

where the CC-LR function for a magnetic and electric dipole moment operator is defined as

$$\langle\langle\boldsymbol{\mu};\mathbf{m}\rangle\rangle_\omega = \frac{1}{2}\hat{C}^{\pm\omega}\hat{P}(\boldsymbol{\mu}(-\omega),\mathbf{m}(\omega))\left[\langle 0|\hat{\Lambda}\left[\bar{\boldsymbol{\mu}},\hat{X}^{\omega}_{\mathbf{m}}\right]|0\rangle + \frac{1}{2}\langle 0|\hat{\Lambda}\left[\left[\bar{H},\hat{X}^{\omega}_{\boldsymbol{\mu}}\right],\hat{X}^{-\omega}_{\mathbf{m}}\right]|0\rangle\right] \tag{5.3}$$

where $\hat{P}$ is a symmetric permutation operator, $\hat{C}^{\pm\omega}$ simultaneously changes the sign of ω and takes the complex conjugate of the equation. The $\hat{\Lambda}$ operators are de-excitation operators, analogous to $\hat{T}$, that characterize the left-hand states of the non-hermitian, similarity transformed Hamiltonian, $\bar{H}$ (*e.g.*, $\bar{H} = e^{-\hat{T}}\hat{H}e^{\hat{T}}$). The set of $\hat{X}^{\pm\omega}_{\mathbf{A}}$ are perturbed wave function parameters specific to each perturbation and sign of ω, solved by

$$\sum_\sigma \langle\nu|(\bar{H}-\omega)|\sigma\rangle\langle\sigma|\hat{X}^{\pm\omega}_{\mathbf{A}}|0\rangle + \langle\nu|\hat{\mathbf{A}}|0\rangle = 0 \tag{5.4}$$

where ν and σ represent excited determinants. It is worth noting that the above definition of the CC-LR functions has been constructed to neglect orbital relaxation effects, relying on the singly excited perturbed amplitudes to account for orbital relaxation. The use of singles

to account for orbital relaxation has been shown to have a negligible effect on response-type properties[34] with the added advantage of avoiding artifactual CPHF poles.[35]

Applying the local correlation approach developed by Saebø and Pulay requires consistent domains for all quantities in the CC-LR function. In other words, the domains used to calculate the ground-state $\hat{T}$ amplitudes must also be applied to the left-hand analog, $\hat{\Lambda}$, and the perturbed wave function amplitudes, $\hat{X}_{\mathbf{A}}^{\pm\omega}$, defined in eqn. (5.4). The consistent domain requirement is to ensure static response properties calculated by the CC-LR function of eqn. (5.3) match those calculated via numerical and analytical differentiation techniques.

We have chosen to use the charge-maximization procedure of Pipek and Mezey[74] to localize the occupied orbital space. The Pipek-Mezey localization procedure maintains orthonormality within the occupied space and provides well localized chemically intuitive bond types. (*i.e.*, σ, π, lone pairs, etc.) The virtual orbital space is handled via a projection operator,

$$|\tilde{\nu}\rangle = \Big(1 - \sum_i |\psi_i\rangle\langle\psi_i|\Big)|\nu\rangle \tag{5.5}$$

which removes all occupied pieces of the original AO basis, to form a set of PAOs (projected AOs), denoted by the tilde. The set of PAOs is localized to atom centers and orthogonal to the occupied space, but not to each other.

Given the above set of localized occupied and virtual orbitals, we can implement a spatial criterion to discriminate and neglect insignificant excitations. (*i.e.* T amplitudes) A subset of the PAOs is assigned to each occupied orbital and becomes that orbital's domain, or correlation space. Boughton and Pulay[75] have developed a completeness check to automatically define orbital domains:

$$f_i(\mathbf{C}') = \min\left[\int(\phi_i - \phi_i')^2 d\tau\right] = 1 - \sum_{\nu\in[i]}\sum_{\sigma} C_\nu'^i S_{\nu\sigma} C_\sigma^i. \tag{5.6}$$

Where ϕ_i' is an approximation to ϕ_i for the current subset of AOs, with associated MO coefficients $C_\nu'^i$. Typically a cutoff of 0.02 is sufficient to retain *ca.* 98% of the correlation energy. However, the domains derived from eqn. (5.6), throughout this work referred to as BP

domains, only consider electronic interaction within the molecular system. It is important to consider how various perturbations will alter the localizability of the molecular system and how the domains must be altered to account for an applied perturbation(s).

We have proposed solutions to the coupled-perturbed Hartree-Fock (CPHF) equations to predict the effects of applied perturbations.[68] Our previous work focused only on polarizabilities and domain definitions required solutions to only the electric dipole moment perturbed CPHF equations. A single element of the electric dipole polarizability tensor, within CPHF, is

$$\alpha_{xy} = \sum_{i}^{\text{occ}} \sum_{a}^{\text{vir}} U_{ai}^{x} \mu_{ai}^{y} \tag{5.7}$$

where U_{ai}^{x} are solutions to the CPHF equations and μ_{ai}^{y} are dipole moment integrals. The virtual orbitals in the above expression can be 'back-transformed' into the AO basis making it trivial to write an expression for individual atomic contributions for a particular occupied orbital as

$$\alpha_{xy}^{iK} = \sum_{\rho \in K}^{\text{AO}} U_{\rho i}^{x} \mu_{\rho i}^{y} \tag{5.8}$$

where ρ is an AO basis function and α_{xy}^{iK} is the atomic contribution of the AO basis functions centered on atom K to occupied orbital ψ_i. Writing the CPHF polarizability tensor in this form lends itself to a completeness check similar to the BP domain definitions described by eqn. (5.6).

Implementing a completeness check based on eqn. (5.8) as it is written would be a mistake due to the potential sign differences between individual AO contributions to the polarizability. In other words, significant contributions to the polarizability may be ignored due to a cancellation of positive and negative contributions to α_{xy}^{iK} resulting artifactually small domain sizes. Instead, we propose using absolute values to calculate a difference between the untruncated and current estimate of the 'pseudo'-polarizability:

$$\epsilon_{xy}^{i} = \sum_{\rho}^{\text{AO}} \left| U_{\rho i}^{x} \mu_{\rho i}^{y} \right| - \sum_{\rho \in [i]}^{\text{AO}} \left| U_{\rho i}^{x} \mu_{\rho i}^{y} \right| \tag{5.9}$$

where the notation $\rho \in [i]$ indicates that only the AOs associated with the current domain of orbital ψ_i are included in the summation and ϵ^i_{xy} is a prescribed cutoff to assess 'completeness'. The domain for occupied orbital ψ_i is assigned by first ranking the atoms by decreasing 'pseudo'-polarizability and then incorporating AOs on an atom-wise basis until the value of ϵ^i_{xy} falls below a certain value. The PAOs centered on the atoms used to bring ϵ^i_{xy} below the prescribed cutoff are incorporated into the final domain of occupied orbital ψ_i.

The inclusion of electric dipole perturbed CPHF-based domains is sufficient for the calculation of polarizabilities,[68] which uses only the electric dipole moment operator. However, optical rotation employs the electric and magnetic dipole moment operators via the β tensor in eqn. (5.1), requiring solutions to the magnetic perturbed CPHF equations to augment the orbital domains similar to eqn. (5.9), *e.g.*,

$$\epsilon^i_{xy} = \sum_{\rho}^{\mathrm{AO}} \left| M^x_{\rho i} m^y_{\rho i} \right| - \sum_{\rho \in [i]}^{\mathrm{AO}} \left| M^x_{\rho i} m^y_{\rho i} \right| \tag{5.10}$$

where $M^x_{\rho i}$ are solutions to the magnetic perturbed CPHF equations and $m^y_{\rho i}$ are magnetic dipole integrals. The final domain of occupied orbital ψ_i is taken to be the union of the BP domains from eqn. (5.6) and the electric and magnetic dipole perturbed CPHF-based domain definitions from eqns. (5.9) and (5.10), *e.g.*, $[i] = [i]_{\mathrm{BP}} \cup [i]_{\boldsymbol{\mu}} \cup [i]_{\mathbf{m}}$. This domain selection results in domains that are much larger than the original BP domains leading to increased computational expense and much smaller localization errors (*vide infra*).

The domains are determined immediately following the Hartree-Fock reference calculation and held constant throughout all facets of the CC-LR calculation, as noted above. Pair domains for excitation and de-excitation operators involving orbitals ψ_i and ψ_j are taken as the union of the single excitation domains for each individual orbital (*e.g.*, $[ij] = [i] \cup [j]$). These pairwise operators can be classified as 'strong' or 'weak' pairs to further reduce the scaling of the method.[62,63] We have chosen to treat all pairs as strong pairs to assess the localizability of optical rotation and provide a 'best-case' scenario for the calculation of optical rotation within the local correlation framework. We have also chosen to leave all single domains untruncated due to the unique role X_1 operators play as orbital relaxation

parameters.[34]

5.3 Computational Details

We have chosen to perform CC2 (approximation to CCSD)[33] level optical rotation calculations due to $O(N^5)$ scaling compared to $O(N^6)$ associated with CCSD (coupled-cluster singles and doubles), allowing calculations to be performed on larger molecular systems. Canonical- and local-MO CC2-LR optical rotation calculations using spin-restricted Hartree-Fock (RHF) orbitals were carried out using the Psi3 quantum chemical program package.[96] The local-CC2 calculations performed on 'pilot' code which uses the canonical version of the program then filters all T, Λ and X quantities to simulate the local correlation treatment.[59,63,65,68]

Optical rotation calculations have been performed on a series of 1-fluoroalkanes ranging from 1-fluoropropane to 1-fluoroundecane, a series of [n]-triangulanes from [4]-triangulane to [6]-triangulane and the model system β-pinene. All of the structures in this work have been optimized using Hartree-Fock theory in a 6-31G** basis set. All calculations in this work used the split-valence 6-31G* and 6-31+G* basis sets of Pople and co-workers.[117]

5.4 Results and Discussion

Fig. 5.1 plots the localization error for CC2 optical rotation calculations at 589 nm with a 6-31G* basis set for a series of 1-fluoroalkanes ranging from 1-fluoropropane to 1-fluoroundecane. The corresponding data is reported in Table 5.1 as well the the ratio of the number of T_2 amplitudes in the local calculation to the number of T_2 amplitudes in the canonical calculation. Two different domain definitions have been reported, the standard BP domains defined by eqn. 5.6 and the CPHF-based domains proposed above with cutoffs from 0.01 to 0.20. Looking at the smallest cutoff of 0.01 it is clear that % errors are sufficiently small with

no absolute value exceeding 1%. However, the crossover point, when the local correlation calculation becomes computationally advantageous, occurs at 1-fluorononane. We prefer the crossover point to occur at a smaller molecular size.

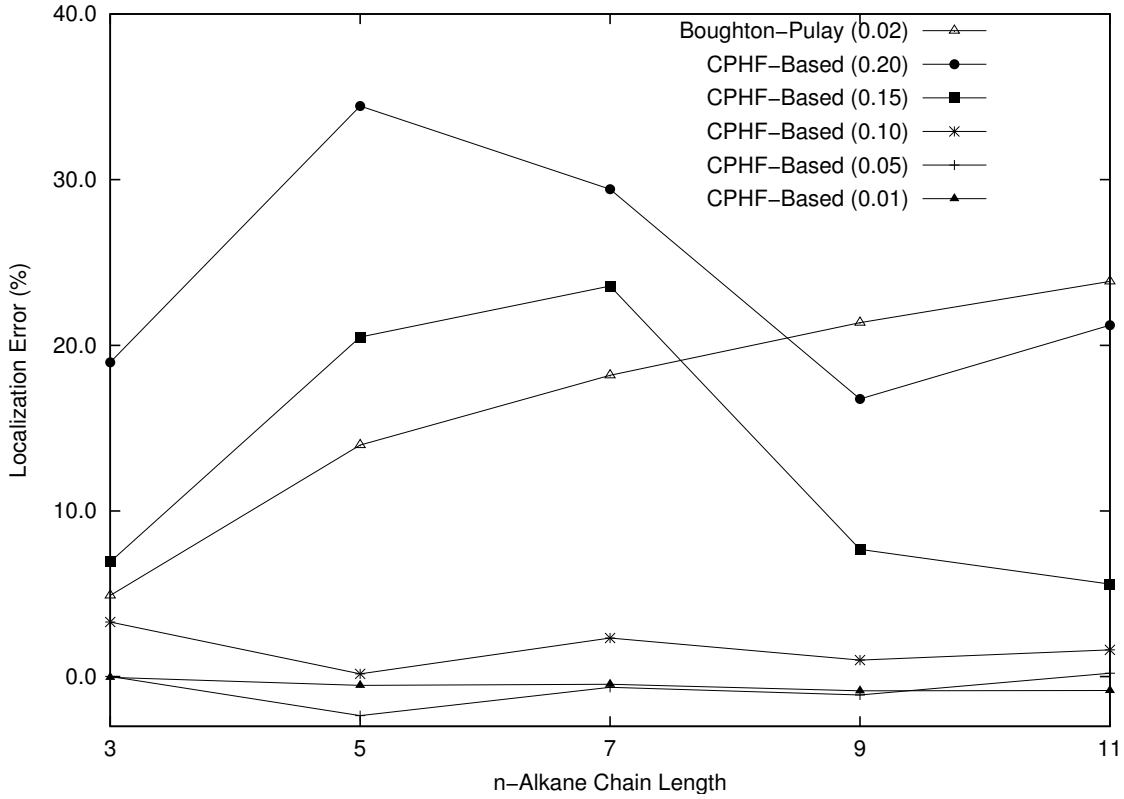

Figure 5.1: Localization errors (%) for CC2/6-31G* optical rotation for 1-fluoroalkane chains using Boughton-Pulay and CPHF-based domain structures.

The most disturbing feature of the plot in Fig. 5.1 are the CPHF-based cutoffs of 0.15 and 0.20 which have larger % errors than the % errors from the original BP domains. This means that increasing the domain size has resulted in a less accurate calculation of optical rotation. Decreasing the cutoff to 0.10 drops the error to below 5% for each 1-fluoroalkane in the series. It appears as though the CPHF-based domains with a 0.15 and 0.20 cutoff suffer from an unbalanced domain structure leading to large % errors. It is not until the 0.10 cutoff that the domains become balanced and consistently small % errors are achieved.

Realizing the source of the optical activity is due to the stereogenic center at the C_1 carbon may lead to the notion that the PAOs centered on atoms near the stereo center are the most important to include in the domains of nearby occupied orbitals. We tried augmenting the BP domains of spatially close occupied orbitals with PAOs centered on all atoms attached to the C_1 carbon but % errors were still very large. In the case of 1-fluoropropane the % error actually increased from 4.9% to 10.6%. We next attempted to augment the CPHF-based domains with cutoffs of 0.15 and 0.20 in the same manner as we did for the BP domains. The localization errors were still far too large, falling in the range of 5-7% error.

We have also looked at leaving the section of the molecule near the stereogenic center completely untruncated. For the case of 1-fluoropentane, the region of the molecule containing the fluorine atom and carbons 1, 2, and 3 as well as all attached hydrogens were treated in its entirety, without truncation. The remaining area of the molecule employed BP domains, resulting in a 7.62% error in the optical rotation. An analogous calculation on 1-fluoroheptane returned a localization error of 5.67%, indicating that significant contributions to the optical rotation arising from other parts of the molecule outside of the region immediately surrounding the chiral center.

Fig. 5.2 plots the number of T_2 amplitudes used in the various calculations including the number of canonical and local T_2 amplitudes for various local schemes ranging from the BP domains to the CPHF-based domains. It is clear that significant savings are possible with a 0.10 cutoff while maintaining satisfactorily small localization errors. The BP domains show an extreme amount of computational savings but this is at the cost of accuracy in terms of the optical rotation. For 1-fluoroundecane, the BP domains retained only 5% of the T_2 amplitudes to calculate an optical rotation that is off by over 25%. This is simply not acceptable. By contrast, the CPHF-based domains with a cutoff of 0.10 retains 38% of the wave function and returns only a 1.6% error in the optical rotation.

It is worth noting that we have looked at the localization errors at a wavelength of 355 nm. While the actual values of the optical rotation changed greatly, as compared to 589 nm, the %

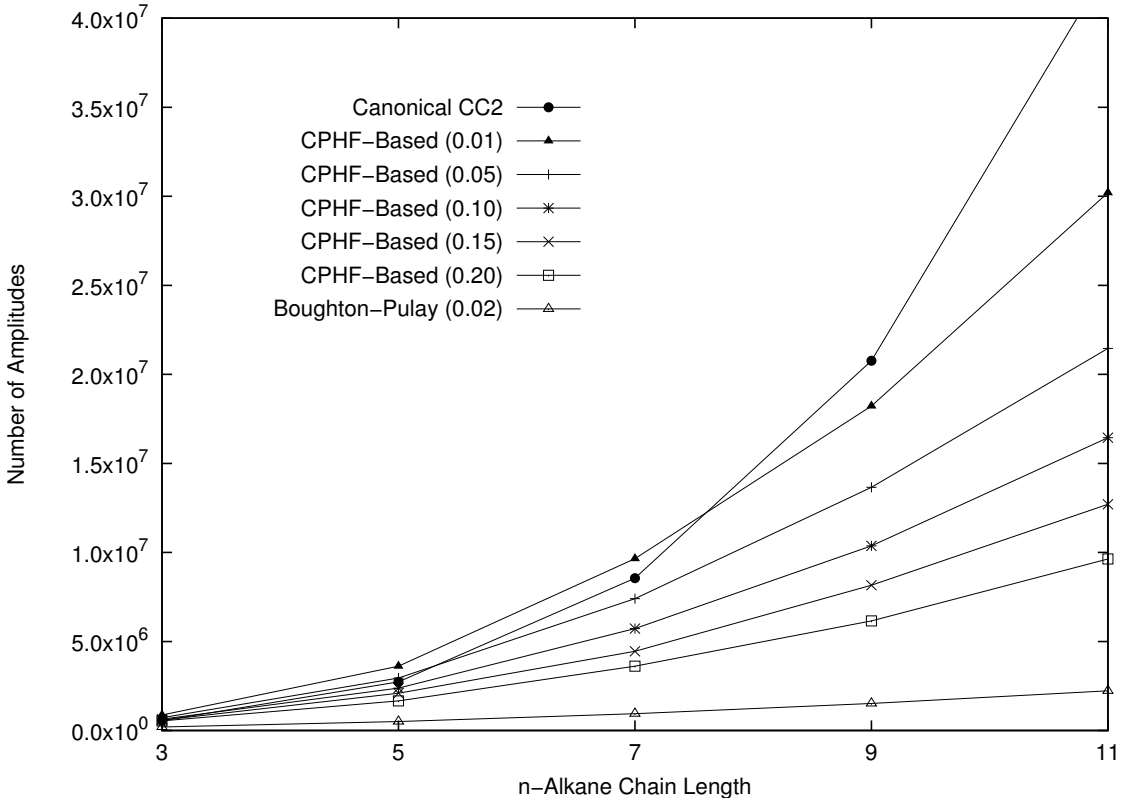

Figure 5.2: Localization errors (%) for CC2/6-31G* optical rotation for 1-fluoroalkane chains using Boughton-Pulay and CPHF-based domain structures.

localization errors changed only very slightly with no qualitative difference in the localization errors between the two wavelengths. Due to the lack of orbital domain dependence on the incident wavelength we can avoid the costly recalculation of all facets of the coupled-cluster calculation with various domain structures, allowing the *a priori* selection of orbital domains immediately following the orbital localization.

Table 5.1: Canonical and local CC2-LR optical rotation (at 589 nm) and % localization errors for a series of 1-fluoroalkane chains using a 6-31G* basis set.

1-Fluoroalkane	Canonical	0.01		0.05		0.10		0.15		0.20		BP	
	$[\alpha]_{589}$	% Error	T_2 Ratio	% Error	T_2 Ratio	% Error	T_2 Ratio	% Error	T_2 Ratio	% Error	T_2 Ratio	% Error	T_2 Ratio
1-fluoropropane	-35.60	-0.04	1.59	0.01	1.30	3.30	1.16	6.93	1.07	18.97	0.99	4.90	0.37
1-fluoropentane	-39.50	-0.53	1.32	-2.35	1.08	0.17	0.87	20.50	0.77	34.45	0.651	13.98	0.18
1-fluoroheptane	-36.89	-0.46	1.13	-0.64	0.87	2.33	0.67	23.58	0.52	29.42	0.42	18.19	0.11
1-fluorononane	-34.83	-0.86	0.88	-1.11	0.66	1.00	0.50	7.68	0.39	16.76	0.30	21.37	0.07
1-fluoroundecane	-33.42	-0.84	0.70	0.21	0.50	1.62	0.38	5.59	0.30	21.21	0.22	23.86	0.05

Table 5.2: Canonical and local CC2-LR optical rotation (at 589 nm) and % localization errors for a series of 1-fluoroalkane chains using a 6-31+G* basis set.

1-Fluoroalkane	Canonical	0.05		0.10		0.15		0.20		BP	
	$[\alpha]_{589}$	% Error	T_2 Ratio	% Error	T_2 Ratio	% Error	T_2 Ratio	% Error	T_2 Ratio	% Error	T_2 Ratio
1-fluoropropane	-79.73	-0.30	1.28	0.27	1.16	4.95	1.13	3.50	1.09	21.79	0.35
1-fluoropentane	-62.55	0.85	1.14	1.45	1.02	0.92	0.96	3.44	0.87	21.38	0.18
1-fluoroheptane	-53.74	1.48	0.99	4.44	0.82	2.59	0.78	1.06	0.71	23.29	0.11
1-fluorononane	-41.93	0.03	0.84	3.10	0.71	2.67	0.62	2.53	0.56	24.29	0.07
1-fluoroundecane	-35.03	-1.10	0.75	2.23	0.61	3.53	0.51	1.80	0.56	25.49	0.05

Table 5.3: Canonical and local CC2-LR optical rotation (at 589 nm) and % localization errors for a series of [n]-triangulanes using a 6-31G* basis set.

[n]-Triangulane	Canonical	0.05		0.10		0.15		BP	
	$[\alpha]_{589}$	% Error	T_2 Ratio	% Error	T_2 Ratio	% Error	T_2 Ratio	% Error	T_2 Ratio
[4]-triangulane	167.94	0.44	0.87	0.99	0.71	1.10	0.63	15.50	0.16
[5]-triangulane	347.40	1.78	0.73	2.08	0.55	1.17	0.50	19.98	0.11
[6]-triangulane	473.28	3.33	0.55	3.78	0.44	4.04	0.40	22.55	0.08
[7]-triangulane	569.44	2.95	0.49	3.97	0.37	4.48	0.32	24.36	0.07

Table 5.4: Canonical and local CC2-LR optical rotation (at 589 nm) and % localization errors for a series of [n]-triangulanes using a 6-31+G* basis set.

[n]-Triangulane	Canonical	0.05		0.10		0.15		BP	
	$[\alpha]_{589}$	% Error	T_2 Ratio	% Error	T_2 Ratio	% Error	T_2 Ratio	% Error	T_2 Ratio
[4]-triangulane	195.54	1.09	1.13	-0.36	1.01	1.68	0.89	14.84	0.16
[5]-triangulane	409.32	0.54	1.04	1.27	0.91	1.50	0.79	14.69	0.12
[6]-triangulane	553.53	0.35	0.97	1.15	0.85	2.18	0.71	14.58	0.13

Table 5.5: Canonical and local CC2-LR optical rotation (at 589 nm) and % localization errors for a β-pinene using a 6-31G* and 6-31+G* basis set.

Basis Set	Canonical	0.01		0.05		0.10		0.15		BP	
	$[\alpha]_{589}$	% Error	T_2 Ratio	% Error	T_2 Ratio	% Error	T_2 Ratio	% Error	T_2 Ratio	% Error	T_2 Ratio
6-31G*	32.68	1.35	1.28	2.66	0.94	3.70	0.57	-9.26	0.51	57.17	0.11
6-31+G*	43.97	-0.53	1.27	-3.33	1.13	-3.15	1.06	-2.94	0.94	63.75	0.14

Plots the optical rotation for the same series of 1-fluoroalkanes as in Fig. 5.1 at 589 nm with a 6-31+G* basis set using the BP and CPHF-based domains with cutoffs from 0.05 to 0.20 are shown in Fig. 5.3. The inclusion of diffuse functions into the basis set made very little difference in the % errors associated of the BP domains, except at the smaller molecular sizes where the error is much larger for the 6-31+G* basis set. However, the asymptotic limit of the % error appears to be approximately the same between the two basis sets. By contrast, the % errors for the CPHF-based domains change drastically as diffuse functions are added to the basis set. The largest CPHF-based cutoff of 0.20 provide localization errors below 5% for all 1-fluoroalkanes. However, to ensure errors below *ca.* 2% it is necessary to use a cutoff of 0.05.

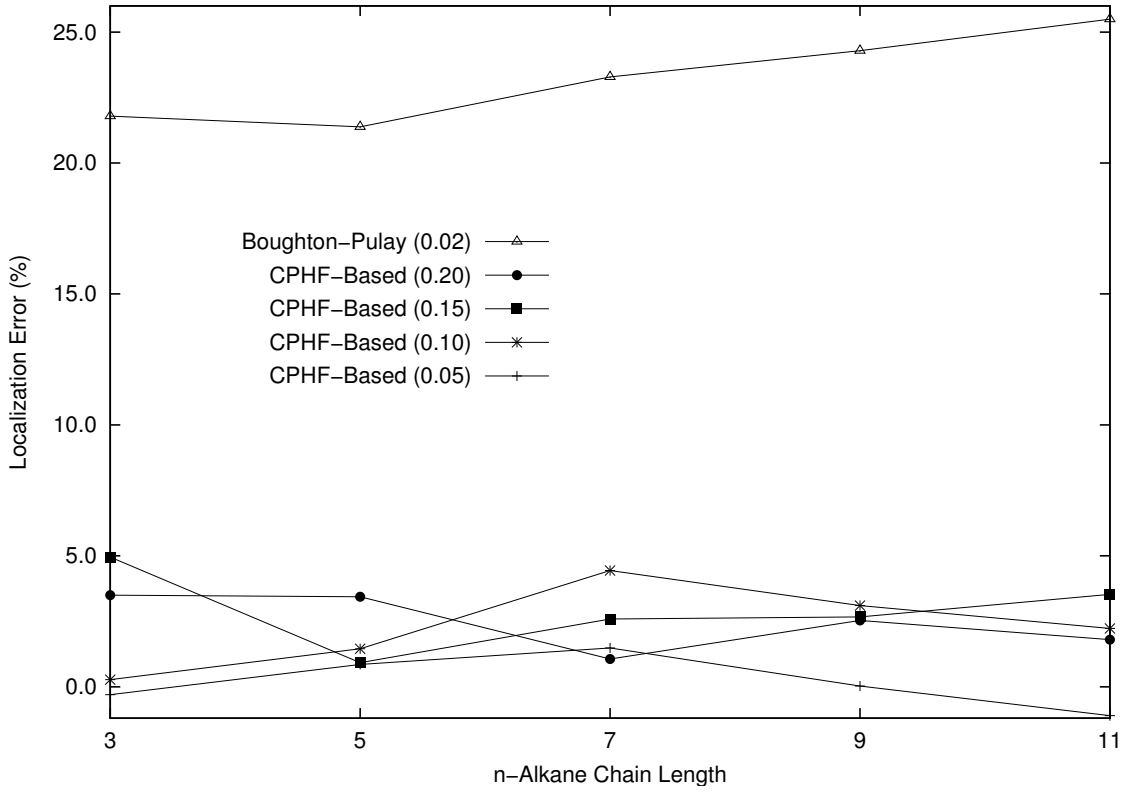

Figure 5.3: Localization errors (%) for CC2/6-31+G* optical rotation for 1-fluoroalkane chains using Boughton-Pulay and CPHF-based domain structures.

The difference in the CPHF-based domain structure due to the inclusion of diffuse basis

functions is easy to glean from figs. 5.2 and 5.4. It is clear that the decrease in localization error is due, in part, to the larger domains associated with 6-31+G* basis set as evidenced by the steeper slope in the Fig. 5.4 than in Fig. 5.2. The domain sizes shift from about 5-6 atoms in the 6-31G* basis to about 6-8 atoms in the 6-31+G* basis set for a 0.10 cutoff.

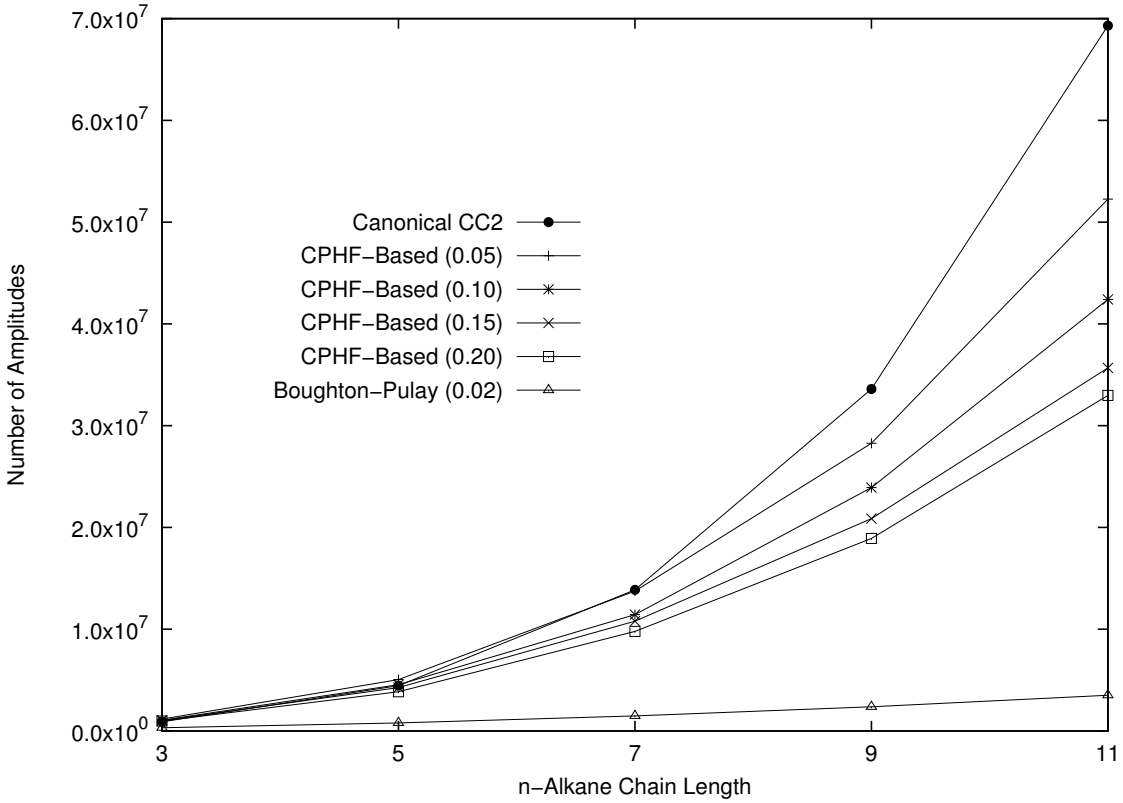

Figure 5.4: Localization errors (%) for CC2/6-31+G* optical rotation for 1-fluoroalkane chains using Boughton-Pulay and CPHF-based domain structures.

We have also performed calculations on a series of [n]-triangulanes ranging from [4]-triangulane to [6]-triangulane, reported in Table 5.3 and 5.4 for 6-31G* and 6-31+G* basis sets, respectively. One notable difference between the series of 1-fluoroalkanes and [n]-triangulanes are the much smaller localization errors for the [n]-triangulanes in the 6-31G* basis. Localization errors fall below 5% and 2% for all [n]-triangulanes using a 6-31G* and 6-31+G* basis set, respectively, within the CPHF-based domain structure. The BP domains also show lower localization errors for the [n]-triangulanes as compared to the series of 1-fluoroalkanes.

The localization errors are still far too large with, ranging from 15-20% and just under 15% for the 6-31G* and 6-31+G* basis sets, respectively. The difference in localization errors could be due to the manifestation of optical activity within each molecular system. The [n]-triangulanes are helical structures with C_2 symmetry and have a chiral axis as compared to the 1-fluoroalkanes, which have no symmetry and a chiral center.

The most troubling aspect comparing the 1-fluoroalkane chains to the series of [n]-triangulanes is the fact that the optical rotation is relatively invariant to chain length for the 1-fluoroalkanes, which implies that the source of the optical activity is localized to the CH_2F- end of the molecule. However, based on the local correlation calculations performed here, it is clear that significant contributions to the optical rotation arise from other parts of the molecule away from the stereogenic carbon. By contrast, the series of [n]-triangulanes changes dramatically as the molecule increases length, indicating that the source of optical activity is distributed across the entire molecular framework. However, the localization error associated with the set [n]-triangulanes is smaller than those for the 1-fluoroalkanes.

We have also performed optical rotation calculations on the β-pinene molecule which has two stereogenic centers. Table 5.5 lists the localization errors for the BP and CPHF-based domains. It is clear that this molecular system proposes an even greater challenge to obtaining small localization errors than the series of 1-fluoroalkanes. This is most likely due to the fact the β-pinene has two chiral centers, leading to localization errors ranging from about 3-9% for the CPHF based domains. The BP domains exhibit a gross shortcoming in predicting the optical rotation with a localization error of 57% within the 6-31G* basis and over 63% for the 6-31+G* basis set. It is clear that further work must be done to achieve small localization errors in the optical rotation for molecules that possess one or more a chiral centers.

5.5 Conclusions

The ability to predict the local domain structure for achieve a reduced scaling algorithm with sufficiently small % errors has achieved limited success for the calculation of optical rotation. The 1-fluoroalkane chains have proved to be much more problematic than expected, especially with a 6-31G* basis set. However, most of the difficulty disappears with the inclusion of diffuse basis functions. Surprisingly, the series of [n]-triangulanes were better behaved than the 1-fluoroalkanes. Our preliminary conclusion is that this is due to the source of optical activity. It appears as though a chiral axis lends itself to a local correlation description more readily than does a molecule with a stereogenic center. This is further confirmed by β-pinene, whose % localization errors are even larger than those calculated for the series of 1-fluoroalkanes, most likely due to the two stereogenic carbons within the framework of the β-pinene molecule.

Chapter 6

Efficient Implementation of Local Correlation for the Calculation of Molecular Energies

Implementing local correlation within quantum chemical methods introduces several complications. First, the Pipek-Mezey localization procedure destroys the canonical nature of the MOs, leading to an iterative algorithm for solving the MP2 amplitude equations. A second complication introduced by local correlation is the use of a nonorthogonal, redundant virtual space, requiring a pairwise transformation of the T amplitudes and residuals (*vide infra*) at each iteration, along with the removal of linear dependencies for each pair. Also, all equations written in the virtual MO basis must be transformed into the PAO basis resulting in multiplications of the overlap matrix, $\tilde{\mathbf{S}}$. The manner of dealing with these complications will be addressed in the following sections as well as a complete reformulation of the MP2 and CC2 amplitude equations.

6.1 Impact of Noncanonical MOs

Recall the MP2 amplitude equation as

$$\langle ab||ij\rangle + \sum_e \left(t_{ij}^{ae} f_{eb} + t_{ij}^{eb} f_{ae}\right) - \sum_m \left(t_{im}^{ab} f_{mj} + t_{mj}^{ab} f_{im}\right) = 0 \tag{6.1}$$

Employing canonical MOs (*i.e.* $f_{p\neq q} = 0$), eliminates the summations in the above equation and the MP2 T_2 amplitudes can be solved directly though the use of energy denominators (see eqn. 1.68). A basis for which the Fock matrix is not diagonal results in a coupling of the T_2 amplitudes to themselves and the set of T_2 equations must be solved iteratively.

Iteratively solving the T_2 amplitude equations requires an initial guess as well as an update procedure. The initial guess is usually taken to be the two-electron integrals (*i.e.* $R_{ij}^{ab} = \langle ab||ij\rangle$, which is the leading term in the MP2 T_2 equation) and a set of residuals are commonly used to provide updates to the T_2 amplitudes:

$$\Delta t_{ij}^{ab} = \frac{R_{ij}^{ab}}{f_{ii} + f_{jj} - f_{aa} - f_{bb}} \tag{6.2}$$

Where the residuals, R_{ij}^{ab}, are defined as

$$R_{ij}^{ab} = \langle ab||ij\rangle + \sum_e \left(t_{ij}^{ae} f_{be} + t_{ij}^{eb} f_{ae}\right) - \sum_m \left(t_{im}^{ab} f_{mj} + t_{mj}^{ab} f_{im}\right) \tag{6.3}$$

The ΔT_2 from eqn. 6.2 is added to the original T_2's to recompute the residual from eqn. 6.3. The new residual leads to a new ΔT_2 and so on, until the norm of the residual falls below a prescribed cutoff. Convergence is normally accelerated through the use of DIIS (direct inversion of the iterative subspace).[139,140]

6.2 Impact of a Nonorthogonal, Redundant Virtual Space

The iterative solution to the MP2 and CC2 amplitude equations requires the use of diagonal elements of the Fock matrix (*e.g.*, eqn. 6.2), assumed to be diagonally dominant. However,

the use of a nonorthogonal, redundant virtual space destroys the diagonal dominance in the virtual-virtual block of the Fock matrix, causing convergence problems. Dividing the residual by diagonal elements of the Fock matrix, as in eqn. 6.2 requires a transformation to a basis for which Fock matrix is diagonally dominant (we will go one step further and enforce a canonical basis). A matrix, $\mathbf{W}_{[ij]}$, is constructed to handle the transformation from the PAO space to an orthogonal, nonredundant (and canonical) virtual space specific for each ij pair, denoted by the subscript $[ij]$. This process can be viewed as a 'mini-canonicalization' of the PAO space specific to each ij pair.

The residuals from eqn. 6.3, rewritten in the PAO space ($R^{\alpha\beta}_{[ij]}$), are transformed to the mini-canonical space by the $\mathbf{W}_{[ij]}$ matrix:

$$\bar{R}^{ab}_{[ij]} = \sum_{\alpha\beta} W^{\alpha a}_{[ij]} \tilde{R}^{\alpha\beta}_{[ij]} W^{\beta b}_{[ij]} \tag{6.4}$$

where the over-bar denotes a quantity in the mini-canonical space and reiterated by indices $a, b, \ldots$ and the Greek indices $\alpha, \beta, \ldots$ are used to denote an AO basis function. The update to the T_2 amplitude equations, in the canonical space, can now be obtained by

$$\Delta\bar{t}^{ab}_{[ij]} = \frac{\bar{R}^{ab}_{[ij]}}{f_{ii} + f_{jj} - \epsilon^{a}_{[ij]} - \epsilon^{b}_{[ij]}} \tag{6.5}$$

where the $\epsilon^{a}_{[ij]}$ and $\epsilon^{b}_{[ij]}$ are diagonal elements of the orbital energies within the mini-canonical space. The $\Delta\bar{t}^{ab}_{[ij]}$ is then transformed back to the original PAO space using the $W_{[ij]}$ matrix similar to eqn. 6.4,

$$\Delta\tilde{t}^{\alpha\beta}_{[ij]} = \sum_{ab} W^{\alpha a}_{[ij]} \Delta\bar{t}^{ab}_{[ij]} W^{\beta b}_{[ij]} \tag{6.6}$$

where the $\Delta\tilde{t}^{\alpha\beta}_{[ij]}$ can easily be added to the original $\tilde{t}^{\alpha\beta}_{[ij]}$ amplitudes to obtain a new set of T_2 amplitudes. What remains now is to build the $\mathbf{W}_{[ij]}$ matrix for each ij pair.

Constructing the $\mathbf{W}_{[ij]}$ Matrices

A separate $\mathbf{W}_{[ij]}$ matrix is constructed for each ij pair to transform the residuals and T amplitudes from the nonorthogonal, redundant PAO space to a virtual space that is orthogonal,

nonredundant and also canonical. There are several steps that need to be taken to build the set of $\mathbf{W}_{[ij]}$ matrices. We have chosen to follow the procedure outlined by Hampel and Werner.[63] The first step is to diagonalize the overlap matrix in the PAO basis, *e.g.*,

$$\mathbf{X}^{\dagger}\tilde{\mathbf{S}}\mathbf{X} = \tilde{\mathbf{s}} \tag{6.7}$$

where $\tilde{\mathbf{s}}$ and $\mathbf{X}$ are the eigenvalues and eigenfunctions, respectively. The subscript $[ij]$ in the above and all remaining equations in this section have been omitted for the sake of readability. Small eigenvalues correlate to linear dependencies in the PAO space and are thus eliminated followed by renormalizing the eigenvectors:

$$X_{ab} = \begin{cases} \frac{X_{ab}}{\sqrt{\tilde{s}_b}} & \text{if } \tilde{s}_b > 10^{-6} \\ 0 & \text{if } \tilde{s}_b \leq 10^{-6} \end{cases} \tag{6.8}$$

The remaining eigenfunctions form an orthonormal basis and are used to transform the Fock matrix as

$$\bar{\mathbf{F}} = \mathbf{X}^{\dagger}\tilde{\mathbf{F}}\mathbf{X} \tag{6.9}$$

The Fock matrix is now represented in an orthogonal, nonredundant basis that spans the same space as the original PAO basis. This new Fock matrix can now be diagonalized in a similar manner to the overlap matrix to obtain eigenvectors and eigenvalues by

$$\mathbf{U}^{\dagger}\bar{\mathbf{F}}\mathbf{U} = \epsilon \tag{6.10}$$

The $\mathbf{U}$ matrix is the usual unitary transformation matrix normally associated with the Fock matrix in the canonical basis (restricted to a particular ij pair) and ϵ are the eigenvalues.

The $\mathbf{X}$ defined in eqn. 6.8 provides a transformation from the PAO basis to an orthogonal, nonredundant basis that spans the same space as the original PAO space. The $\mathbf{U}$ matrix from eqn. 6.10 furnishes a transformation from the orthogonal, nonredundant basis to a canonical basis. Combing these two matrices forms the $\mathbf{W}$ transformation matrix:

$$\mathbf{W} = \mathbf{X}\mathbf{U} \tag{6.11}$$

The procedure used to build the $\mathbf{W}$ matrix is repeated for each ij pair producing a different $\mathbf{W}$ matrix for each ij pair, represented by the subscript $[ij]$ as, $\mathbf{W}_{[ij]}$.

6.3 Local MP2 and CC2

In order to efficiently implement local correlation within the MP2 or CC2 framework, we must present the T amplitude equations in terms of the PAO basis. One way to achieve this is to use a tensor based formulation and completely rederive the T amplitude equations already presented by Head-Gordon *et al.*[52] Another method is to 'back-transform' the normal MO expression into the PAO basis using a transformation matrix, which will be shown in this work. Since the PAOs are just 'pieces' of AOs, the transformation properties that apply for quantities in the AO basis also apply to quantities in the PAO basis, with the only difference being the specific transformation matrix employed. Quantities in the PAO or AO basis can be easily transformed to the MO basis using the $\tilde{\mathbf{C}}$ or $\mathbf{C}$ matrix, respectively. In the final T amplitude equations, the transformation matrix multiplications are relegated to multiplications by the PAO, or AO, basis overlap matrix, $\tilde{\mathbf{S}}$, or $\mathbf{S}$ *vide infra.* For this reason we will formulate all equations using the AO basis and the $\mathbf{C}$ matrix, where in the end all occurrences of $\mathbf{S}$ are replaced by $\tilde{\mathbf{S}}$ to represent the use of a PAO basis. As a result, the PAO to MO transformation matrix, $\tilde{\mathbf{C}}$, never needs to be formulated, only the PAO basis overlap matrix, $\tilde{\mathbf{S}}$.

Quantities in the AO basis can be easily transformed to the MO basis using the coefficient matrix, $\mathbf{C}$, defined by Hartree-Fock theory. For example,

$$S_{pq} = \sum_{\mu\nu} C_{\mu p} S_{\mu\nu} C_{\nu q} \tag{6.12}$$

Where μ and ν represent AOs and p and q represent MOs. Transforming the MO basis quantities to the AO basis is achieved by multiplying the above equations by $\mathbf{C}^{-1}$, as

$$S_{\mu\nu} = \sum_{pq} C^{-1}_{\mu p} S_{pq} C^{-1}_{\nu q} \tag{6.13}$$

Recalling that the overlap matrix in the MO basis is the identity matrix ($S_{pq} = \delta_{pq}$), reveals a special relationship between the AO basis overlap matrix and the $\mathbf{C}^{-1}$ matrix,

$$S_{\mu\nu} = \sum_{a} C^{-1}_{\mu p} C^{-1}_{\nu p} \tag{6.14}$$

The residuals of eqn. 6.3 function similarly to the Fock and overlap matrices above with the exception that the transformation must be performed separately for each ij pair, *e.g.*,

$$R^{\alpha\beta}_{[ij]} = \sum_{ab} C^{-1}_{\alpha a} R^{ab}_{[ij]} C^{-1}_{\beta b} \tag{6.15}$$

$$R^{ab}_{[ij]} = \sum_{\alpha\beta} C_{\alpha a} R^{\alpha\beta}_{[ij]} C_{\beta b} \tag{6.16}$$

where we have used a and b to represent virtual MOs and the indices α and β to represent AOs specifically transformed from the virtual MO space.

All of the above quantities have units of energy, by contrast, the T amplitudes are unitless. Thus, their transformation properties are reversed from those listed above[47,141,142]

$$t^{\alpha\beta}_{[ij]} = \sum_{ab} C_{\alpha a} t^{ab}_{[ij]} C_{\beta b} \tag{6.17}$$

$$t^{ab}_{[ij]} = \sum_{\alpha\beta} C^{-1}_{\alpha a} t^{\alpha\beta}_{[ij]} C^{-1}_{\beta b} \tag{6.18}$$

In summary, the pertinent equations for transforming from the MO basis to the PAO basis (instead of the AO basis) are listed below:[142]

$$\tilde{S}_{\alpha\beta} = \sum_{p} C^{-1}_{\alpha a} C^{-1}_{\beta p} \tag{6.19}$$

$$S_{ab} = \sum_{\alpha\beta} C_{\alpha a} \tilde{S}_{\alpha\beta} C_{\beta b} \tag{6.20}$$

$$F_{ab} = \sum_{\alpha\beta} C_{\alpha a} \tilde{F}_{\alpha\beta} C_{\beta b} \tag{6.21}$$

$$K^{ab}_{[ij]} = \sum_{\alpha\beta} C_{\alpha a} \tilde{K}^{\alpha\beta}_{[ij]} C_{\beta b} \tag{6.22}$$

$$R^{ab}_{[ij]} = \sum_{\alpha\beta} C_{\alpha a} \tilde{R}^{\alpha\beta}_{[ij]} C_{\beta b} \tag{6.23}$$

$$t^{ab}_{[ij]} = \sum_{\alpha\beta} C^{-1}_{\alpha a} \tilde{t}^{\alpha\beta}_{[ij]} C^{-1}_{\beta b} \tag{6.24}$$

Where the tildes represent quantities in the PAO basis and the indices α and β are used to re-enforce that only the virtual orbitals are in the PAO basis. We have introduced a two-electron integral as $K^{ab}_{[ij]} = \langle ab||ij\rangle$, which is the leading term in the MP2 amplitude equations (eqn. 6.3)

6.3.1 The MP2 Equations in a Nonorthogonal Virtual Basis

Starting from the MO expression for the MP2 amplitude from eqn. 6.3, and using the expressions from eqns. 6.19-6.24, the MP2 amplitude equations can be rewritten as

$$\begin{aligned}\sum_{\alpha'\beta'} C_{\alpha' a}\tilde{R}^{\alpha'\beta'}_{[ij]}C_{\beta' b} &= \sum_{\alpha'\beta'} C_{\alpha' a}\tilde{K}^{\alpha'\beta'}_{[ij]}C_{\beta' b} \\ &+ \sum_{e}\left(\sum_{\alpha'\epsilon} C^{-1}_{\alpha' a}\tilde{t}^{\alpha'\epsilon}_{[ij]}C^{-1}_{\epsilon e}\sum_{\beta'\epsilon} C_{\epsilon e}\tilde{f}_{\epsilon\beta'}C_{\beta' b} + \sum_{\alpha'\epsilon} C_{\alpha' a}\tilde{f}_{\alpha'\epsilon}C_{\epsilon e}\sum_{\beta'\epsilon} C^{-1}_{\epsilon e}\tilde{t}^{\epsilon\beta'}_{[ij]}C^{-1}_{\beta' b}\right) \\ &- \sum_{m}\left(\sum_{\alpha'\beta'} C^{-1}_{\alpha' a}\tilde{t}^{\alpha'\beta'}_{[im]}C^{-1}_{\beta' b}f_{mj} + \sum_{\alpha'\beta'} C^{-1}_{\alpha' a}\tilde{t}^{\alpha'\beta'}_{[mj]}C^{-1}_{\beta' b}f_{im}\right) \qquad (6.25)\end{aligned}$$

Where we have use α' and β', due to subsequent multiplications by $C^{-1}_{\alpha a}$ and $C^{-1}_{\beta b}$ (*vide infra*). Looking at both terms that depend on the summation over e we see only two quantities that depend on the e index, $C^{-1}_{\epsilon e}$ and $C_{\epsilon e}$. Performing the summation over e reveals the identity matrix (*i.e.*, $\mathbf{C}^{-1}\mathbf{C} = \mathbf{1}$). Eqn. 6.25 can be further simplified by multiplying by $C^{-1}_{\alpha a}$ on the left and $C^{-1}_{\beta b}$ on the right. Substituting all instances of $\sum_a C^{-1}_{\alpha a}C_{\alpha' a}$ with the identity matrix yields

$$\begin{aligned}\tilde{R}^{\alpha\beta}_{[ij]} &= \tilde{K}^{\alpha\beta}_{[ij]} + \sum_{a\alpha'\epsilon}(C^{-1}_{\alpha a}C^{-1}_{\alpha' a})\tilde{t}^{\alpha'\epsilon}_{[ij]}\tilde{f}_{\epsilon b} + \sum_{b\beta'\epsilon}(C^{-1}_{\beta b}C^{-1}_{\beta' b})\tilde{t}^{\epsilon\beta'}_{[ij]}\tilde{f}_{\alpha\epsilon} \qquad (6.26) \\ &- \sum_{m}\left(\sum_{ab\alpha'\beta'}(C^{-1}_{\alpha a}C^{-1}_{\alpha' a})\tilde{t}^{\alpha'\beta'}_{[im]}(C^{-1}_{\beta b}C^{-1}_{\beta' b})f_{mj} + \sum_{ab\alpha'\beta'}(C^{-1}_{\alpha a}C^{-1}_{\alpha' a})\tilde{t}^{\alpha'\beta'}_{[mj]}(C^{-1}_{\beta b}C^{-1}_{\beta' b})f_{im}\right)\end{aligned}$$

This equation can be greatly simplified by replacing $\mathbf{C}^{-1}\mathbf{C}^{-1}$ by the overlap matrix in the PAO basis, *i.e.*

$$\sum_{a} C^{-1}_{\alpha a}C^{-1}_{\alpha' a} = \tilde{S}^{\alpha}_{\alpha'} \qquad (6.27)$$

The final form of the MP2 T_2 equations is

$$\begin{aligned}\tilde{R}^{\alpha\beta}_{[ij]} &= \tilde{K}^{\alpha\beta}_{[ij]} + \sum_{\alpha'\epsilon}(S^{\alpha_{[ij]}}_{\alpha'_{[ij]}}\tilde{t}^{\alpha'\epsilon}_{[ij]})f_{\epsilon_{[ij]}\beta_{[ij]}} + \sum_{\beta'\epsilon}(S^{\beta_{[ij]}}_{\beta'_{[ij]}}\tilde{t}^{\epsilon\beta'}_{[ij]})f_{\alpha_{[ij]}\epsilon_{[ij]}} \\ &- \sum_{m\alpha'\beta'}(S^{\alpha_{[ij]}}_{\alpha'_{[im]}}\tilde{t}^{\alpha'\beta'}_{[im]}S^{\beta_{[ij]}}_{\beta'_{[im]}})f_{mj} - \sum_{m\alpha'\beta'}(S^{\alpha_{[ij]}}_{\alpha'_{[mj]}}\tilde{t}^{\alpha'\beta'}_{[mj]}S^{\beta_{[ij]}}_{\beta'_{[mj]}})f_{im} \qquad (6.28)\end{aligned}$$

Where the subscript $[ij]$ has been added to explicitly indicate the domain of each PAO index (except POA indices on four-dimensional quantities where the domain is obvious due to the already included subscript $[ij]$). The inclusion of domains on each PAO index further reveals the need for multiplications by the PAO basis overlap matrix where the domains of α and α' can be different. In some cases, the multiplication by $\tilde{\mathbf{S}}$ can be thought of as a domain transformation between the the domains of α and α'.

6.3.2 The CC2 Equations in a Nonorthogonal Virtual Basis

Formulating the CC2 equations in the PAO basis employs all of the same concepts and identities described above for the transformation of the MP2 T_2 equations. The biggest difference between CC2 and MP2 is that CC2 has a T_1 and T_2 equation and there are many more terms in the T_2 equation. CC2 T_1 and T_2 equations in the MO basis are, for the T_1 equation

$$\begin{aligned} R_i^a &= f_{ai} + \sum_e t_i^e f_{ae} - \sum_m t_m^a f_{mi} - \sum_{me} t_i^e t_m^a f_{me} + \sum_{me} t_m^e \langle am||ie\rangle + \sum_{mef} t_i^e t_m^f \langle am||ef\rangle \\ &\quad - \sum_{mne} t_m^a t_n^e \langle mn||ie\rangle - \sum_{mnef} t_m^a t_i^e t_n^f \langle mn||ef\rangle + \sum_{me} t_{im}^{ae} f_{me} + \frac{1}{2}\sum_{mef} t_{im}^{ef} \langle am||ef\rangle \\ &\quad - \frac{1}{2}\sum_{mne} t_{mn}^{ae} \langle mn||ie\rangle + \sum_{mnef} t_{im}^{ae} t_n^f \langle mn||ef\rangle - \frac{1}{2}\sum_{mnef} t_i^e t_{mn}^{af} \langle mn||ef\rangle - \frac{1}{2}\sum_{mnef} t_m^a t_{in}^{ef} \langle mn||ef\rangle \end{aligned} \tag{6.29}$$

and for the T_2 equation

$$\begin{aligned} R_{ij}^{ab} &= \langle ab||ij\rangle + P(ab)\sum_e t_{ij}^{ae} f_{eb} - P(ij)\sum_m t_{im}^{ab} f_{mj} + P(ij)\sum_e t_i^e \langle ab||ej\rangle - P(ab)\sum_m t_m^a \langle mb||ij\rangle \\ &\quad + P(ij)\sum_{ef} t_i^e t_j^f \langle ab||ef\rangle + P(ab)\sum_{mn} t_m^a t_n^b \langle mn||ij\rangle - P(ij)P(ab)\sum_{me} t_i^e t_m^a \langle mb||ej\rangle \\ &\quad - \frac{1}{2}P(ij)P(ab)\sum_{mef} t_i^e t_j^f t_m^b \langle am||ef\rangle - \frac{1}{2}P(ij)P(ab)\sum_{mne} t_j^e t_m^a t_n^b \langle mn||ie\rangle \\ &\quad + \frac{1}{4}P(ij)P(ab)\sum_{mnef} t_i^e t_j^f t_m^a t_n^b \langle mn||ef\rangle \end{aligned} \tag{6.30}$$

The CC2 T_1 and T_2 equations are never implemented as shown in eqns. 6.29 and 6.30. The T_1 and T_2 equations are always factorized by intermediate quantities to greatly reduce the

scaling from $\mathcal{O}(N^8)$, as shown, to $\mathcal{O}(N^5)$.

As stated above, the same procedure for transforming the MP2 T_2 equations from the MO to the PAO basis can be applied to transform the CC2 T amplitude equations. After transformation, the T_1 equation becomes

$$\begin{aligned}
R^{\alpha}_{[i]} &= f_{\alpha_{[i]}i} + \sum_{\epsilon} t^{\epsilon}_{[i]} f_{\alpha_{[i]}\epsilon_{[i]}} - \sum_{m\alpha'} (t^{\alpha'}_{[m]} S^{\alpha_{[i]}}_{\alpha'_{[m]}}) f_{mi} - \sum_{m\epsilon\alpha'} t^{\epsilon}_{[i]} (t^{\alpha'}_{[m]} S^{\alpha_{[i]}}_{\alpha'_{[m]}}) f_{m\epsilon_{[i]}} \\
&+ \sum_{m\epsilon} t^{\epsilon}_{[m]} \langle \alpha_{[i]} m || i \epsilon_{[m]} \rangle + \sum_{m\epsilon\gamma} t^{\gamma}_{[m]} t^{\epsilon}_{[i]} \langle \alpha_{[i]} m || \epsilon_{[i]} \gamma_{[m]} \rangle \\
&- \sum_{mn\epsilon\alpha'} t^{\epsilon}_{[n]} (t^{\alpha'}_{[m]} S^{\alpha_{[i]}}_{\alpha'_{[m]}}) \langle mn || i \epsilon_{[n]} \rangle - \sum_{mn\epsilon\gamma\alpha'} t^{\gamma}_{[n]} t^{\epsilon}_{[i]} (t^{\alpha'}_{[m]} S^{\alpha_{[i]}}_{\alpha'_{[m]}}) \langle mn || \epsilon_{[i]} \gamma_{[n]} \rangle \\
&+ \sum_{m\epsilon\alpha'} (t^{\alpha'\epsilon}_{[im]} S^{\alpha_{[i]}}_{\alpha'_{[im]}}) f_{m\epsilon_{[im]}} + \frac{1}{2} \sum_{m\epsilon\gamma} t^{\epsilon\gamma}_{[im]} \langle \alpha_{[i]} m || \epsilon_{[im]} \gamma_{[im]} \rangle \\
&- \frac{1}{2} \sum_{mn\epsilon\alpha'} (t^{\alpha'\epsilon}_{[mn]} S^{\alpha_{[i]}}_{\alpha'_{[mn]}}) \langle mn || i \epsilon_{[mn]} \rangle + \sum_{mn\epsilon\gamma\alpha'} t^{\gamma}_{[n]} (t^{\alpha'\epsilon}_{[im]} S^{\alpha_{[i]}}_{\alpha'_{[im]}}) \langle mn || \epsilon_{[im]} \gamma_{[n]} \rangle \\
&- \frac{1}{2} \sum_{mn\epsilon\gamma\alpha'} t^{\epsilon}_{[i]} (t^{\alpha'\gamma}_{[mn]} S^{\alpha_{[i]}}_{\alpha'_{[mn]}}) \langle mn || \epsilon_{[i]} \gamma_{[mn]} \rangle \\
&- \frac{1}{2} \sum_{mn\epsilon\gamma\alpha'} t^{\epsilon\gamma}_{[in]} (t^{\alpha'}_{[m]} S^{\alpha_{[i]}}_{\alpha'_{[m]}}) \langle mn || \epsilon_{[in]} \gamma_{[in]} \rangle
\end{aligned} \tag{6.31}$$

and the T_2 equation

$$\begin{aligned}
R^{\alpha\beta}_{[ij]} &= \langle \alpha_{[ij]} \beta_{[ij]} || ij \rangle + P(\alpha\beta) \sum_{\epsilon\beta'} (t^{\beta'\epsilon}_{[ij]} S^{\beta_{[ij]}}_{\beta'_{[ij]}}) f_{\alpha_{[ij]}\epsilon_{[ij]}} - P(ij) \sum_{m\alpha'\beta'} (t^{\alpha'\beta'}_{[jm]} S^{\alpha_{[ij]}}_{\alpha'_{[jm]}} S^{\beta_{[ij]}}_{\beta'_{[jm]}}) f_{mi} \\
&+ P(ij) \sum_{\epsilon} t^{\epsilon}_{[i]} \langle \alpha_{[ij]} \beta_{[ij]} \epsilon_{[i]} || j \rangle - P(\alpha\beta) \sum_{m\alpha'} (t^{\alpha'}_{[m]} S^{\alpha_{[ij]}}_{\alpha'_{[m]}}) \langle m \beta_{[ij]} || ij \rangle \\
&+ P(ij) \sum_{\epsilon\gamma} t^{\epsilon}_{[i]} t^{\gamma}_{[j]} \langle \alpha_{[ij]} \beta_{[ij]} || \epsilon_{[i]} \gamma_{[j]} \rangle + P(\alpha\beta) \sum_{mn\alpha'\beta'} (t^{\alpha'}_{[m]} S^{\alpha_{[ij]}}_{\alpha'_{[m]}}) (t^{\beta'}_{[n]} S^{\beta_{[ij]}}_{\beta'_{[n]}}) \langle mn || ij \rangle \\
&- P(ij) P(\alpha\beta) \sum_{m\epsilon\alpha'} t^{\epsilon}_{[i]} (t^{\alpha'}_{[m]} S^{\alpha_{[ij]}}_{\alpha'_{[m]}}) \langle m \beta_{[ij]} || \epsilon_{[i]} j \rangle \\
&- \frac{1}{2} P(ij) P(\alpha\beta) \sum_{m\epsilon\gamma\beta'} t^{\epsilon}_{[i]} t^{\gamma}_{[j]} (t^{\beta'}_{[m]} S^{\beta_{[ij]}}_{\beta'_{[m]}}) \langle \alpha_{[ij]} m || \epsilon_{[i]} \gamma_{[j]} \rangle \\
&- \frac{1}{2} P(ij) P(\alpha\beta) \sum_{mn\epsilon\alpha'\beta'} t^{\epsilon}_{[j]} (t^{\alpha'}_{[m]} S^{\alpha_{[ij]}}_{\alpha'_{[m]}}) (t^{\beta'}_{[n]} S^{\beta_{[ij}}_{\beta'_{[n]}}) \langle mn || i \epsilon_{[j]} \rangle \\
&+ \frac{1}{4} P(ij) P(\alpha\beta) \sum_{mn\epsilon\gamma\alpha'\beta'} t^{\epsilon}_{[i]} t^{\gamma}_{[j]} (t^{\alpha'}_{[m]} S^{\alpha_{[ij]}}_{\alpha'_{m]}}) (t^{\beta'}_{[n]} S^{\beta_{[ij]}}_{\beta'_{[n]}}) \langle mn || \epsilon_{[i]} \gamma_{[j]} \rangle
\end{aligned} \tag{6.32}$$

6.3.3 Intermediate Quantities

The T_1 and T_2 equations can be factored into a much more efficient form as follows, for T_1

$$\begin{aligned} R^{\alpha}_{[i]} &= f_{\alpha_{[i]}i} + \sum_{\epsilon} t^{\epsilon}_{[i]} F_{\alpha_{[i]}\epsilon_{[i]}} - \sum_{m\alpha'} (t^{\alpha'}_{[m]} S^{\alpha_{[i]}}_{\alpha'_{[m]}}) F_{mi} - \sum_{m\epsilon\alpha'} (t^{\alpha'\epsilon}_{[im]} S^{\alpha_{[i]}}_{\alpha'_{[m]}}) F_{m\epsilon_{[im]}} + \sum_{m\epsilon} t^{\epsilon}_{[im]} \langle \alpha_{[i]} m || i\epsilon_{[m]} \rangle \\ &+ \frac{1}{2} \sum_{m\epsilon\gamma} t^{\epsilon\gamma}_{[im]} \langle \alpha_{[i]} m || \epsilon_{[im]} \gamma_{[im]} \rangle - \frac{1}{2} \sum_{mn\epsilon\alpha'} (t^{\alpha'\epsilon}_{[mn]} S^{\alpha_{[i]}}_{\alpha'_{[mn]}}) W_{mni\epsilon_{[mn]}} \end{aligned} \tag{6.33}$$

and for T_2

$$\begin{aligned} R^{\alpha\beta}_{[ij]} &= \langle \alpha_{[ij]} \beta_{[ij]} || ij \rangle + P(\alpha\beta) \sum_{\epsilon\beta'} (t^{\beta'\epsilon}_{[ij]} S^{\beta_{[ij]}}_{\beta'_{[ij]}}) f_{\alpha_{[ij]}\epsilon_{[ij]}} - P(ij) \sum_{m\alpha'\beta'} (t^{\alpha'\beta'}_{[jm]} S^{\alpha_{[ij]}}_{\alpha'_{[jm]}} S^{\beta_{[ij]}}_{\beta'_{[jm]}}) f_{mi} \\ &- P(\alpha\beta) \sum_{m\alpha'} (t^{\alpha'}_{[m]} S^{\alpha_{[ij]}}_{\alpha'_{[m]}}) W_{m\beta_{[ij]}ij} + P(ij) \sum_{\epsilon} t^{\epsilon}_{[i]} W_{\alpha_{[ij]}\beta_{[ij]}\epsilon_{[i]}j} \end{aligned} \tag{6.34}$$

The F intermediates are defined as,

$$F_{m\epsilon_{[x]}} = f_{m\epsilon_{[x]}} + \sum_{n\gamma} t^{\gamma}_{[n]} \langle mn || \epsilon_{[x]} \gamma_{[n]} \rangle \tag{6.35}$$

$$F_{\alpha_{[i]}\epsilon_{[i]}} = f_{\alpha_{[i]}\epsilon_{[i]}} + \sum_{m\gamma} t^{\gamma}_{[m]} \langle \alpha_{[i]} m || \epsilon_{[i]} \gamma_{[m]} \rangle \tag{6.36}$$

$$F_{mi} = f_{mi} + \sum_{\epsilon} t^{\epsilon}_{[i]} F_{m\epsilon_{[i]}} + \sum_{n\epsilon} t^{\epsilon}_{[n]} \langle mn || i\epsilon_{[n]} \rangle + \sum_{n\epsilon\gamma} t^{\epsilon\gamma}_{[in]} \langle mn || \epsilon_{[in]} \gamma_{[in]} \rangle \tag{6.37}$$

Notice, the $F_{m\epsilon_{[x]}}$ intermediate is used twice, once in the fourth term of the T_1 equation and once in the F_{mi} intermediate, each with a different domain for ϵ. The generic $[x]$ domain is used to denote that the domain of ϵ depends on where $F_{m\epsilon_{[x]}}$ is used. The W intermediates

are defined as,

$$W_{mni\epsilon_{[mn]}} = \langle mn||i\epsilon_{[mn]}\rangle + \sum_f t^f_{[i]}\langle mn||\gamma_{[i]}\epsilon_{[mn]}\rangle \tag{6.38}$$

$$W_{mnij} = \langle mn||ij\rangle + P(ij)\sum_\epsilon t^\epsilon_{[j]} Z_{mni\epsilon_{[j]}} \tag{6.39}$$

$$W_{m\beta_{[ij]}ij} = \langle m\beta_{[ij]}||ij\rangle - \frac{1}{2}\sum_{n\beta'}(t^{\beta'}_{[n]} S^{\beta_{[ij]}}_{\beta'_{[n]}})W_{mnij} + P(ij)\sum_\epsilon t^\epsilon_{[i]} Z_{m\beta_{[ij]}\epsilon_{[i]}j} \tag{6.40}$$

$$W_{\alpha_{[ij]}\beta_{[ij]}\epsilon_{[i]}j} = \langle \alpha_{[ij]}\beta_{[ij]}||\epsilon_{[i]}j\rangle + \frac{1}{2}\sum_\gamma t^\gamma_{[j]}\langle \alpha_{[ij]}\beta_{[ij]}||\epsilon_{[i]}\gamma_{[j]}\rangle \tag{6.41}$$

where the Z intermediates are defined as,

$$Z_{mni\epsilon_{[j]}} = \langle mn||i\epsilon_{[j]}\rangle + \frac{1}{2}\sum_\gamma t^\gamma_{[i]}\langle mn||\gamma_{[i]}\epsilon_{[j]}\rangle \tag{6.42}$$

$$Z_{m\beta_{[ij]}\epsilon_{[i]}j} = \langle m\beta_{[ij]}||\epsilon_{[i]}j\rangle + \frac{1}{2}\sum_\gamma t^\gamma_{[j]}\langle m\beta_{[ij]}||\epsilon_{[i]}\gamma_{[j]}\rangle \tag{6.43}$$

Almost all intermediates shown above are identical to those used in the canonical version of CC2 with one difference. Look at the following term in its 'raw' form

$$\tilde{R}^\alpha_i \leftarrow -\frac{1}{2}\sum_{mnef\alpha'} t^\epsilon_{[i]}(t^{\alpha'\gamma}_{[mn]} S^{\alpha_{[i]}}_{\alpha'_{[mn]}})\langle mn||\epsilon_{[i]}\gamma_{[mn]}\rangle \tag{6.44}$$

The order we perform multiplications in the above term determines which intermediate it contributes to. Multiplying the integral by T_2 first would result in a contribution to the $F_{\alpha_{[i]}\epsilon_{[i]}}$ intermediate, which is how this term is handled in the canonical formulation of CC2. However, this is very cumbersome in the local correlation variant of CC2 due to the multiplication by $\tilde{\mathbf{S}}$, resulting in multiple $\mathcal{O}(N^6)$ steps. By contrast, first multiplying the integral by T_1 leads to several $\mathcal{O}(N^5)$ steps that are much less expensive. For this reason the integral is multiplied by T_1 first, which contributes to the $W_{mni\epsilon_{[mn]}}$ intermediate and a proper scaling algorithm.

6.3.4 Comparisons and Timings with 'Pseudo-'Production Level Code

We are currently implementing a production level local correlation program for calculating MP2 and CC2 energies. While there is still much streamlining to be done, we have implemented the MP2 and CC2 equations within the PAO basis as shown in the previous section. Since the localization and domain selection is performed immediately after the Hartree-Fock reference calculation, we should be able to limit the integral transformation to include only the integrals appearing in the above equations similar to the techniques used by Werner *et al.*.[64,69,81] However, our current integral transformation lacks any form of screening. For example, performing an energy calculation on heptadecane in a DZ basis set, we transform nearly 70 GB of integrals but only use about 3.3 GB for the local correlation calculation of the energy neglecting weak pairs or employing an MP2 weak pair correction.

Another major shortcoming in the current status of our code is the assumption that all quantities can be held in memory. At first glance this may seem a ghastly assumption, however, since the local correlation framework limits the virtual orbitals to only certain domains within the PAO space, the quantities become much smaller and more manageable in memory. In the example above, it would be impossible to perform a CC2 calculation within a canonical basis assuming we could hold 70 GB of information in memory (on most computer systems).

Despite the limitations in the current status of our production level code we can still glean a sense of the speedup achievable within a local correlation calculation of energies as well as % localization errors. Table 6.1 lists the energies and time for a series of n-alkane chains ranging from propane to heptadecane using the DZ basis set of Dunning.[143] The energies and time, given as seconds per iteration ($\frac{s}{\text{iter}}$) for the canonical calculation are shown in the first two columns. The remaining columns list % errors and time for various treatments of weak pairs, including, no weak pairs (all pairs treated as strong), neglecting weak pairs, and an MP2 weak pair correction. The localization error (%) are plotted in Fig. 6.1.

Table 6.1: Comparisons of energy and timings between canonical and local correlation for a series of n-alkanes using a DZ basis set. All calculations have been run on the Inferno2 computer system. Energies are in hartrees (E_h) and time is given as seconds per iterations ($\frac{s}{\text{iter}}$).

	Canonical		No Weak Pairs		Neglect Weak Pairs		MP2 Weak Pairs	
n-Alkane	Energy	Time	% Error	Time	% Error	Time	% Error	Time
propane	-0.2648	0.1	3.51	0.9	7.88	0.5	4.04	0.1
pentane	-0.4393	0.6	4.68	4.5	10.21	1.3	5.32	0.2
heptane	-0.6141	2.5	5.19	12.9	11.24	3.0	5.89	0.5
nonane	-0.7888	7.1	5.48	29.3	11.8	5.5	6.20	1.0
undecane	-0.9636	16.4	5.66	111.4	12.17	9.7	6.41	2.4
tridecane	-1.1384	34.4	5.79	119.3	12.42	16.1	6.55	3.8
pentadecane	-1.3131	62.9	5.88	344.4	12.61	34.5	6.65	6.0
heptadecane	-1.4879	162.1	-	-	12.76	24.3	6.73	8.4

Treating all pairs as strong pairs provides the best recovery of the correlation energy compared to the other weak pair treatments. In all cases, the localization error falls below 6%. This seemingly large % error is due to the use of a relatively poor quality DZ basis set, *vide infra*. Treating all pairs as strong pairs has come at the cost of computational expense in terms of both time and storage. In fact, the amount of time required per iteration has actually increased compared to the canonical case. The amount of memory required for treating all pairs as strong pairs for pentadecane is about 11 GB. Neglecting weak pairs or applying the MP2 weak pair correction requires approximately 2.2 GB of memory.

Neglecting weak pairs gives way to a much more favorable result in terms of speedup, but localization errors are far too large, often reaching above 12%. Employing the MP2 weak pair correction greatly improves the localization error at a very small computational cost. Even for the large heptadecane system, less than two minutes were required for the entire MP2 weak pair calculation. Also, no extra storage is required since MP2 uses integrals

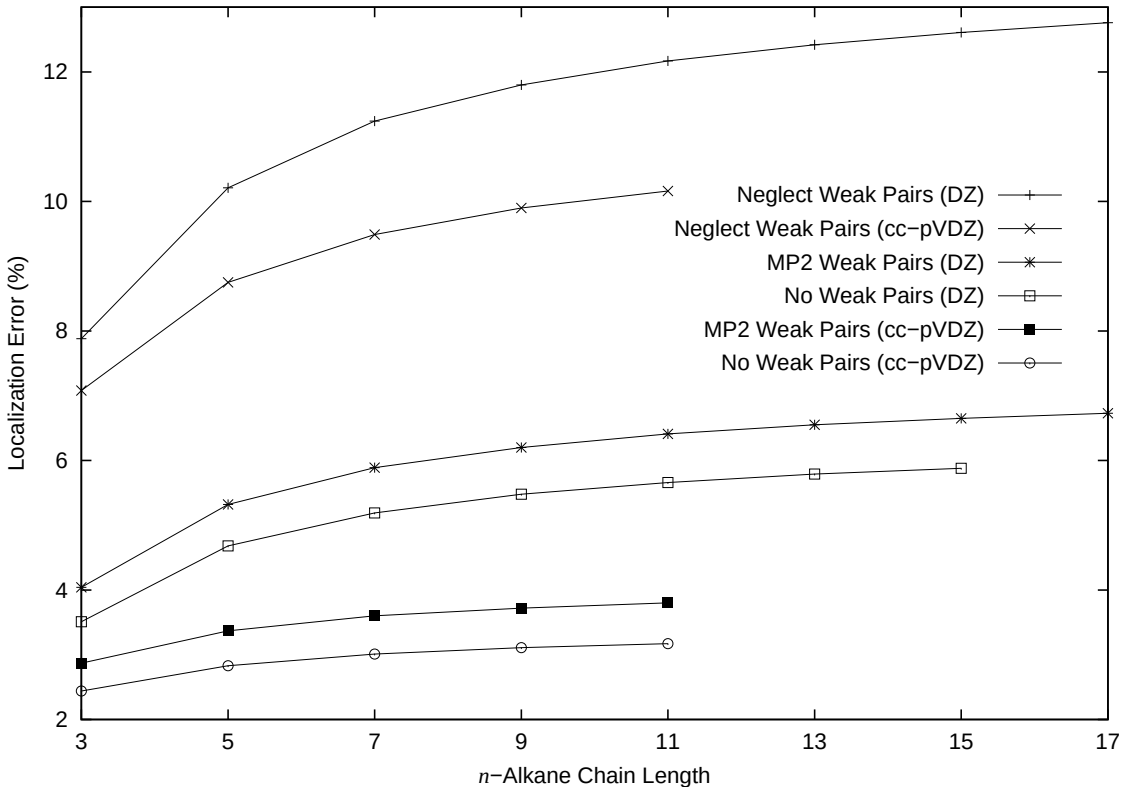

Figure 6.1: Localization errors (%) for CC2 energies on a series of n-alkane chains using various treatments for weak pairs using the DZ and cc-pVDZ basis sets.

already required for the CC2 part of the calculation. It is clear that at least an approximate treatment of weak pairs is necessary for the adequate recovery of correlation energy.

One of the difficulties with using a shared machine like Inferno2 is that there is always a lot of people using it and it is difficult to ensure dedication to any one process, which makes timings very difficult. Therefore, all the timing data in Table 6.1 are only rough estimates. We have also performed the same calculations on one of our own high performance workstations where we can be sure the machine is dedicated to just one process at a time. These calculations are reported in Table 6.2 and plotted in Fig. 6.2 to provide a much better assessment of the times associated with each calculation. Unfortunately, a common high performance workstation (such as those employed in our lab) has much less memory than Inferno2, limiting the largest n-alkane to heptane for treating all pairs as strong and tridecane for the other two methods.

Table 6.2: Comparisons of energy and timings between canonical and local correlation for a series of n-alkanes using a DZ basis set. All calculations have been run on a modern high performance workstation. Energies are in hartrees (E_h) and time is given as seconds per iterations ($\frac{s}{\text{iter}}$).

	Canonical		No Weak Pairs		Neglect Weak Pairs		MP2 Weak Pairs	
n-Alkane	Energy	Time	% Error	Time	% Error	Time	% Error	Time
propane	-0.2648	0.3	3.51	1.1	7.88	0.4	4.04	0.1
pentane	-0.4393	1.9	4.68	5.4	10.21	1.3	5.32	0.6
heptane	-0.6141	6.9	5.19	15.5	11.24	2.8	5.89	1.5
nonane	-0.7888	19.6	-	-	11.80	5.2	6.20	3.2
undecane	-0.9636	46.4	-	-	12.17	8.7	6.41	5.8
tridecane	-1.1384	217.2	-	-	12.42	14.7	6.55	9.8

All energies and % errors in Table 6.2 are identical to those listed in Table 6.1, the only difference is in the time per iteration for all calculations. Again, treating all weak pairs as strong pairs results in times that are longer than the canonical calculation. However, neglecting weak pairs results in a very large speedup over the canonical calculation. For the case of tridecane, seconds per iteration dropped from 217.2 to a mere 14.7. Furthermore, only 9.8 seconds per iteration are required for an MP2 weak pair correction, or a total of about 2.5 minutes.

In this discussion so far we have neglected the influence of symmetry on the timing comparisons. The series of odd number n-alkane chains have C_{2v} symmetry and Psi3 is able to take full advantage of the symmetry inherent to the odd number n-alkane chains. Timings for the canonical calculations reported in all the tables in this section have been performed using the computational advantages of C_{2v} symmetry. However, the Pipek-Mezey localization scheme, as well as our choice of a PAO virtual space destroys the symmetry of the electronic structure. Fig. 6.2 also plots the timings of the n-alkane chains without the computational advantages of symmetry within the canonical formulation. For example, forcing the canoni-

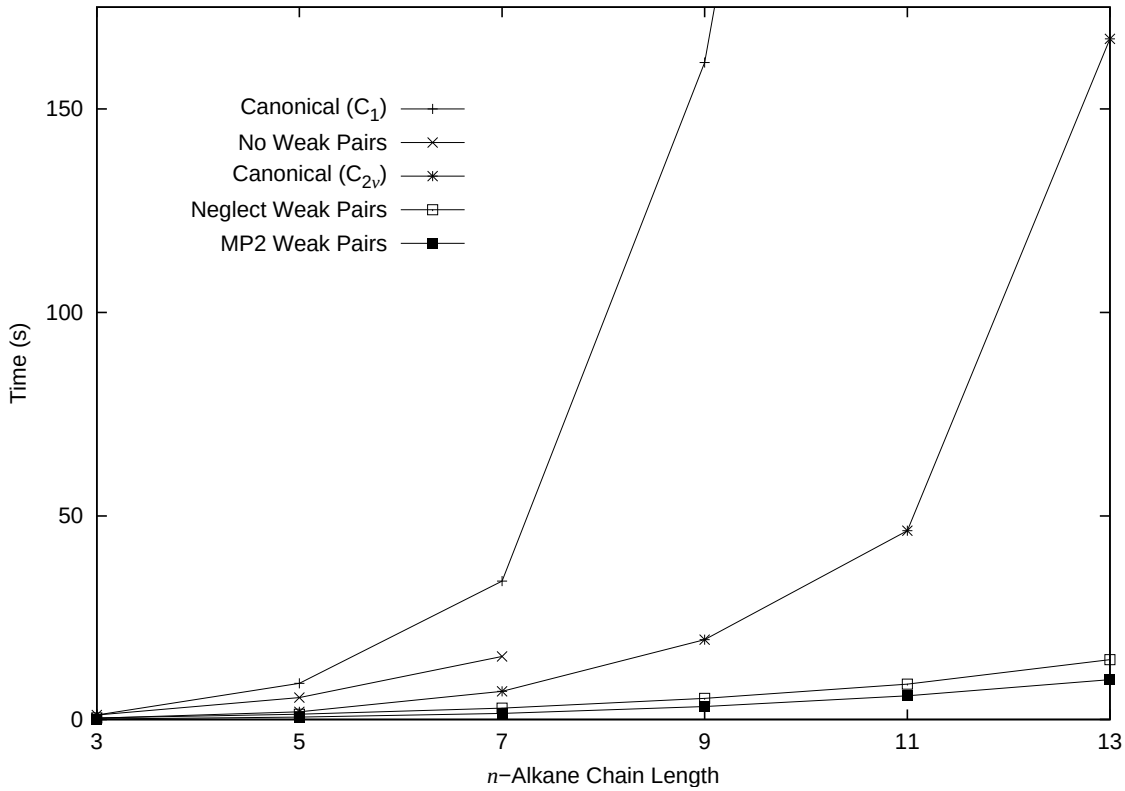

Figure 6.2: Comparisons of time, listed as seconds per iteration ($\frac{s}{\text{iter}}$), for the calculating ground state energies via canonical and local correlation techniques, including various treatments of weak pairs within the local correlation method. All calculations were performed on a modern high performance workstation with 2.0 GB of memory.

cal calculation of tridecane to run in C_1 symmetry on our workstation requires 861.2 seconds per iteration, compared to the time required for the local correlation calculation of only 14.7. Calculations of optical rotation are often performed on molecules with very low or no symmetry. The computational advantages of a local correlation framework become transparent for this particular application.

We chose to use the relatively poor quality DZ basis set in order to allow for the calculation of 'large' molecular system. Looking at Table 6.1 the localization errors are rather large. Some authors have attributed the large % errors within small basis sets to BSSE (basis set superposition error) within the canonical calculation.[61,63,144,145] This implies that a larger,

Table 6.3: Comparisons of energy and timings between canonical and local correlation for a series of n-alkanes using a cc-pVDZ basis set. All calculations have been run on the Inferno2 computer system. Energies are in hartrees (E_h) and time is given as seconds per iterations ($\frac{s}{\text{iter}}$).

	Canonical		No Weak Pairs		Neglect Weak Pairs		MP2 Weak Pairs	
n-Alkane	Energy	Time	% Error	Time	% Error	Time	% Error	Time
propane	-0.4478	0.6	2.44	4.4	7.08	1.9	2.87	0.1
pentane	-0.7363	4.5	2.83	23.5	8.75	5.1	3.37	0.4
heptane	-1.0249	16.4	3.01	49.9	9.49	10.5	3.60	1.1
nonane	-1.3134	47.7	3.11	156.2	9.90	16.2	3.72	2.7
undecane	-1.6020	107.0	3.17	211.4	10.16	49.2	3.80	5.0

more complete, basis set will return smaller localization errors. Table 6.3 lists the energies, localization errors and timings for a set of odd numbered n-alkanes ranging from propane to undecane for canonical and local correlation methods with various treatments of weak pairs using the cc-pVDZ correlation-consistent basis set of Dunning *et al.* The localization errors have also been plotted in Fig. 6.1. The localization errors change dramatically moving from the DZ basis to the cc-pVDZ basis, falling from 5.66% for undecane in a DZ basis to only 3.17% in a cc-pVDZ basis, treating all pairs as strong pairs. Only a small percentage shift is observed when weak pairs are neglected, falling from 12.17% to 10.16%. The MP2 corrected weak pair energies exhibit a similar behavior to the no weak pair energies, dropping from 6.41% to 3.8%. These calculations provide good support that the localization errors are indeed a result of BSSE within the canonical calculation and may provide good reason to trust the local correlation energies over the canonical energies.

Chapter 7

Conclusions

We have examined the occurence of discontinuities in bond-breaking potential energy surfaces given by local correlation methods based on the Pulay-Saebø orbital domain approach. Our analysis focuses on three prototypical dissociating systems: the C−F bond in fluoromethane, the C−C bond in singlet ketene, and the central C−C bond in propadienone. We find that such discontinuities do not occur in cases of homolytic bond cleavage due to the inability of the Pipek-Mezey orbital localization method to separate singlet-coupled charges on distant fragments. However, for heterolytic bond cleavage, such as that observed in singlet ketene and propadienone, discontinuities occur both at stretched geometries and near equilbrium. These discontinuities are usually small, but may be of the same order of magnitude as the localization error in some cases.

We have extended the local coupled cluster approach of Pulay and Saebø, which has seen great success in the computation of ground-state energies, to molecular response properties such as dipole polarizabilities. This scheme uses an atom-based coupled-perturbed Hartree-Fock (CPHF) breakdown of the desired property to expand the usual ground-state orbital domains. Benchmark tests of the static polarizabilities of helium chains, linear alkanes, and non-saturated systems up to N-acetylglycine indicate that the method can reproduce untruncated coupled cluster properties to within 1% given appropriately chosen cutoffs,

even without including orbital relaxation in the method. The method requires increased computational demands, but crossover points between non-local and local approaches are still well within reach of production-level implementations.

We have extended the coupled-perturbed Hartree-Fock (CPHF) domain selection scheme used to calculate static polarizabilities to the calculation of optical rotation. Benchmark calculations of the optical rotation of 1-fluoroalkanes, [n]-triangulanes and β-pinene have been performed with mixed results. Molecules exhibiting a center of chirality require large domain structures and only small scaling reductions have been observed. Our local domain selection has performed well on molecules possessing a chiral axis often able to achieve localization error *ca.* 2% or less with significant reduction in scaling. Our proposed CPHF-based domain structure requires increased computational demands compared to the domain selection scheme of Boughton and Pulay. However, these larger domains are are necessary to achieve small localization errors, but still within reach of a production-level implementation.

We have implemented a 'pseudo-'production level version of locally correlated CC2 capable of significant reduction in scaling and time compared to a conventional canonical formulation. We have also implemented an MP2 weak pair correction allowing a great improvement to the localization error for a very small computational cost. Currently, there are two significant limitations that must be addressed. First, there is no screening algorithm within the integral transformation, leading to the excessive calculation of many integrals that are never used in the CC2 calculation. Second, we have assumed all quantities in the local basis can be stored in memory drastically limiting the size of molecule on which we can perform calculations.

Bibliography

[1] Born, M.; Oppenheimer, R. "Zur Quantentheorie der Molekeln." *Annalen Der Physik* **1927**. 84, 457–484.

[2] Jørgensen, P.; Simons, J. *Second Quantization-Based Methods in Quantum Chemistry.* Academic Press, New York, **1981**.

[3] Schatz, G. C.; Ratner, M. A. *Quantum Mechanics in Chemistry.* Dover Publications, Inc., Mineola, New York, **2002**.

[4] Harris, F. E.; Monkhorst, H. J.; Freeman, D. L. *Algebraic and Diagrammatic Methods in Many-Fermion Theory.* Oxford University Press, New York, **1992**.

[5] Slater, J. C. "Note on Hartree's Method." *Phys. Rev.* **1930**. 35, 210–211.

[6] Roothaan, C. C. J. "New developments in molecular orbital theory." *Rev. Mod. Phys.* **1951**. 23, 69–89.

[7] Jensen, F. *Introduction to Computational Chemistry.* John Wiley & Sons, **1999**.

[8] Hellmann, H. "A New Approximation Method in the Problem of Many Electrons." *J. Chem. Phys.* **1935**. 3, 61.

[9] Stevens, R. M.; Pitzer, R. M.; Lipscomb, W. N. "Perturbed Hartree-Fock Calculations. I. Magnetic Susceptibility and Shielding in the LiH Molecule." *J. Chem. Phys.* **1963**. 38, 550–560.

[10] Yamaguchi, Y.; Osamura, Y.; Goddard, J. D.; Schaefer, H. F. *A New Dimension to Quantum Chemistry: Analytic Derivative Methods in* Ab Initio *Molecular Electronic Structure Theory.* The International Series of Monographs on Chemistry. Oxford University Press, New York, **1994**.

[11] Allen, L. C. "Hartree-Fock Equations with a Perturbing Field." *Phys. Rev.* **1960**. 118, 167–175.

[12] Gerratt, J.; Mills, I. M. "Force Constants and Dipole-Moment Derivatives of Molecules from Perturbed Hartree–Fock Calculations. I." *J. Chem. Phys.* **1968**. 49, 1719–1729.

[13] Helgaker, T.; Ruden, T. A.; Jorgensen, P.; Olsen, J.; Klopper, W. "A priori calculation of molecular properties to chemical accuracy." *J. Phys. Org. Chem.* **2004**. 17, 913–933.

[14] Feller, D.; Peterson, K. A. "An examination of intrinsic errors in electronic structure methods using the Environmental Molecular Sciences Laboratory computational results database and the Gaussian-2 set." *J. Chem. Phys.* **1998**. 108, 154–176.

[15] Cramer, C. J. *Essentials of Computational Chemistry: Theories and Models.* John Wiley & Sons, **2002**.

[16] Smith, C. E.; Crawford, T. D.; Cremer, D. "The structures of *m*-benzyne and tetrafluoro-*m*-benzyne." *J. Chem. Phys.* **2005**. 122, 174309.

[17] Szabo, A.; Ostlund, N. S. *Modern Quantum Chemistry: Introduction to Advanced Electronic Structure Theory.* Dover Publications, Inc., Mineola, New York, 1st ed., **1989**.

[18] Löwdin, P.-O. "Quantum Theory of Many-Particle Systems. I. Physical Interpretations by Means of Density Matrices, Natural Spin-Orbitals, and Convergence Problems in the Method of Configuration Interaction." *Phys. Rev.* **1955**. 97, 1474–1489.

[19] Löwdin, P.-O. "Quantum Theory of Many-Particle Systems. III. Extension of the Hartree-Fock Scheme to Include Degenerate Systems and Correlation Effects." *Phys. Rev.* **1955**. 97, 1509–1520.

[20] Sherrill, C. D.; Schaefer, H. F. "The Configuration Interaction Method: Advances in Highly Correlated Approaches." *Advances in Quantum Chemistry* **1999**. 34, 143–269.

[21] Bartlett, R. J. "Coupled-cluster approach to molecular structure and spectra: A step toward predictive quantum chemistry." *J. Phys. Chem.* **1989**. 93, 1697–1708.

[22] Cole, S. J.; Bartlett, R. J. "Comparison of MBPT and coupled cluster methods with full CI. II. Polarized basis sets." *J. Chem. Phys.* **1987**. 86, 873–881.

[23] Olsen, J.; Christiansen, O.; Koch, H.; Jørgensen, P. "Surprising cases of divergent behavior in Møller-Plesset perturbation theory." *J. Chem. Phys.* **1996**. 105, 5082.

[24] Bauschlicher, C. W.; Taylor, P. R. "A full CI treatment of the $^1A_1 - ^3B_1$ separation in methylene." *J. Chem. Phys.* **1986**. 85, 6510–6512.

[25] Bauschlicher, C. W.; Taylor, P. R. "Benchmark full configuration-interaction calculations on H_2O, F, and F^-." *J. Chem. Phys.* **1986**. 85, 2779–2783.

[26] Bauschlicher, C. W.; Langhoff, S. R. "A full CI treatment of the Ne atom - a benchmark calculation performed on the NAS CRAY 2." *Chem. Phys. Lett.* **1986**. 126, 436.

[27] Bauschlicher, C. W.; Langhoff, S. R.; Taylor, P. R.; Handy, N. C.; Knowles, P. J. "Benchmark full configuration interaction calculations on HF and NH_2." *J. Chem. Phys.* **1986**. 85, 1469–1474.

[28] Bauschlicher, C. W.; Taylor, P. R. "Full CI benchmark calculations on CH_3." *J. Chem. Phys.* **1987**. 86, 5600–5602.

[29] Bauschlicher, C. W.; Taylor, P. R. "Full CI benchmark calculations for several states of the same symmetry." *J. Chem. Phys.* **1987**. 86, 2844–2848.

[30] Bauschlicher, C. W.; Taylor, P. R. "A full CI treatment of the $^1A_1$, $^1B_1$, and $^3B_1$ states of SiH_2." *J. Chem. Phys.* **1987**. 86, 1420–1424.

[31] Møller, C.; Plesset, M. S. "Note on an approximation treatment for many-electron systems." *Phys. Rev.* **1934**. 46, 618–622.

[32] Crawford, T. D.; Schaefer, H. F. "An introduction to coupled cluster theory for computational chemists." In Lipkowitz, K. B.; Boyd, D. B., eds., "Reviews in Computational Chemistry," VCH Publishers, New York, vol. 14. **2000** 33–136.

[33] Christiansen, O.; Koch, H.; Jørgensen, P. "The second-order approximate coupled cluster singles and doubles model CC2." *Chem. Phys. Lett.* **1995**. 243, 409–418.

[34] Salter, E. A.; Sekino, H.; Bartlett, R. J. "Property evaluation and orbital relaxation in coupled cluster methods." *J. Chem. Phys.* **1987**. 87, 502–509.

[35] Koch, H.; Jørgensen, P. "Coupled cluster response functions." *J. Chem. Phys.* **1990**. 93, 3333–3344.

[36] Pedersen, T. B.; Koch, H. "Coupled cluster response functions revisited." *J. Chem. Phys.* **1997**. 106, 8059–8072.

[37] Pople, J. A.; McIver, J. W.; Ostlund, N. S. "Self-Consistent Perturbation Theory. I. Finite Perturbation Methods." *J. Chem. Phys.* **1968**. 49, 2960–2964.

[38] Rosenfeld, L. "Quantenmechanische Theorie der natürlichen optischen Aktivität von Flüssigkeiten und Gasen." *Z. Physik* **1928**. 52, 161.

[39] Ruud, K.; Helgaker, T. "Optical rotation studied by density-functional and coupled-cluster methods." *Chem. Phys. Lett.* **2002**. 352, 533–539.

[40] Ruud, K.; Stephens, P. J.; Devlin, F. J.; Taylor, P. R.; Cheeseman, J. R.; Frisch, M. J. "Coupled-cluster calculations of optical rotation." *Chem. Phys. Lett.* **2003**. 373, 606–614.

[41] Tam, M. C.; Russ, N. J.; Crawford, T. D. "Coupled Cluster Calculations of Optical Rotatory Dispersion of (*S*)-Methyloxirane." *J. Chem. Phys.* **2004**. 121, 3550–3557.

[42] Crawford, T. D.; Owens, L. S.; Tam, M. C.; Schreiner, P. R.; Koch, H. "*Ab Initio* Calculation of Optical Rotation in (*P*)-(+)-[4]Triangulane." *J. Am. Chem. Soc.* **2005**. 127, 1368–1369.

[43] Tam, M. C.; Crawford, T. D. "*Ab Initio* Determination of Optical Rotatory Dispersion in the Conformationally Flexible Molecule *(R)-Epichlorohydrin*." *J. Phys. Chem. A* **2006**. 110, 2290–2298.

[44] Ruud, K.; Zanasi, R. "The Importance of Molecular Vibrations: The Sign Change of the Optical Rotation of Methyloxirane." *Angew. Chem. Int. Ed.* **2005**. 44, 3594–3596.

[45] Kongsted, J.; Pedersen, T. B.; Jensen, L.; Hansen, A. E.; Mikkelsen, K. V. "Coupled Cluster and Density Functional Theory Studies of the Vibrational Contribution to the Optical Rotation of (*S*)-Propylene Oxide." *J. Am. Chem. Soc.* **2006**. 128, 976–982.

[46] Burant, J. C.; Scuseria, G. E.; Frisch, M. J. "A linear scaling method for Hartree-Fock exchange calculations of large molecules." *J. Chem. Phys.* **1996**. 105, 8969–8972.

[47] Scuseria, G. E. "Linear Scaling Density Functional Calculations with Gaussian Orbitals." *J. Phys. Chem. A* **1999**. 103, 4782–4790.

[48] Shao, Y.; Head-Gordon, M. "An improved J matrix engine for density functional theory calculations." *Chem. Phys. Lett.* **2000**. 323, 425–433.

[49] Liang, W.; Head-Gordon, M. "An exact reformulation of the diagonalization step in electronic structure calculations as a set of second order nonlinear equations." *J. Chem. Phys.* **2004**. 120, 10379–10384.

[50] Pulay, P. "Localizability of dynamic electron correlation." *Chem. Phys. Lett.* **1983**. 100, 151–154.

[51] Saebø, S.; Pulay, P. "Local configuration interaction: An efficient approach for larger molecules." *Chem. Phys. Lett.* **1985**. 113, 13–18.

[52] Head-Gordon, M.; Maslen, P. E.; White, C. A. "A tensor formulation of many-electron theory in a nonorthogonal single-particle basis." *J. Chem. Phys.* **1998**. 108, 616–625.

[53] Maslen, P.; Head-Gordon, M. "Non-iterative local second order order Møller-Plesset theory." *Chem. Phys. Lett.* **1998**. 283, 102–108.

[54] Maslen, P. E.; Head-Gordon, M. "Noniterative local second order Møller-Plesset theory: Convergence with local correlation space." *J. Chem. Phys.* **1998**. 109, 7093–7099.

[55] Lee, M. S.; Maslen, P. E.; Head-Gordon, M. "Closely approximating second-order Møller-Plesset perturbation theory with a local triatomics in molecules model." *J. Chem. Phys.* **2000**. 112, 3592–3601.

[56] Flocke, N.; Bartlett, R. J. "Localized correlation treatment using natural bond orbitals." *Chem. Phys. Lett.* **2003**. 367, 80–89.

[57] Flocke, N.; Bartlett, R. J. "Correlation energy estimates in periodic extended systems using the localized natural bond orbital coupled cluster approach." *J. Chem. Phys.* **2003**. 118, 5326–5334.

[58] Pulay, P.; Saebø, S. "Orbital-invariant formulation and second-order gradient evaluation in Møller-Plesset perturbation theory." *Theor. Chim. Acta* **1986**. 69, 357–368.

[59] Saebø, S.; Pulay, P. "Fourth-order Møller-Plesset perturbation theory in the local correlation treatment. I. Method." *J. Chem. Phys.* **1987**. 86, 914–922.

[60] Saebø, S.; Pulay, P. "The local correlation treatment. II. Implementation and tests." *J. Chem. Phys.* **1988**. 88, 1884–1890.

[61] Saebø, S.; Tong, W.; Pulay, P. "Efficient elimination of basis set superposition errors by the local correlation method: Accurate *ab initio* studies of the water dimer." *J. Chem. Phys.* **1993**. 98, 2170–2175.

[62] Saebø, S.; Pulay, P. "Local treatment of electron correlation." *Ann. Rev. Phys. Chem.* **1993**. 44, 213–236.

[63] Hampel, C.; Werner, H.-J. "Local treatment of electron correlation in coupled cluster theory." *J. Chem. Phys.* **1996**. 104, 6286.

[64] Schütz, M.; Werner, H.-J. "Low-order scaling local electron correlation methods. IV. Linear scaling local coupled-cluster (LCCSD)." *J. Chem. Phys.* **2001**. 114, 661–681.

[65] Crawford, T. D.; King, R. A. "Locally Correlated Equation-of-Motion Coupled Cluster Theory for the Excited States of Large Molecules." *Chem. Phys. Lett.* **2002**. 366, 611–622.

[66] Korona, T.; Werner, H.-J. "Local treatment of electron excitations in the EOM-CCSD method." *J. Chem. Phys.* **2003**. 118, 3006–3019.

[67] Korona, T.; Pflüger, K.; Werner, H.-J. "The effect of local approximations in coupled-cluster wave functions on dipole moments and static dipole polarizabilities." *Phys. Chem. Chem. Phys.* **2004**. 6, 2059–2065.

[68] Russ, N. J.; Crawford, T. D. "Local correlation in coupled cluster calculations of molecular response properties." *Chem. Phys. Lett.* **2004**. 400, 104–111.

[69] Schütz, M.; Manby, F. R. "Linear scaling local coupled cluster theory with density fitting. Part I: 4-external integrals." *Phys. Chem. Chem. Phys.* **2003**. 5, 3349–3358.

[70] Boys, S. F. "Construction of Some Molecular Orbitals to Be Approximately Invariant for Changes from One Molecule to Another." *Rev. Mod. Phys.* **1960**. 32, 296–299.

[71] Foster, J. M.; Boys, S. F. "Canonical Configurational Interaction Procedure Construction of Some Molecular Orbitals to Be Approximately Invariant for Changes from One Molecule to Another Construction of Some Molecular Orbitals to Be Approximately Invariant for Changes from One Molecule to Another Construction of Some Molecular

Orbitals to Be Approximately Invariant for Changes from One Molecule to Another Construction of Some Molecular Orbitals to Be Approximately Invariant for Changes from One Molecule to Another." *Rev. Mod. Phys.* **1960**. 32, 300–302.

[72] Edmiston, C.; Ruedenberg, K. "Localized Atomic and Molecular Orbitals." *Rev. Mod. Phys.* **1963**. 35, 457–465.

[73] Edmiston, C.; Ruedenberg, K. "Localized Atomic and Molecular Orbitals. II." *J. Chem. Phys.* **1965**. 43, S97–S116.

[74] Pipek, J.; Mezey, P. G. "A fast intrinsic localization procedure applicable for *ab initio* and semiempirical linear combination of atomic orbital wave functions." *J. Chem. Phys.* **1989**. 90, 4916–4926.

[75] Boughton, J. W.; Pulay, P. "Comparison of the Boys and Pipek-Mezey Localizations in the Local Correlation Approach and Automatic Virtual Basis Selection." *J. Comput. Chem.* **1993**. 14, 736–740.

[76] Hetzer, G.; Pulay, P.; Werner, H.-J. "Multipole approximation of distant pair energies in local MP2 calculations." *Chem. Phys. Lett.* **1998**. 290, 143–149.

[77] Schütz, M.; Hetzer, G.; Werner, H.-J. "Low-order scaling local electron correlation methods. I. Linear scaling local MP2." *J. Chem. Phys.* **1999**. 111, 5691–5705.

[78] Häser, M.; Almlöf, J. "Laplace transform techniques in Møller-Plesset perturbation theory." *J. Chem. Phys.* **1992**. 96, 489–595.

[79] Ayala, P. Y.; Scuseria, G. E. "Linear scaling second-order Moller-Plesset theory in the atomic orbital basis for large molecular systems." *J. Chem. Phys.* **1999**. 110, 3660–3671.

[80] Scuseria, G. E.; Ayala, P. Y. "Linear scaling coupled cluster and perturbation theories in the atomic orbital basis." *J. Chem. Phys.* **1999**. 111, 8330–8343.

[81] Hetzer, G.; Schütz, M.; Stoll, H.; Werner, H.-J. "Low-order scaling local correlation methods II: Splitting the Coulomb operator in linear scaling local second-order Møller-Plesset perturbation theory." *J. Chem. Phys.* **2000**. 113, 9443–9455.

[82] Rauhut, G.; Werner, H.-J. "Analytical energy gradients for local coupled-cluster methods." *Phys. Chem. Chem. Phys.* **2001**. 3, 4853–4862.

[83] Schütz, M. "A new, fast, semi-direct implementation of linear scaling local coupled cluster theory." *Phys. Chem. Chem. Phys.* **2002**. 4, 3941–3947.

[84] Maslen, P. E.; Lee, M. S.; Head-Gordon, M. "An accurate local model for triple substitutions in fourth order Møller-Plesset theory and in perturbative corrections to singles and doubles coupled cluster methods." *Chem. Phys. Lett.* **2000**. 319, 205–212.

[85] Schütz, M.; Werner, H.-J. "Local perturbative triples correction (T) with linear cost scaling." *Chem. Phys. Lett.* **2000**. 318, 370–378.

[86] Schütz, M. "Low-order scaling local electron correlation methods. III. Linear scaling local perturbative triples correction (T)." *J. Chem. Phys.* **2000**. 113, 9986–10001.

[87] Constans, P.; Ayala, P.; Scuseria, G. "Scaling reduction of the perturbative triples correction (T) to coupled cluster theory via Laplace transform formalism." *J. Chem. Phys.* **2000**. 113, 10451–10458.

[88] Schütz, M. "Low-order scaling local electron correlation methods. V. Connected triples beyond (T): Linear scaling local CCSDT-1b." *J. Chem. Phys.* **2002**. 116, 8772–8785.

[89] Subotnik, J. E.; Head-Gordon, M. "A local correlation model that yields intrinsically smooth potential-energy surfaces." *J. Chem. Phys.* **2005**. 123, 064108.

[90] Subotnik, J. E.; Dutoi, A. D.; Head-Gordon, M. "Fast localized orthonormal virtual orbitals which depend smoothly on nuclear coordinates." *J. Chem. Phys.* **2005**. 123, 114108.

[91] Pople, J. A. "Theoroetical models for chemistry." In Smith, D. W.; McRae, W. B., eds., "Energy, Structure, and Reactivity," John Wiley, New York. **1973** 51–61.

[92] Kestner, N. R. "He-He Interaction in the SCF-MO Approximation." *J. Chem. Phys.* **1968**. 48, 252–257.

[93] van Lenthe, J. H.; van Duijneveldt-van de Rijdt, J. G. C. M.; van Duijneveldt, F. B. "Weakly bonded systems." *Adv. Chem. Phys.* **1987**. 69, 521–566.

[94] Boys, S. F.; Bernardi, F. "The calculation of small molecular interactions by the differences of seperate total energies. Some procedures with reduced errors." *Mol. Phys.* **1970**. 19, 553–566.

[95] Bartlett, R. J. "Coupled-cluster theory: An overview of recent developments." In Yarkony, D. R., ed., "Modern Electronic Structure Theory," World Scientific, Singapore, vol. 2 of *Advanced Series in Physical Chemistry*. **1995** 1047–1131.

[96] Crawford, T. D.; Sherrill, C. D.; Valeev, E. F.; Fermann, J. T.; King, R. A.; Leininger, M. L.; Brown, S. T.; Janssen, C. L.; Seidl, E. T.; Kenny, J. P.; Allen, W. D. "PSI 3.2.", **2003**.

[97] Dunning, T. H. "Gaussian basis sets for use in correlated molecular calculations. I. The atoms boron through neon." *J. Chem. Phys.* **1989**. 90, 1007–1023.

[98] Dutta, A.; Sherrill, C. D. "Full configuration interaction potential energy curves for breaking bonds to hydrogen: An assessment of single-reference correlation methods." *J. Chem. Phys.* **2003**. 118, 1610–1619.

[99] Allen, W. D.; Schaefer, H. F. "Reaction paths for the dissociation of $\tilde{a}\ ^3A''$ $CH_2O \rightarrow \tilde{X}\ ^3B_1$ $CH_2 + \tilde{X}\ ^1\Sigma^+$ CO." *J. Chem. Phys.* **1988**. 89, 329–344.

[100] Kim, S. K.; Choi, Y. S.; Pibel, C. D.; Zheng, Q.-K.; Moore, C. B. "Determination of the singlet/triplet branching ratio in the photodissociation of ketene." *J. Chem. Phys.* **1991**. 94, 1954–1960.

[101] Yu, J.; Kliipenstein, S. J. "Variational Calculation of the Rate of Dissociation of CH_2CO into $^1CH_2$ and CO on an ab Initio Determined Potential Energy Surface." *J. Phys. Chem.* **1991**. 95, 9882–9889.

[102] Green, W. H.; Moore, C. B.; Polik, W. F. "Transition-States and Rate Constants for Unimolecular Reactions." *Ann. Rev. Phys. Chem.* **1992**. 43, 591–626.

[103] Klippenstein, S. J.; East, A. L. L.; Allen, W. D. "A first principles theoretical determination of the rate constant for the dissociation of singlet ketene." *J. Chem. Phys.* **1994**. 101, 9198–9201.

[104] East, A. L. L.; Allen, W. D.; Klippenstein, S. J. "The Anharmonic Force Field and Equilibrium Molecular-Structure of Ketene." *J. Chem. Phys.* **1995**. 102, 8506–8532.

[105] Cui, Q.; Morokuma, K. "Ab initio study of nonadiabatic interactions in the photodissociation of ketene." *J. Chem. Phys.* **1997**. 107, 4951–4959.

[106] East, A. L. L. "The kinkiness of cumulenones: H_2C_3O, H_2C_4O, and H_2C_5O." *J. Chem. Phys.* **1998**. 108, 3574–3584.

[107] Olsen, J.; Jørgensen, P. "Time-dependent response theory with applications to seld-consistent field and multiconfigurational self-consistent field wave functions." In Yarkony, D., ed., "Modern Electronic Structure Theory," World Scientific, Singapore, vol. 2 of *Advanced Series in Physical Chemistry*. **1995** 857–990.

[108] Rowe, D. J. "Equations-of-Motion Method and the Extended Shell Model." *Rev. Mod. Phys.* **1968**. 40, 153–166.

[109] Casida, M. E. "Time-Dependent Density Functional Response Theory for Molecules." In Chong, D. P., ed., "Recent Advances in Density Functional Methods," World Scientific, Singapore, vol. 1. **1995** .

[110] Jamorski, C.; Casida, M. E.; Salahub, D. R. "Dynamic polarizabilities and excitation spectra from a molecular implementation of time-dependent density-functional response theory: N_2 as a case study." *J. Chem. Phys.* **1996**. 104, 5134–5147.

[111] Gauss, J. "The coupled-cluster method." In Schleyer, P.; Allinger, N. L.; Clark, T.; Gasteiger, J.; Kollman, P. A.; Schaefer III, H. F.; Schreiner, P. R., eds., "Encyclopedia of Computational Chemistry," John Wiley & Sons, Chichester. **1998** 615–636.

[112] Lee, T. J.; Scuseria, G. E. "Achieving chemical accuracy with coupled-cluster theory." In Langhoff, S. R., ed., "Quantum Mechanical Electronic Structure Calculations with Chemical Accuracy," Kluwer Academic Publishers, Dordrecht. **1995** 47–108.

[113] Larsen, H.; Olsen, J.; Hättig, C.; Jørgensen, P.; Christiansen, O.; Gauss, J. "Polarizabilities and first hyperpolarizabilities of HF, Ne, and BH from full configuration interaction and coupled cluster calculations." *J. Chem. Phys.* **1999**. 111, 1917–1925.

[114] Stanton, J. F.; Bartlett, R. J. "The equation of motion coupled-cluster method. A systematic biorthogonal approach to molecular excitation energies, transition probabilities, and excited state properties." *J. Chem. Phys.* **1993**. 98, 7029–7039.

[115] Pedersen, T. B.; Fernández, B.; Koch, H. "Gauge invariant coupled cluster response theory using optimized nonorthogonal orbitals." *J. Chem. Phys.* **2001**. 114, 6983–6993.

[116] Kendall, R. A.; Dunning, T. H.; Harrison, R. J. "Electron effinities of the first-row atoms revisited. Systematic basis sets and wave functions." *J. Chem. Phys.* **1992**. 96, 6796–6806.

[117] Hariharan, P. C.; Pople, J. A. "The Influence of Polarization Functions on Molecular Orbital Hydrogenation Energies." *Theor. Chim. Acta* **1973**. 28, 213–222.

[118] Wipf, P.; Uto, Y.; Yoshimura, S. "Total Synthesis of a Stereoisomer of Bistramide C and Assignment of Configuration of the Natural Product." *Chem. Eur. J.* **2002**. 8, 1670–1681.

[119] Stephens, P.; Devlin, F.; Cheeseman, J.; Frisch, M.; Bortolini, O.; Besse, P. "Determination of Absolute Configuration Using Ab Initio Calculation of Optical Rotation." *Chirality* **2003**. 15, S57–S64.

[120] Polavarapu, P. L. "Optical Rotation: Recent Advances in Determining the Absolute Configuration." *Chirality* **2002**. 14, 768–781.

[121] Grimme, S. "Calculation of frequency dependent optical rotation using density functional response theory." *Chem. Phys. Lett.* **2001**. 339, 380–388.

[122] Polavarapu, P. L.; Chakraborty, D. K. "Absolute Stereochemistry of Chiral Molecules from ab Initio Theoretical and Experimental Molecular Optical Rotations." *J. Am. Chem. Soc.* **1998**. 120, 6160–6164.

[123] Polavarapu, P. L. "*Ab initio* molecular optical rotations and absolute configurations." *Mol. Phys.* **1997**. 91, 551–554.

[124] Pao, Y.-H.; Santry, D. P. "A Molecular Orbital Theory of Optical Rotatory Strengths of Molecules." *J. Am. Chem. Soc.* **1966**. 88, 4157–4163.

[125] Bouman, T. D.; Voigt, B.; Hansen, A. E. "Optical Activity of Saturated Ketones. Ab Initio Localized Orbital Analysis of a Model Ketone in the Random-Phase Approximation." *J. Am. Chem. Soc.* **1979**. 101, 550–558.

[126] Polavarapu, P. L. "Quantum mechanical predictions of chiroptical vibrational properties." *Int. J. Quantum Chem.* **2006**. 106, 1809–1814.

[127] Stephens, P. J.; Devlin, F. J. "Determination of the Structure of Chiral Molecules Using Ab Initio Vibrational Circular Dichroism Spectroscopy." *Chirality* **2000**. 12, 172–179.

[128] Stephens, P. J. "Theory of Vibrational Circular Cichroism." *J. Phys. Chem.* **1985**. 89, 748–752.

[129] Pecul, M.; Ruud, K. "Ab Initio Calculation of Vibrational Raman Optical Activity." *Int. J. Quantum Chem.* **2005**. 104, 816–829.

[130] Barron, L. D.; Hecht, L.; McColl, I. H.; Blanch, E. W. "Raman optical activity comes of age." *Mol. Phys.* **2004**. 102, 731–744.

[131] Polavarapu, P. L. "Ab Initio Vibrational Raman and Raman Optical Activity Spectra." *J. Phys. Chem.* **1990**. 94, 8106–8112.

[132] Kongsted, J.; Pedersen, T. B.; Strange, M.; Osted, A.; Hansen, A. E.; Mikkelsen, K. V.; Pawlowski, F.; Jørgensen, P.; Hättig, C. "Coupled cluster calculations of the optical rotation of *S*-propylene oxide in gas phase and solution." *Chem. Phys. Lett.* **2005**. 401, 385–392.

[133] Stephens, P. J.; Devlin, F. J.; Cheeseman, J. R.; Frisch, M. J.; Rosin, C. "Determination of Absolute Configuration Using Optical Rotation Calculated Using Density Functional Theory." *Org. Lett.* **2002**. 4, 4595–4598.

[134] Hansen, A. E.; Bouman, T. D. "Natural Chiroptical Spectroscopy: Theory and Computations." In Prigogine, I.; Rice, S. A., eds., "Advances in Chemical Physics," John Wiley & Sons, vol. 44. **1980** 545–644.

[135] Koch, H.; Aa. Jensen, H. J.; Jørgensen, P.; Helgaker, T. "Excitation energies from the coupled cluster singles and doubles linear response function (CCSDLR). Applications to Be, CH^+, CO, and H_2O." *J. Chem. Phys.* **1990**. 93, 3345–3350.

[136] Goedecker, S. "Linear scaling electronic structure methods." *Rev. Mod. Phys.* **1999**. 71, 1085–1123.

[137] Russ, N. J.; Crawford, T. D. "Potential energy surface discontinuities in local correlation methods." *J. Chem. Phys.* **2004**. 121, 691–696.

[138] Olsen, J.; Jørgensen, P. "Linear and nonlinear response functions for an exact state and for an MCSCF state." *J. Chem. Phys.* **1985**. 82, 3235–3264.

[139] Pulay, P. "Convergence acceleration of iterative sequences. The case of the SCF iteration." *Chem. Phys. Lett.* **1980**. 73, 393–398.

[140] Scuseria, G. E.; Lee, T. J.; Schaefer, H. F. "Accelerating the convergence of the coupled-cluster approach. The use of the DIIS method." *Chem. Phys. Lett.* **1986**. 130, 236–239.

[141] Pulay, P.; Saebø, S.; Meyer, W. "An efficient reformulation of the closed-shell self-consistent electron pair theory." *J. Chem. Phys.* **1984**. 81, 1901–1905.

[142] Saebø, S.; Baker, J.; Wolinski, K.; Pulay, P. "An efficient atomic orbital based second-order Møller–Plesset gradient program." *J. Chem. Phys.* **2004**. 120, 11423–11431.

[143] Dunning, T. H. "Gaussian basis functions for use in molecular calculations. I. Contraction of $(9s5p)$ atomic basis sets for the first-row atoms." *J. Chem. Phys.* **1970**. 53, 2823–2833.

[144] Meyer, W.; Frommhold, L. "*Ab initio* calculation of the dipole moment of He-Ar and the collision-induced absorption spectra." *Phys. Rev. A* **1986**. 33, 3807–3814.

[145] Schütz, M.; Rauhut, G.; Werner, H.-J. "Local Treatment of Electron Correlation in Molecular Clusters: Structures and Stabilities of (H_2O), n = 2-4." *J. Phys. Chem. A* **1998**. 102, 5997–6003.

VITA

Nicholas Joel Russ was born on October 30, 1978 to Mike and Carol Russ. He is the second of two children with a sister named Angi Frederick. Nick graduated from Northern York County High School located in Dillsburg, PA. He later attended college at Eastern Mennonite University majoring in Chemistry and Mathematics. Currently, Nick is pursuing a Ph.D. at Virginia Tech under the guidance of Prof. T. Daniel Crawford. Recently, Nick found himself completely smitten by a young beautiful woman named Jenny Kile, whom he wooed, courted and finally married on September 24, 2005. Upon completion of his doctorate, Nick plans to take a postdoctoral position at a small quantum chemistry software company called Q-Chem located in Pittsburgh, PA.